DMD Fast Forward. Published on September 10, 2019 as DOI: 10.1124/dmd.119.086918
This article has not been copyedited and formatted. The final version may differ from this version.

DMD # 86918

Systematic Development and Verification of A Physiologically-Based Pharmacokinetic Model of Rivaroxaban

Eleanor Jing Yi Cheong[1], Denise Wun Xi Teo[1], Denise Xin Yi Chua[1] and Eric Chun Yong Chan[1,2]

[1]Department of Pharmacy, Faculty of Science, National University of Singapore, 18 Science Drive 4, Singapore 117543; [2]National University Cancer Institute, Singapore (NCIS), NUH Medical Centre (NUHMC), 5 Lower Kent Ridge Road, Singapore 119074

Note: Eleanor Jing Yi Cheong, Denise Wun Xi Teo and Denise Xin Yi Chua contributed equally to the manuscript.

Downloaded from dmd.aspetjournals.org at ASPET Journals on April 20, 2024

DMD Fast Forward. Published on September 10, 2019 as DOI: 10.1124/dmd.119.086918
This article has not been copyedited and formatted. The final version may differ from this version.

Running title: PBPK Modeling of Rivaroxaban

Address correspondence to:

Professor Eric Chun Yong Chan, Department of Pharmacy, Faculty of Science, National University of Singapore, 18 Science Drive 4, Singapore 117543, Singapore.

Email: phaccye@nus.edu.sg; Telephone: 65-6516 6137; Fax: +65-67791554

Number of Text Pages	21
Number of Tables	6
Number of Figures	6
Number of References	54
Number of Words in the Abstract	246
Number of Words in the Introduction	687
Number of Words in the Discussion	1719

ABBREVIATIONS

AF	Atrial Fibrillation
AUC	Area under the plasma concentration-time curve
CL/F	Apparent clearance
CLu_{int}	Unbound intrinsic clearance
CL_{PD}	Passive diffusion clearance

Downloaded from dmd.aspetjournals.org at ASPET Journals on April 20, 2024

DMD Fast Forward. Published on September 10, 2019 as DOI: 10.1124/dmd.119.086918
This article has not been copyedited and formatted. The final version may differ from this version.

CL_R	Renal clearance
CYP2J2	Cytochrome P450 2J2
CYP3A4	Cytochrome P450 3A4
C_{max}	Peak plasma concentration
DDI	Drug-Drug Interaction
DDDI	Drug-Drug-Disease Interaction
DOAC	Direct oral anticoagulant
USFDA	United States Food and Drug Administration
IVIVE	*In vitro* to *in vivo* extrapolation
J_{max}	Maximum rate of active transport
K_m	Michaelis constant
$K_{m:w}$	Bile micelle: water partition coefficient
K_p	Tissue: plasma partition coefficient
P_{app}	*In vitro* apparent permeability
PBPK	Physiologically-based pharmacokinetic
$P_{eff,man}$	Effective permeability in human
P-gp	P-glycoprotein
PTCPGK	Proximal tubular cells per gram kidney
S_0	Intrinsic Solubility

Downloaded from dmd.aspetjournals.org at ASPET Journals on April 20, 2024

DMD Fast Forward. Published on September 10, 2019 as DOI: 10.1124/dmd.119.086918
This article has not been copyedited and formatted. The final version may differ from this version.

ABSTRACT

Rivaroxaban is indicated for stroke prevention in nonvalvular atrial fibrillation (AF). Its elimination is mediated by both hepatic metabolism and renal excretion. Consequently, its clearance is susceptible to both intrinsic (pathophysiological) and extrinsic (concomitant drugs) variabilities that in turn implicate bleeding risks. Upon systematic model verification, physiologically-based pharmacokinetic (PBPK) models are qualified for the quantitative rationalization of complex drug-drug-disease interactions (DDDIs). Hence, this study aimed to develop and verify a PBPK model of rivaroxaban systematically. Key parameters required to define rivaroxaban's disposition were either obtained from *in vivo* data or generated via *in vitro* metabolism and transport kinetic assays. Our developed PBPK model successfully predicted rivaroxaban's clinical PK parameters within predefined success metrics. Consideration of basolateral organic anion transporter 3 (OAT3)-mediated proximal tubular uptake in tandem with apical P-glycoprotein (P-gp)-mediated efflux facilitated mechanistic characterization of the renal elimination of rivaroxaban in both healthy and renal impaired patients. Retrospective drug-drug interaction (DDI) simulations, incorporating *in vitro* metabolic inhibitory parameters, accurately recapitulated clinically observed attenuation of rivaroxaban's hepatic clearance due to enzyme-mediated DDIs with CYP3A4/2J2 inhibitors (verapamil and ketoconazole). Notably, transporter-mediated DDI simulations between rivaroxaban and P-gp inhibitor ketoconazole yielded minimal increases in rivaroxaban's systemic exposure when P-gp-mediated efflux was solely inhibited but were successfully characterized when concomitant basolateral uptake inhibition was incorporated in the simulation. In conclusion, our developed PBPK model of rivaroxaban is systematically verified for prospective interrogation and management of untested yet clinically relevant DDDIs pertinent to AF management using rivaroxaban.

Downloaded from dmd.aspetjournals.org at ASPET Journals on April 20, 2024

DMD Fast Forward. Published on September 10, 2019 as DOI: 10.1124/dmd.119.086918
This article has not been copyedited and formatted. The final version may differ from this version.

SIGNIFICANCE STATEMENT

Rivaroxaban is susceptible to drug-drug-disease interactions (DDDIs) comprising renal impairment, P-gp and CYP3A4/2J2 inhibition. Here, systematic construction and verification of a PBPK model of rivaroxaban, with the inclusion of a mechanistic kidney component, provided insight into the previously arcane role of OAT3-mediated basolateral uptake in influencing both clinically-observed renal elimination of rivaroxaban and differential extents of transporter-mediated DDIs. The verified model holds potential for investigating clinically-relevant DDDIs involving rivaroxaban and designing dosing adjustments to optimize its pharmacotherapy in atrial fibrillation.

Downloaded from dmd.aspetjournals.org at ASPET Journals on April 20, 2024

DMD Fast Forward. Published on September 10, 2019 as DOI: 10.1124/dmd.119.086918
This article has not been copyedited and formatted. The final version may differ from this version.

VISUAL ABSTRACT

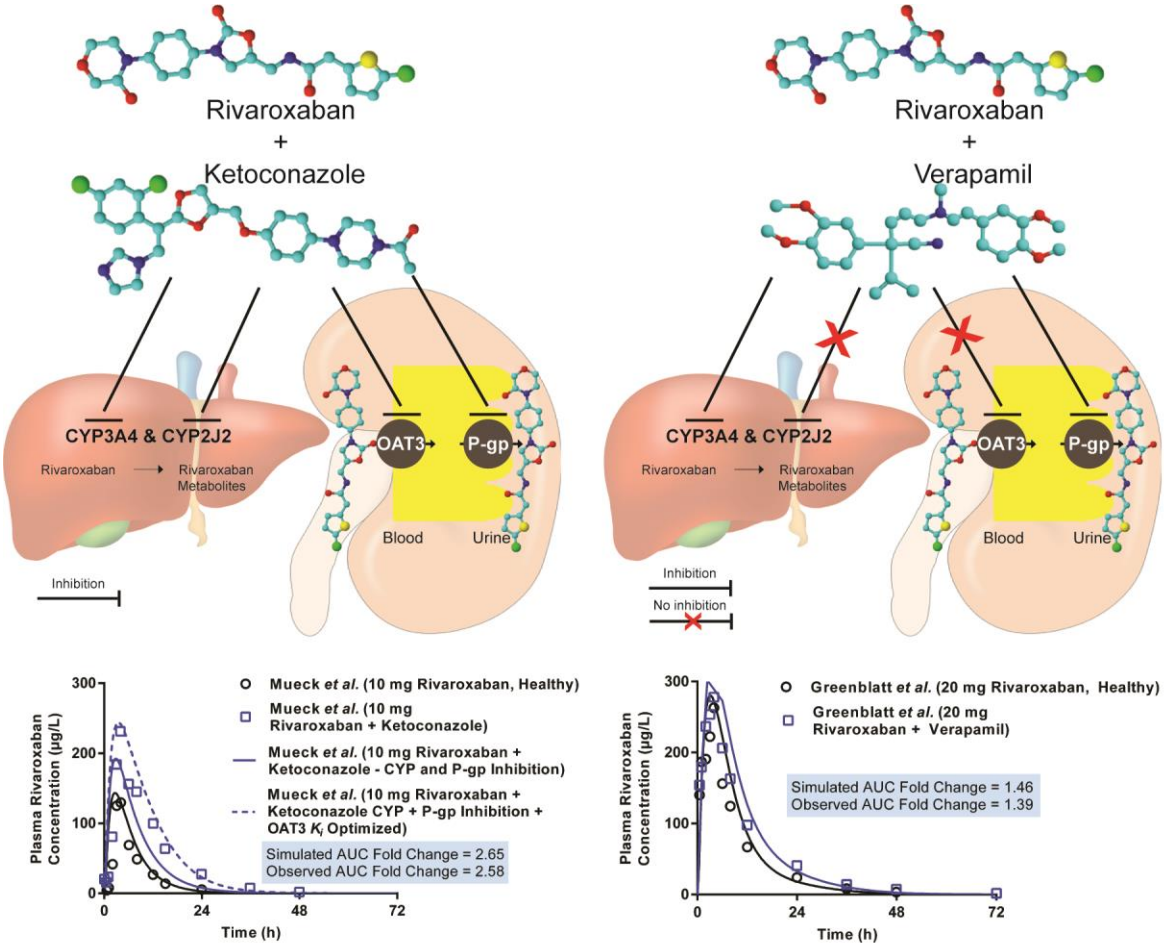

Downloaded from dmd.aspetjournals.org at ASPET Journals on April 20, 2024

DMD Fast Forward. Published on September 10, 2019 as DOI: 10.1124/dmd.119.086918
This article has not been copyedited and formatted. The final version may differ from this version.

INTRODUCTION

Atrial fibrillation (AF) is the most common and clinically significant cardiovascular rhythm disorder. The Global Burden of Diseases, Injuries, and Risk Factors 2010 study indicated that the previous two decades have witnessed a progressive increase in the worldwide prevalence and incidence of AF, with significant effects on associated morbidity and mortality (Chugh *et al.*, 2014). Therapeutic mainstays of AF management can be chiefly divided into symptomatic treatment of arrhythmia by either rate or rhythm control, and prevention of thromboembolic complications by anticoagulation (January *et al.*, 2014).

In recent years, direct oral anticoagulants (DOACs) have emerged as preferred alternatives to warfarin, particularly due to predictable dose response relationships that eliminate the need for routine laboratory monitoring (Scaglione, 2013). Rivaroxaban, a non-vitamin K antagonist OAC approved by the United States Food and Drug Administration (USFDA) in 2010, is indicated for stroke prevention in nonvalvular AF. Rivaroxaban possesses a unique dual mode of elimination: where two thirds of the systematically absorbed dose undergo cytochrome P450 (CYP) 3A4/2J2-mediated metabolism while the remaining one third is excreted unchanged in the urine, primarily via P-glycoprotein (P-gp)-mediated efflux (Mueck *et al.*, 2013). This inevitably increases rivaroxaban's susceptibility to drug-drug-disease interactions (DDDIs) attributed to simultaneous impairment of its multiple clearance pathways (Grillo *et al.*, 2012).

The likelihood of drug-drug interactions (DDIs) is markedly increased when we consider that many rhythm and rate control agents (e.g. amiodarone, carvedilol and diltiazem) likely to be co-administered with rivaroxaban in AF are known CYP3A4/2J2 and/or P-gp inhibitors (Wessler *et al.*, 2013; US FDA, 2017). Furthermore, given that the prevalence of AF burgeons in the elderly population (Chugh *et al.*, 2014), assessing the implications of age-related physiological decline on the extent of these clinically relevant DDIs also becomes essential to guide pharmacotherapy. Nevertheless, practical constraints often restrict the number of dedicated trials that can be conducted to evaluate all clinically plausible

Downloaded from dmd.aspetjournals.org at ASPET Journals on April 20, 2024

DMD Fast Forward. Published on September 10, 2019 as DOI: 10.1124/dmd.119.086918
This article has not been copyedited and formatted. The final version may differ from this version.

permutations. Consequently, physiologically-based pharmacokinetic (PBPK) modeling has emerged as a valuable tool in the quantitative rationalization of PK variabilities due to complex DDDIs.

By coupling the defining properties of rivaroxaban and the biological system with trial design, minimal PBPK models developed by Grillo *et al.* (Grillo *et al.*, 2012) and Ismail *et al.* (Ismail *et al.*, 2018) have prospectively established clinically significant DDDIs between rivaroxaban and erythromycin or verapamil in renally impaired patients. Findings were instrumental in substantiating cautionary language discouraging concomitant administration of rivaroxaban with moderate CYP3A4/P-gp inhibitors in patients with renal dysfunction (US FDA, 2011b). Nevertheless, subsequent model verification using clinical DDI data uncovered a key limitation of the current minimal PBPK models where major physiological compartments (except the liver) are combined with the plasma compartment. While these PBPK models incorporated interactions comprising both CYP3A4 and P-gp pathways, clinical urinary excretion data revealed negligible decreases in the renal clearance of rivaroxaban when it was co-administered with either erythromycin or verapamil in healthy patients (Moore *et al.*, 2014; Greenblatt *et al.*, 2018). This invalidated the initial assumption of a transporter-mediated component mediating the observed DDDI. Hence, to justify PBPK-guided extrapolation beyond the clinical trial population in the investigation of potential DDDIs involving rivaroxaban, mechanistic delineation of passive and active processes governing the renal clearance of rivaroxaban becomes essential.

Consequently, this study aims to develop and verify a full PBPK model for rivaroxaban, via incorporation of both *in vivo* clinical PK data as well as *in vitro* experimental measurements, which can be utilized to inform drug-specific parameters through *in vitro* to *in vivo* extrapolation (IVIVE). Upon successful recapitulation of observed rivaroxaban PK and urinary excretion profiles in both healthy and renal impaired patients, *in vitro* inhibitory parameters utilizing rivaroxaban as the probe substrate would be quantified and employed in retrospective DDI simulations linking rivaroxaban with prototypical CYP3A4/2J2 and P-gp inhibitors (ketoconazole and verapamil which yield different quantitative effects on the renal clearance of rivaroxaban). We envision that this systematic approach to PBPK model verification would eventually instill confidence in acting on model-generated insights to support the

Downloaded from dmd.aspetjournals.org at ASPET Journals on April 20, 2024

DMD Fast Forward. Published on September 10, 2019 as DOI: 10.1124/dmd.119.086918
This article has not been copyedited and formatted. The final version may differ from this version.

rational dose selection of rivaroxaban in previously untested, albeit realistically complex clinical scenarios. The long-term aim is to minimize inadvertent increases in the systemic exposure of rivaroxaban while preserving its anticoagulant efficacy.

Downloaded from dmd.aspetjournals.org at ASPET Journals on April 20, 2024

DMD Fast Forward. Published on September 10, 2019 as DOI: 10.1124/dmd.119.086918
This article has not been copyedited and formatted. The final version may differ from this version.

MATERIALS AND METHODS

The workflow schematic adopted for PBPK model development, verification and iterative refinement is illustrated in **Fig. 1**. Mechanistic modeling of permeability and transport kinetics was implemented with the Simcyp *In Vitro* Analysis (SIVA) toolkit (Version 3). All PK simulations presented herein were conducted using a population-based absorption, distribution, metabolism and excretion simulator (version 17, Simcyp®, Sheffield, UK).

1.1 Model Development

PBPK Model of Rivaroxaban. Key drug-dependent parameters necessary for simulation of the kinetics of rivaroxaban are delineated in **Table 1**. Oral absorption of rivaroxaban was predicted with the Advanced Dissolution, Absorption, Metabolism (ADAM) model implemented in Simcyp. The effective permeability of rivaroxaban in human ($P_{eff,man}$) was derived from *in vitro* apparent permeability (P_{app}) measured in Caco-2 cell monolayers (Gnoth *et al.*, 2011) using the P_{app}-P_{eff} correlation model within the simulator. Upon defining its intrinsic solubility (S_0) (Takács-Novák *et al.*, 2013), the dissolution rate of rivaroxaban was estimated with the diffusion layer model developed by Wang and Flanagan (Wang and Flanagan, 1999). The effects of bile on the *in vivo* solubility estimated in each segment of the gastrointestinal tract was quantified via the bile micelle:water partition coefficient ($K_{m:w}$), calculated from the predefined log P via a quantitative structure activity relationship model developed by Glomme *et al* (Glomme *et al.*, 2007). Simulated solubility outputs were compared with experimental biorelevant solubility measurements (Takács-Novák *et al.*, 2013) and $K_{m:w}$ was manually adjusted to achieve concordance. Subsequently, a whole body PBPK model was applied to describe the distribution of rivaroxaban, where tissue to plasma distribution equilibrium ratios (K_p) were calculated via mechanistic tissue composition equations developed by Rodgers and Rowland (Rodgers and Rowland, 2006). The volume of distribution at steady state (V_{ss}) was predicted to be 0.2 L/kg, which is lower than the observed *in vivo* V_{ss} of approximately 0.62 L/kg (Mueck *et al.*, 2014). Hence, a K_p scalar (applied equally to all tissues) of 2.2 was applied to optimize V_{ss}.

Downloaded from dmd.aspetjournals.org at ASPET Journals on April 20, 2024

DMD Fast Forward. Published on September 10, 2019 as DOI: 10.1124/dmd.119.086918
This article has not been copyedited and formatted. The final version may differ from this version.

Hepatic Metabolism. Apparent oral and renal clearance (CL/F and CL_R) data were collated from primary literature sources following administration of rivaroxaban to healthy adult subjects (**Supplemental Table 1**). Overall weighted mean clearances were calculated using **eq. 1**.

$$W\bar{X} = \frac{\sum_{j=1}^{J} n_j . \bar{x}_j}{\sum_{j=1}^{J} n_j} \quad (\mathbf{1})$$

where $W\bar{X}$ is the weighted mean, n_j is the number of subjects in the jth study, and x_j is the mean of the jth study. Here a "study" is defined as the data associated with a group of subjects being administered a specific dose and dosing regimen of rivaroxaban, on a particular occasion, with "n" number of subjects. Based on a fractional metabolism in the liver of 0.37 for CYP3A4 and 0.29 for CYP2J2 as reported by Grillo *et al* (Grillo *et al.*, 2012), the unbound intrinsic clearances (CLu_{int}) of rivaroxaban mediated by CYP3A4 and CYP2J2 were derived from the weighted mean of CL/F after accounting for the contribution of CL_R, via retrograde application of the well-stirred model.

Mechanistic Kidney Model Development. The differential contribution of the primary processes governing the renal disposition of rivaroxaban (i.e. glomerular filtration, tubular secretion and tubular reabsorption) was quantified via by the mechanistic kidney model (MechKiM) within the simulator. *In vitro* transport assays investigating the P-gp-mediated efflux kinetics of rivaroxaban were first performed in Madin Darby canine kidney (MDCK) subclone I cells transfected with multidrug resistance protein (MDR1). To account for the bidirectional passive permeability of rivaroxaban across the apical (A) and basolateral (B) membranes in addition to apical P-gp-mediated efflux driven by unbound intracellular rivaroxaban concentrations, time- (60-420 min) and concentration- (3-100 µM donor rivaroxaban) dependent data, measured in the absorptive (A to B) direction, were fitted to a mechanistic model that dynamically simulates flux in rivaroxaban concentrations within the apical, basolateral and intracellular compartments of the transwell apparatus. Derived *in vitro* estimates of the maximum rate of active transport (J_{max}), Michaelis constant (K_m) and passive permeability (P_{pass}) were subsequently subjected to quantitative IVIVE scaling as highlighted in **eqs. 2** and **3** to simulate the

Downloaded from dmd.aspetjournals.org at ASPET Journals on April 20, 2024

DMD Fast Forward. Published on September 10, 2019 as DOI: 10.1124/dmd.119.086918
This article has not been copyedited and formatted. The final version may differ from this version.

intrinsic clearance attributed to *in vivo* P-gp-mediated tubular secretion ($CLu_{int,T\ per\ kidney}$) and passive diffusion clearances ($CL_{PD,kidney}$) that contribute to tubular reabsorption respectively.

$$CLu_{int,T\ per\ kidney} = \frac{J_{max}}{K_{m,u}} / CL_{u,int} \times REF_{PTC} \times PTCPGK \times kidney\ weight \quad (2)$$

$$CL_{PD,kidney} = \frac{P_{pass} \times Nephron\ Surface\ Area\ based\ on\ 2\ kidneys}{PTCPGK \times kidney\ weight} \quad (3)$$

In **eq. 2**, J_{max} (pmol/min) generated was first normalized to protein concentration in each transwell insert, quantified using the BCA protein assay. J_{max} was subsequently converted from pmol/min/mg protein to pmol/min/10^6 cells based on 1 million MDCK cells containing 0.08 mg of total protein (Scotcher *et al.*, 2017). Differential P-gp mRNA expression data in the kidney, intestine and MDCK cells was used to inform the relative expression factor (REF_{PTC}) (Scotcher *et al.*, 2017). In **eq. 3**, total nephron surface area (291 cm^2), kidney weight (341.5 g) and the number of proximal tubular cells per gram kidney, PTCPGK (60 million in a healthy population) were used as IVIVE scaling factors to convert *in vitro* P_{app} to CL_{PD} (Emami Riedmaier *et al.*, 2016).

Further details on the chemicals, culture techniques, modeling and fitting procedures used are highlighted in **Supplemental Methods Section 1.1**.

PBPK Models of Inhibitors (Ketoconazole and Verapamil). Ketoconazole, verapamil and its primary metabolite, norverapamil, are prototypical CYP3A4/2J2 as well as P-gp inhibitors that have been implicated in clinical DDIs with rivaroxaban (Mueck *et al.*, 2013; Greenblatt *et al.*, 2018). In the construction of PBPK-DDI models, the verified compound file of ketoconazole provided in Simcyp® (version 17) was used. In the case of verapamil, although the compound file provided in Simcyp® (version 17) allowed adequate modeling of the PK profile of an immediate release formulation, co-administration of rivaroxaban and sustained release verapamil capsules in the trial by Greenblatt *et al* necessitated further refinement of verapamil's absorption kinetics. As described in **Supplemental Fig.**

Downloaded from dmd.aspetjournals.org at ASPET Journals on April 20, 2024

DMD Fast Forward. Published on September 10, 2019 as DOI: 10.1124/dmd.119.086918
This article has not been copyedited and formatted. The final version may differ from this version.

1, a sequential one stage convolution procedure was implemented that models the relationship between the *in vitro* dissolution profile and the observed plasma concentration-time profile of verapamil. Final model parameters for ketoconazole and verapamil are summarized in **Supplemental Tables 2.1-2.3.**

2.1 Model Verification – PK Simulations

Verification of Basal PBPK Model of Rivaroxaban and Verapamil. PK profiles following single or multiple administration of clinically relevant doses to healthy subjects using the default healthy 'NEurCaucasian" population available within Simcyp were first simulated to verify the performance of the PBPK models of rivaroxaban and verapamil. During the model verification process, the population, number of participants, dose and regimen selected for the simulations were matched to the corresponding clinical study designs (**Supplemental Table 3**). A total of 10 trials were simulated to assess variability across groups. The predictive accuracies of the PBPK models were evaluated via visual predictive checks against average plasma concentration-time data digitized using a WebPlotDigitizer (version 4.0, https://automeris.io/WebPlotDigitizer). Additionally, a metric approach detailed by Abduljalil *et al.* that considers both the intrinsic variability of observed PK parameters (i.e. area under the curve, AUC; peak plasma concentration, C_{max}) as well as the clinical sample size was also applied to assess simulated values (Abduljalil *et al.*, 2014).

Simulation of Rivaroxaban's CL_R Using the Mechanistic Kidney Model in a Healthy Population and in Patients with Mild Renal Impairment. Simulations of rivaroxaban's plasma concentration-time and urinary excretion profiles in a healthy population using the final mechanistic model were first compared with the PBPK model of rivaroxaban where weighted mean CL_R collated from 7 independent studies was defined as a single input parameter (**Supplemental Table 1**). Upon verification of the predictive capabilities of the mechanistic kidney model in healthy subjects, system-dependent parameters within the model were further modified to reflect potential physiological changes synonymous with renal impairment. Based on the intact nephron hypothesis (INH) by Bricker, damaged nephrons stop working completely while undamaged nephrons function normally (Bricker, 1969). Consequently, proportional reductions in tubular secretion and glomerular filtration would likely be

Downloaded from dmd.aspetjournals.org at ASPET Journals on April 20, 2024

DMD Fast Forward. Published on September 10, 2019 as DOI: 10.1124/dmd.119.086918
This article has not been copyedited and formatted. The final version may differ from this version.

observed in chronic kidney disease (CKD). In this study, a decline in PTCPGK was utilized to represent the loss of tubular cells and hence active secretion that is consistent with the INH concept. Consequently, the default value of 60 million PTCPGK corresponding to the representative GFR of a healthy population (136.4 mL/min) was scaled down proportionally to 28.6 million according to the median GFR that occurs in mild renal impairment (GFR= 65 mL/min in a range of 50 to 79 mL/min) (Scotcher *et al.*, 2017; Hsueh *et al.*, 2018) (**Supplemental Table 4**). This newly defined population was subsequently used to predict the observed attenuations in rivaroxaban's CL_R in mild renal impairment (**Supplemental Methods, Modelling Supplemental Data File 1**).

2.2 Model Verification – Retrospective DDI Simulations

Upon accurate recapitulation of rivaroxaban's PK, performance verification in both the uninhibited and inhibited states is essential to ascertain that rivaroxaban has been adequately characterized as a DDI victim (Shebley *et al.*, 2018). Hence, PBPK-DDI models were constructed via the incorporation of *in vitro* inhibitory parameters describing the inhibitory potential of verapamil, norverapamil and ketoconazole against the CYP3A4/2J2-mediated metabolism as well as P-gp-mediated secretion of rivaroxaban (**Supplemental Methods Section 2, Modelling Supplemental Data Files 2 and 3**). For DDI simulations, statistical analyses were performed using SPSS Version 22. AUC, C_{max} and CL of rivaroxaban were analyzed assuming log normally distributed data. Student's t test was used to analyze the difference in these parameters in the absence and presence of concomitant inhibitors. Point estimates and exploratory 90% confidence intervals (CIs) for the ratios were calculated by retransformation of the logarithmic results. Based on these analyses, a refined predictive measure proposed by Guest *et al.* incorporating PK variability coupled with variable prediction boundaries dependent on the extent of interaction was applied in defining the success of DDI simulations (Guest *et al.*, 2011).

3 Model Refinement

Incorporation of Organic Anion Transporter 3 (OAT3)-Mediated Basolateral Uptake of Rivaroxaban. Consideration of glomerular filtration, tubular reabsorption via passive permeability clearances and apical P-gp-mediated secretion resulted in an underestimation of rivaroxaban's CL_R,

Downloaded from dmd.aspetjournals.org at ASPET Journals on April 20, 2024

DMD Fast Forward. Published on September 10, 2019 as DOI: 10.1124/dmd.119.086918
This article has not been copyedited and formatted. The final version may differ from this version.

alluding to potential undefined mechanisms governing rivaroxaban's renal disposition. Tsuruya *et al.* reported the specific uptake of rivaroxaban in mouse OAT3-expressing cells, with J_{max} and K_m in mOAT3-transfected cells determined to be 72.9 ± 46.8 pmol/min/mg protein and 1.01 ± 0.70 µM respectively (Tsuruya *et al.*, 2017). In the absence of transporter abundance or expression to facilitate allometric scaling, rivaroxaban uptake was independently investigated in this study using hOAT3-transfected HEK cell lines obtained from Dr. Kathleen Giacomini (University of California, San Francisco, CA). Details on the culture techniques, uptake assay protocol, two compartmental modeling and fitting procedures are highlighted in **Supplemental Methods Section 1.1**. Derived *in vitro* active uptake clearance (CL_{int}) was similarly subjected to IVIVE using **eq. 3**. correcting for measured protein (0.15 mg) per million HEK cells. An alternative top-down approach was further utilized to estimate the CLu_{int} governing OAT3-mediated uptake. Using sensitivity analysis optimization, the CLu_{int} was determined to be the value producing a simulated CL_R that converged with the weighted mean CL_R of 3.1L/h when serum creatinine was fixed at 80 µmol/L (corresponding to GFR = 120 mL/min in healthy volunteers) (Scotcher *et al.*, 2017).

Downloaded from dmd.aspetjournals.org at ASPET Journals on April 20, 2024

DMD Fast Forward. Published on September 10, 2019 as DOI: 10.1124/dmd.119.086918
This article has not been copyedited and formatted. The final version may differ from this version.

RESULTS

1 Development and Verification of the PBPK Models of Rivaroxaban and Verapamil

Basal PBPK Model of Rivaroxaban Recapitulated Clinically Observed PK Profiles. The weighted mean CL/F and CL_R of rivaroxaban collated from 7 independent studies in healthy volunteers were 8.6 L/h and 3.1 L/h respectively (**Supplemental Table 1**). Using the retrograde model, CLu_{int} attributed to CYP2J2 and CYP3A4 were calculated to be 5.69 and 0.064 µL/min/pmol of isoform, with additional liver clearance defined to be 23.5 µL/min/mg of liver microsomal protein. The effect of food in enhancing rivaroxaban's bioavailability at the 20 mg dose strength was recapitulated by considering the differential influences of fasted versus fed conditions on the extent of bile micelle-mediated solubilization (**Fig. 2A**, **Table 2**). As highlighted in **Table 2**, simulated geometric mean AUC was 1512 µg.h/L in the fasted state compared to 2127 µg.h/L in the fed state. This predicted 1.41-fold increase in the presence of food was aligned with the 1.39-fold change observed in a Phase I confirmatory food effect trial (Stampfuss *et al.*, 2013). Model predictive performance was further assessed using external verification datasets from independent clinical trials not utilized in model development. Plasma concentration-time profiles of 10 mg (**Fig. 2B**) and 20 mg (**Fig. 2C**) doses of rivaroxaban (**Modelling Supplemental Data File 4**) compared well with the reference published studies by Mueck *et al.* and Greenblatt *et al* (Mueck *et al.*, 2013; Greenblatt *et al.*, 2018) respectively, with observed PK parameters (AUC, C_{max} and CL) falling within the pre-specified PK prediction criteria (**Table 2**).

Three-Compartmental Analysis Enabled Accurate Determination of Kinetic Constants Governing the *In Vitro* P-gp-Mediated Efflux of Rivaroxaban. Approximately one third (36%) of the absorbed dose of rivaroxaban is excreted unchanged in the kidney, with active tubular secretion accounting for 30% (Mueck *et al.*, 2013). As a result, accurate estimation of kinetic parameters governing the P-gp-mediated efflux of rivaroxaban based on *in vitro* data is critical for successful IVIVE of its renal disposition. Preliminary analyses of bidirectional MDCK-MDR1 transport assays via the conventional Michaelis-Menten approach established time-linear conditions for both absorptive (**Supplemental Fig. 2A**) and basolateral rivaroxaban transport (**Supplemental Fig. 2B**) as well as the

Downloaded from dmd.aspetjournals.org at ASPET Journals on April 20, 2024

DMD Fast Forward. Published on September 10, 2019 as DOI: 10.1124/dmd.119.086918
This article has not been copyedited and formatted. The final version may differ from this version.

superior sensitivity of absorptive flux (**Supplemental Fig. 2C**) compared to basolateral flux (**Supplemental Fig. 2D**) in response to apical P-gp efflux activity. Yet, as seen in **Supplemental Fig. 2C**, solubility limitations prevented saturation of rivaroxaban transport in the absorptive direction. Hence, to account for the interaction of P-gp with unbound intracellular concentrations of rivaroxaban, mechanistic three-compartmental modeling was subsequently applied to analyze both time- and concentration-dependent data describing rivaroxaban's absorptive transport. Unbound rivaroxaban concentrations in the extracellular (fu_{media}) and intracellular (fu_{cell}) compartments, determined via ultrafiltration experiments to be 1 and 0.023 respectively, were incorporated as fixed drug-dependent parameters (**Supplemental Table 5**). $J_{max,app}$ and $K_{m,app}$ (97.98 pmol/min and 836.8 µM respectively) determined using the conventional Michaelis Menten approach were also utilized as *a priori* information for naïve pooled fitting via both hybrid and local (Nelder Mead) optimization procedures. As highlighted in **Table 3**, the convergence of J_{max} and K_m estimates from two different optimization methods attested to the robustness of the three-compartmental approach and established that fitting outcomes were minimally influenced by initial J_{max} and K_m values. Visual predictive checks also demonstrated consistency between experimental measurements and simulated rivaroxaban concentration-time profiles in the basolateral compartment (**Fig. 3A** and **B**). Given that Nelder Mead optimization resulted in lower Akaike information criterion (AIC) and difference in small sample size corrected version of AIC (ΔAIC_c) values, J_{max} = 37.83 pmol/min, K_m = 9.42 µM and P_{pass} = 12.88 × 10^6 cm/s were subjected to quantitative IVIVE via **eqs. 2** and **3** to generate $CLu_{int,T\ per\ kidney}$ (J_{max} = 80.921 pmol/min/10^6 cells and $K_{m,u}$ = 9.42 µM) and $CL_{PD,kidney}$ (1.09 × 10^{-5} µL/min/10^6 cells)for parameterization of the mechanistic kidney model (**Table 1**).

IVIVE of Rivaroxaban's Renal Clearance Revealed the Pivotal Role of Basolateral Uptake. Using the mechanistic kidney model, the relative contribution of various processes (i.e. glomerular filtration, tubular reabsorption and active secretion) involved in rivaroxaban's renal excretion clearance was assessed in a stepwise manner. Expectedly, consideration of either glomerular filtration in isolation or both glomerular filtration and passive tubular reabsorption resulted in a substantial underprediction of rivaroxaban's CL_R (predicted CL_R of 0.41 and 0.36 L/h respectively) (**Fig. 4A**) and a corresponding

Downloaded from dmd.aspetjournals.org at ASPET Journals on April 20, 2024

DMD Fast Forward. Published on September 10, 2019 as DOI: 10.1124/dmd.119.086918
This article has not been copyedited and formatted. The final version may differ from this version.

overestimation of its systemic exposure (**Fig. 4B**), underscoring the significance of active renal secretion in mediating rivaroxaban's renal disposition. However, sole incorporation of P-gp-mediated apical efflux demonstrated marginal effects on both CL_R and systemic exposure (**Fig. 4A** and **B**). As highlighted in **Table 4**, without OAT3-mediated basolateral uptake, CL_R was underpredicted by 85% and the predicted AUC was 1.51-fold higher than that reported by Greenblatt *et al.*, falling outside the prespecified success criteria (Greenblatt *et al.*, 2018). Hence, this provided the impetus for mechanistic investigation of OAT3-mediated rivaroxaban uptake.

Kinetic Constants Governing *In Vitro* OAT3-Mediated Uptake of Rivaroxaban were Comparable to Top-Down Estimates of OAT3-Mediated Intrinsic Clearance. Upon establishing the functionality of the OAT3/OAT1-transfected systems (**Supplemental Fig. 3A** and **3B**), preliminary investigation of potential rivaroxaban uptake was performed. The uptake of rivaroxaban by hOAT3-expressing cells was higher than that by the empty-vector transfected cells at 5 min and was further inhibited by a prototypical OAT inhibitor, probenecid (50 μM) (**Supplemental Fig. 3C**). In contrast, the uptake of rivaroxaban by hOAT1-expressing cells was comparable to that of the empty vector transfected cells at 5 min (**Supplemental Fig. 3D**). Taken together, rivaroxaban is a substrate of hOAT3 but not hOAT1. Time-dependent rivaroxaban uptake was subsequently evaluated, and linearity was preserved up to 2 min (**Supplemental Fig. 3E).** Consequently, concentration-dependent transport of rivaroxaban (0.5-100 μM) was investigated under time-linear conditions in both wild type and OAT3-transfected cells (**Supplemental Fig. 3G**). Total rivaroxaban uptake (solid black line, **Supplemental Fig. 3H**) was fitted via the conventional two-step approach (**eq. S14**). Accounting for passive diffusion (**Supplemental Fig. 3F**), calculated to be 22.65 μL/min/10^6 cells, saturable active uptake (grey solid line) was observed with transporter-mediated intrinsic clearance ($CL_{int,T}$) estimated to be 33.91 μL/min/10^6 cells (**Supplemental Fig. 3H**). Given that data from 2 min incubations have been shown to produce large standard errors in the estimation of CL_{PD} (Menochet *et al.*, 2012), $CL_{PD,kidney}$ (1.09×10^{-5} μL/min/10^6 cells obtained previously via IVIVE scaling) and $CL_{int,T}$ derived from the two step approach were eventually utilized as initial estimates for naïve pooled fitting of measured time-and concentration-dependent data via two-compartmental modeling. Visual predictive checks demonstrated consistency between experimental

Downloaded from dmd.aspetjournals.org at ASPET Journals on April 20, 2024

DMD Fast Forward. Published on September 10, 2019 as DOI: 10.1124/dmd.119.086918
This article has not been copyedited and formatted. The final version may differ from this version.

measurements and simulated intracellular rivaroxaban concentration-time profiles (**Fig. 3C** and **D**). OAT3 $CLu_{int,T}$ was determined to be 41.33 µL/min/10^6 cells (**Table 3**) and compared well with estimates obtained via a sensitivity analysis-based approach that simulated variations in rivaroxaban's CL_R as a function of OAT3 $CLu_{int,T}$ and serum creatinine input parameter values. The optimal $CLu_{int,T}$ for uptake governed by OAT3 (43 µL/min/10^6 cells) was taken at the intersection of the simulated rivaroxaban CL_R with the observed weighted CL_R of 3.1 L/h (green plane) at a serum creatinine of 80 µmol/L (which corresponds to simulated GFR∼120 ml/min in healthy volunteers) (**Supplemental Fig. 4**).

Concurrent Basolateral Uptake and Apical Efflux were Necessary to Recapitulate Rivaroxaban's Renal Clearance. The optimized $CLu_{int,T}$ of OAT3 mediated uptake was incorporated into the mechanistic kidney model. In a hypothetical scenario where basolateral OAT3 uptake was present but apical P-gp efflux was disregarded, although simulations managed to recapitulate the observed plasma concentration-time profile of rivaroxaban (**Fig. 4B**), the amount excreted unchanged in urine remained underestimated (**Fig. 4A** and **Table 4**). Hence, our simulations demonstrate that accounting for basolateral uptake in conjunction with apical efflux was crucial in ensuring that simulated plasma concentration-time (**Fig. 4B**) and urinary excretion rate profiles (**Fig. 4A**) matched the observed clinical data, with PK parameters (AUC, C_{max} and CL_R) satisfying the prespecified success criteria (**Table 4, Modelling Supplemental Data File 5**).

Simulations using the Mild Renal Impairment Population Adequately Predicted Increases in the Systemic Exposure of Rivaroxaban. Upon successful verification of the mechanistic kidney model in healthy subjects, which affirmed the accuracy of drug-dependent parameters defined for rivaroxaban, the ability of the PBPK model to predict the altered PK of rivaroxaban in mild renal impairment was subsequently investigated. With the application of INH, assuming proportional reductions in GFR and tubular secretion, simulated geometric mean rivaroxaban AUC and CL_R fold changes were 1.20-fold and 0.54-fold respectively (**Table 4**). These point estimates fell within the range of clinical success determined based on the clinically observed AUC and CL_R fold changes of 1.11 and 0.93 (**Table 4, Modelling Supplemental File 1**). Modeled plasma-concentration time profiles also reasonably

Downloaded from dmd.aspetjournals.org at ASPET Journals on April 20, 2024

DMD Fast Forward. Published on September 10, 2019 as DOI: 10.1124/dmd.119.086918
This article has not been copyedited and formatted. The final version may differ from this version.

characterized the increase in rivaroxaban's systemic exposure with concomitant mild renal impairment (**Fig. 4C**).

PBPK Models of Immediate Release Verapamil and Norverapamil Recapitulated Clinically Observed PK Profiles. In the first step of the two stage IVIVC framework (**Supplemental Fig. 1**), using the verified verapamil and norverapamil compound files provided within the Simcyp simulator, simulated PK profiles following a single 80 mg immediate release dose of verapamil were aligned with the reference published study by Haeri *et al.* (**Fig. 5A**) (Haeri *et al.*, 2014). Additionally, the model effectively predicted the observed AUC data within the calculated prediction criteria (**Supplemental Table 6**). This affirms that *in vivo* disposition parameters were accurately defined before proceeding with IVIVC.

PBPK Models of Verapamil and Norverapamil Described Absorption Kinetics following Administration of a Sustained Release Formulation. IVIVC convolution was subsequently applied to predict the PK following administration of a single 120 mg dose of controlled release verapamil based on an initial *in vitro* dissolution input (**Fig. 5B**) (Wise, 2000). Simulated and observed plasma concentrations reported by Frishman *et al.* were compared and discrepancies prompted iterative refinement of dissolution parameters to produce an *in vivo* dissolution profile (**Fig. 5B**) that adequately described absorption kinetics following single dose administration of a sustained release verapamil capsule (**Fig. 5C**) (Frishman and Lazar, 1992). Accumulation of verapamil following multiple dosing (i.e. 120mg on day 1, 240mg on day 2 and 360mg from day 3 to day 10) was also in line with clinical data (**Fig. 5D**) (Greenblatt *et al.*, 2018).

2 Retrospective Simulations of Enzyme- and Transporter-Mediated DDIs between Rivaroxaban and Verapamil/Ketoconazole

Although preliminary PK simulations verified the predictive potential of the basal compound model of rivaroxaban, given that the PBPK model of rivaroxaban is intended to be applied for the characterization of complex DDIs involving potential enzyme-transporter interplay, it becomes essential to further

Downloaded from dmd.aspetjournals.org at ASPET Journals on April 20, 2024

DMD Fast Forward. Published on September 10, 2019 as DOI: 10.1124/dmd.119.086918
This article has not been copyedited and formatted. The final version may differ from this version.

evaluate its predictive performance against observed DDIs with CYP3A4/2J2 and/or P-gp inhibitors (Shebley *et al.*, 2018).

DDDIs between Rivaroxaban and Verapamil were Successfully Modeled. The capability of verapamil and its major metabolite norverapamil to elicit both mechanism-based inactivation (MBI) as well as reversible inhibition of CYP3A4 has been established previously (Orr *et al.*, 2012). Nevertheless, in our study, *in vitro* inhibitory parameters (i.e. k_{inact}: the theoretical maximum inactivation rate constant at infinite inactivator concentration; K_I: the inactivator concentration yielding an inactivation rate at half of k_{inact} and K_i: the equilibrium dissociation constant for the enzyme inhibitor complex) were quantified using rivaroxaban as probe substrate.

Collectively, *in vitro* inhibition studies affirmed the MBI (**Supplemental Fig. 5A-D**) and reversible inhibition (**Supplemental Fig. 6A-D**) of CYP3A4-mediated metabolism of rivaroxaban by verapamil and norverapamil. A summary of the *in vitro* inhibition parameters derived is presented in **Table 5**. Conversely, our preliminary studies suggest the absence of MBI of CYP2J2 by verapamil and norverapamil (**Supplemental Fig. 5E** and **5F**). Similarly, reversible inhibition by verapamil and norverapamil against CYP2J2 yielded large K_i values of 12.2 and 161.8 µM respectively (**Supplemental Fig. 6E-H**). R_1 ratios (**Table 5**) were both less than the threshold of 1.02 recommended by FDA, hence eliminating the need for further assessment of DDI potential.

Notably, despite a previous *in vitro* study demonstrating an inhibitory effect of verapamil against the P-gp-mediated efflux of rivaroxaban (**Table 5**) (Gnoth *et al.*, 2011), *in vivo* data revealed that the amount of rivaroxaban excreted unchanged in urine was elevated in the presence of verapamil (Greenblatt *et al.*, 2018). This *in vitro in vivo* disconnect alluded to the negligible role of transporters in perpetrating the eventual DDI between rivaroxaban and verapamil. Subsequent assimilation of derived CYP3A4 inhibitory parameters into the PBPK-DDI model accurately recapitulated the observed DDI magnitude (**Fig. 6A**) and the increase in CL_R (**Fig. 6B**). Simulated geometric mean (90% CI) AUC and CL ratios of 1.46 (1.33, 1.61) and 0.68 (0.62, 0.75) were within the range of acceptable performance calculated based on the clinically observed AUC and CL-fold changes of rivaroxaban in the presence

Downloaded from dmd.aspetjournals.org at ASPET Journals on April 20, 2024

DMD Fast Forward. Published on September 10, 2019 as DOI: 10.1124/dmd.119.086918
This article has not been copyedited and formatted. The final version may differ from this version.

of verapamil (**Table 6, Modelling Supplemental Data File 2**). In patients with underlying mild renal impairment, verapamil co-administration resulted in simulated geometric mean AUC and CL-fold changes of 1.70 and 0.59 respectively, meeting success criteria defined in **Table 6**, hence attesting to the ability of the PBPK-DDI model to accurately recapitulate an enzymatic DDDI scenario (**Fig. 6C**).

Extent of DDIs between Rivaroxaban and Ketoconazole was Underestimated Despite Consideration of CYP3A4, CYP2J2 and P-gp Inhibition. *In vitro* investigations verified the inhibition of CYP3A4, CYP2J2-mediated metabolism as well as P-gp-mediated efflux of rivaroxaban with co-administration of ketoconazole (**Supplemental Fig. 7A-F**). Simulated fold reduction in CL_H met the success criteria delineated in **Table 6**, reliably supporting conclusions that the extent of enzyme-mediated DDI was accurately reproduced. Nevertheless, as illustrated in **Fig. 6D**, the modeled plasma concentration-time profile in the presence of ketoconazole evidently demonstrated an underestimation of DDI magnitude (blue solid line). Moreover, PK parameters (AUC, C_{max} and CL_R) fell outside the prespecified acceptance criteria (**Table 6**), suggesting that the nature and potency of transporter-mediated interactions between rivaroxaban and ketoconazole have not been adequately elucidated. Results of a subsequent sensitivity analysis (**Supplemental Fig. 8A**) corroborated this postulation and demonstrated that sole inhibition of P-gp-mediated efflux is unlikely to substantially affect rivaroxaban's systemic exposure. In contrast, AUC-fold change was highly sensitive to inhibition of OAT3-mediated basolateral uptake. *In vitro* inhibition experiments further established inhibition of OAT3-mediated uptake by ketoconazole (IC_{50} = 15.77 μM) (**Supplemental Fig. 7G**). Nevertheless, direct incorporation of the measured *in vitro* K_i was unable to recapitulate the clinically observed DDI magnitude (data not shown) and further optimization of the K_i value of ketoconazole to 0.01 μM was eventually required (blue dashed line in **Fig. 6D, Table 6, Modelling Supplemental Data File 3**).

Downloaded from dmd.aspetjournals.org at ASPET Journals on April 20, 2024

DMD Fast Forward. Published on September 10, 2019 as DOI: 10.1124/dmd.119.086918
This article has not been copyedited and formatted. The final version may differ from this version.

DISCUSSION

In the US, 30–50% of adverse drug reactions are due to dosing errors (Neely, 2017), largely implicating vulnerable populations that incidentally constitute the exclusion criteria of pivotal clinical trials (Darwich *et al.*, 2017). PBPK modeling has proven to be a panacea for the perennial challenge of suboptimal therapeutic outcomes in such complex and untested, albeit clinically relevant scenarios. Its unique ability to quantitatively integrate the multitude of drug- and system-dependent parameters, that can influence an individual's dose response, has guided refined dosing in multiple clinical applications, particularly involving DDIs and special populations (Sager *et al.*, 2015; Jamei, 2016).

Using PBPK modeling, Grillo *et al.* predicted clinically significant increases in rivaroxaban exposure due to renal impairment and moderate CYP3A4/P-gp inhibition by erythromycin (Grillo *et al.*, 2012). The findings informed current product labeling where concomitant use of rivaroxaban with a combined weak to moderate inhibitor of CYP3A4 and an inhibitor of P-gp and/or BCRP should be avoided under any degree of renal impairment. Given that such cautionary language hampers the utility of relevant drug combinations in AF management, Ismail *et al.* proposed dosing modifications in renal impairment and concomitant verapamil administration via correlating PBPK-predicted increases in rivaroxaban exposure with bleeding risk outcomes (Ismail *et al.*, 2018). Lastly, Xu *et al.* interrogated the exacerbation of rivaroxaban DDIs by hepatic dysfunction (Xu *et al.*, 2018).

Prior to application, a PBPK model must be qualified as fit for purpose (Shebley *et al.*, 2018) (**Fig. 1**). The four principal aspects essential for robust model qualification are namely, (1) evaluating model relevance to research context; (2) assessing sources of uncertainty and implications; (3) capturing known variabilities in clinical outcomes; and (4) ensuring that model results are qualitatively and quantitatively consistent with test data (Friedrich, 2016). Fulfilling the third and fourth criteria, the abovementioned and our developed models demonstrated qualitative and quantitative reproduction of rivaroxaban's essential clinical PK characteristics, such as rapid and near complete oral absorption, dose proportional increases in rivaroxaban exposure under fed conditions (**Fig. 2B** and **2C**), lack of

Downloaded from dmd.aspetjournals.org at ASPET Journals on April 20, 2024

DMD Fast Forward. Published on September 10, 2019 as DOI: 10.1124/dmd.119.086918
This article has not been copyedited and formatted. The final version may differ from this version.

accumulation upon multiple dosing (Kubitza, Becka, Voith, *et al.*, 2005; Kubitza, Becka, Wensing, *et al.*, 2005; Zhao *et al.*, 2009), and true representation of interindividual variability (Jamei *et al.*, 2009); (US FDA, 2011a). Nevertheless, the intended application of the PBPK model of rivaroxaban to the interrogation of DDIs importantly entails that the first and second criteria are also adequately satisfied. Ensuring that the model scope is sufficiently mechanistic in delineating **1)** the renal disposition of rivaroxaban and **2)** inhibition of the metabolic/transport pathways of rivaroxaban elimination, is required to facilitate rigorous identification and assessment of biological uncertainties that may result in incongruities between predictions and actual outcomes.

Our PBPK model is novel and mechanistically detailed in parameterizing the renal disposition of rivaroxaban. Previously, its CL_R was defined as a function of glomerular filtration and net secretion (calculated as the difference between absolute secretion and absolute reabsorption) (Grillo *et al.*, 2012; Ismail *et al.*, 2018; Xu *et al.*, 2018). Conflating these distinct processes precludes mechanistic characterization of their differential contributions to CL_R of rivaroxaban. Additionally, by ascribing renal elimination of rivaroxaban to the apparent plasma compartment (i.e. minimal PBPK model), both Grillo *et al.* and Ismail *et al.* were unable to predict urinary excretion data for direct assessment of model-predicted CL_R. The significance of such mechanistic detail is further underscored with *in vitro* evidence demonstrating how consideration of P-gp-mediated efflux and passive permeability produced adequate fits for high permeability compounds (e.g. amprenavir and quinidine) but not for low permeability substrates (e.g. loperamide and digoxin) (Acharya *et al.*, 2008). For loperamide and digoxin, observed efflux kinetics were substantially greater than could be fitted by passive permeability alone and improvement in fitting outcomes was contingent on the addition of a basolateral uptake transporter (Acharya *et al.*, 2008). Consistently, evaluating the extent of passive permeability becomes diagnostic for the kinetic necessity of basolateral uptake (Lumen *et al.*, 2013; Huang and Isoherranen, 2018). In this study, incorporating passive permeability (P_{pass} = 12.88 × 10^{-6} cm/s, **Table 3**) estimates from three-compartment modeling yielded a CL_{PD} of 1.09 × 10^{-5} μL/min/10^6 cells when scaled using tubular surface area. When considered in tandem with P-gp efflux kinetics (**Table 3**), the clinically observed CL_R of rivaroxaban remained underestimated by our simulation (**Fig. 4A**). Nevertheless,

Downloaded from dmd.aspetjournals.org at ASPET Journals on April 20, 2024

DMD Fast Forward. Published on September 10, 2019 as DOI: 10.1124/dmd.119.086918
This article has not been copyedited and formatted. The final version may differ from this version.

without independent verification of specific model assumptions governing passive diffusion clearance in the kidneys, it is inevitable that certainty in the quantitative contribution of active transport to renal clearance remains low and interdependent on the error in predicted diffusion clearance (Huang and Isoherranen, 2018). Hence, using a 35-compartment mechanistic kidney model developed by Huang and Isoherranen, where *in vitro* to *in vivo* predictions of renal clearance using plasma unbound fraction and permeability data have been systematically verified for a set of 46 compounds (Huang and Isoherranen, 2018), we demonstrate that renal clearance predicted via MechKiM in the Simcyp simulator was within twofold of that simulated using the 35-compartment model when a P_{pass} of 12.88 $\times 10^{-6}$ cm/s was incorporated (**Supplemental Table 8**), verifying the passive diffusion component of the mechanistic kidney model constructed for rivaroxaban in this study.

With a verified passive diffusion process, the inability to recapitulate the CL_R of rivaroxaban can be thus be confidently attributed to the presence of knowledge gaps in transporter-mediated clearance that imposes constraints on the exclusive utilization of bottom-up approaches. In such scenarios, the utility of a middle-out approach has received increasing recognition (Rostami-Hodjegan, 2018). Using reverse translational modeling, clinical data of rivaroxaban obtained with co-administration of ketoconazole revealed surprising fold reductions in Vd/F (0.53) in addition to CL/F (0.39), such that half-life was minimally affected (US FDA, 2011a). Coupled with experimental demonstration of rivaroxaban uptake in human OAT3 expressing cells, the convergence of evidences reinforces the plausibility of our postulated renal basolateral uptake process. Sensitivity analyses in this study further underscored the relative insensitivity of observed CL_R to P-gp REF (**Supplemental Fig. 8B**) and confirmed that sole inhibition of P-gp-mediated efflux is unlikely to produce significant increases in rivaroxaban's systemic exposure (**Fig. 6D**, **Supplemental Fig. 8A**). Hence, it becomes apparent that reliable quantitative extrapolation of *in vitro* derived OAT3-mediated J_{max} and K_m is essential to accurately define the renal excretion of rivaroxaban. With the emergence of quantitative transporter abundance data in kidney samples (reported OAT3 abundance of 3.5 ± 1.6 pmol/mg of total membrane protein) (Prasad *et al.*, 2016), IVIVE scaling factors can be accurately determined, removing the need for top down

Downloaded from dmd.aspetjournals.org at ASPET Journals on April 20, 2024

DMD Fast Forward. Published on September 10, 2019 as DOI: 10.1124/dmd.119.086918
This article has not been copyedited and formatted. The final version may differ from this version.

optimization (**Supplemental Fig. 4**) where estimates of OAT3 CLu_{int} may be biased based on the mean CL_R and serum creatinine parameters defined.

Acknowledging the pivotal role of basolateral uptake in mediating the renal disposition of rivaroxaban enables informed analysis of the likelihood of observing transporter-mediated DDIs with rivaroxaban. A case in point would be verapamil, a known P-gp inhibitor that demonstrated *in vitro* inhibition of rivaroxaban's efflux in L-MDR1 cells (Gnoth *et al.*, 2011; US FDA, 2017). However, concomitant verapamil administration did not result in significant decrease in rivaroxaban's renal clearance, as highlighted in a DDI study by Greenblatt *et al* (Greenblatt *et al.*, 2018). This observation is substantiated by verapamil having a high mOAT3 K_i value of 31 µM (Ahn *et al.*, 2009). Consistently, our *in vitro* experiments also demonstrated negligible inhibition of OAT3-mediated uptake of rivaroxaban by verapamil up to 100 µM (**Supplemental Fig. 7H**). Furthermore, examining the drugs that have been shown to produce significant transporter-mediated DDIs with rivaroxaban (i.e. ketoconazole and ritonavir) (Mueck *et al.*, 2013) revealed *in vitro* evidence of OAT3 inhibition. Both ketoconazole and ritonavir inhibit estrone sulfate transport in transfected HEK-OAT3 cell lines (IC_{50} = 0.86 and 8.1 µM for ketoconazole and ritonavir respectively) (Vermeer *et al.*, 2016; Shebley *et al.*, 2017). When rivaroxaban was used as the probe substrate in this study, uptake inhibition by ketoconazole was also observed (**Supplemental Fig. 7G**). Nevertheless, further optimization of the K_i value of ketoconazole was required to recapitulate the clinically observed DDI magnitude (**Fig. 6D, Table 6**). Our observed underprediction in transporter K_i remains aligned with previous attempts to recapitulate transporter-mediated DDIs for solute carriers (Hsu et al., 2014; Burt et al., 2016). Such incongruity may reflect the incorrect assumption of a competitive mode of inhibition. Additionally, although the assumed concentration for inhibition (that added to the incubation media) should be largely consistent with that at the transporter binding site, the lipophilic nature of ketoconazole could have resulted in non-specific binding processes both *in vitro* and *in vivo*, further confounding interpretation of the inhibition data. Given that drugs that are likely to be co-administered with rivaroxaban have been reported to be P-gp inhibitors with unknown effects on OAT3-mediated uptake (e.g. amiodarone), elucidating the dynamic

Downloaded from dmd.aspetjournals.org at ASPET Journals on April 20, 2024

DMD Fast Forward. Published on September 10, 2019 as DOI: 10.1124/dmd.119.086918
This article has not been copyedited and formatted. The final version may differ from this version.

interplay between apical P-gp efflux and basolateral OAT3 uptake using alternative approaches such as double-transfected cell lines with rivaroxaban as probe substrate becomes imperative.

Our second novelty lies in our adoption of rivaroxaban as the probe substrate when quantifying inhibition of metabolic and/or transport processes by verapamil and ketoconazole. In the previous PBPK-DDI model developed by Grillo *et al.*, a K_i value of 11 μM derived from an *in vitro* study using digoxin as substrate was utilized to describe the inhibitory potential of erythromycin on the P-gp-mediated efflux of rivaroxaban (Grillo *et al.*, 2012). However, Gnoth *et al.* reported that the directed efflux of rivaroxaban across P-gp-overexpressing L-MDR1 cells was unaffected by erythromycin (Gnoth *et al.*, 2011). A clinical DDI study by Moore *et al.* further demonstrated negligible inhibition of the active renal secretion of rivaroxaban by erythromycin (Moore *et al.*, 2014), underscoring how the nature and potency of DDIs are often unique to each substrate-inhibitor pair. This probe substrate specificity was similarly reflected in our *in vitro* experiments. For instance, verapamil has been reported to exhibit reversible inhibition against CYP2J2 when index substrates were used (Lee et al., 2012; Ren et al., 2013), but yielded minimal inhibition against CYP2J2-mediated metabolism of rivaroxaban (**Supplemental Fig. 6 E-H** and **Table 5**). Additionally, the *in vitro* MBI potencies of verapamil and norverapamil against CYP3A4 using index substrates were less potent (k_{inact}/K_I ratios of 0.9 and 1.74 $h^{-1}\mu M^{-1}$ respectively) than our experimentally derived parameters when rivaroxaban was used as the probe substrate (k_{inact}/K_I ratio of 2.37 and 8.59 $h^{-1}\mu M^{-1}$ respectively) (**Supplemental Table 7**). Finally, the *in vitro* reversible inhibition potency of ketoconazole against CYP3A4 using index substrate was more potent (K_i of 0.015 μM) than our experimentally measured potency using rivaroxaban as substrate (K_i of 0.094 μM) (**Supplemental Table 7**). Hence, it is evident that accurate recapitulation of enzyme-mediated and transporter-mediated DDIs involving rivaroxaban is contingent on generating reliable *in vitro* inhibitory estimates for parameterization of the PBPK-DDI model.

The future intended application of the current PBPK model of rivaroxaban is in extrapolation to untested scenarios implicating both enzyme- and transporter-mediated DDDIs. Assuming the INH and investigating the effect of mild renal impairment alone, our simulated AUC and CL_R fold changes of

Downloaded from dmd.aspetjournals.org at ASPET Journals on April 20, 2024

DMD Fast Forward. Published on September 10, 2019 as DOI: 10.1124/dmd.119.086918
This article has not been copyedited and formatted. The final version may differ from this version.

rivaroxaban fell within predefined success criteria (**Table 4, Fig, 4C**). Additionally, as presented in **Supplemental Fig. 8C**, alterations in either PTCPGK or transporter abundance (**Supplemental Table 9**), two independent pathophysiological mechanisms that have been proposed to account for the reduction in tubular secretion (Naud *et al.*, 2011; Hsu *et al.*, 2014), yielded comparable effects on the renal clearance of rivaroxaban. Hence, it is conceptually reasonable to predict transporter-mediated DDDIs in mild-moderate CKD by empirically applying a scaling factor to account for the linear reduction in tubular secretion in accordance with GFR (either via PTCPGK or adjustment of transporter abundance) while accounting for inhibition against OAT3/P-gp-mediated transport. However, it is important to note that reductions of GFR and tubular secretion become disproportional in severe CKD, with the activity of OATs directly inhibited by uremic solutes at clinically relevant concentrations (Hsueh *et al.*, 2016, 2018), Although rivaroxaban is currently contraindicated in severe CKD (CrCL < 30 mL/min), the possibility of expanding rivaroxaban use to such patients has been raised (Dias *et al.*, 2016). Therefore, improved understanding of underlying mechanisms behind changes in tubular secretion in severe CKD is crucial.

In conclusion, the iteratively verified PBPK model of rivaroxaban is applicable to the investigation of enzyme and transporter-mediated DDDIs involving clinically relevant inhibitors and mild-moderate CKD, except in severe CKD where additional understanding of the effects of pathophysiology on transporter-mediated processes is required.

Downloaded from dmd.aspetjournals.org at ASPET Journals on April 20, 2024

DMD Fast Forward. Published on September 10, 2019 as DOI: 10.1124/dmd.119.086918
This article has not been copyedited and formatted. The final version may differ from this version.

AUTHORSHIP CONTRIBUTIONS

Participated in research design:	Cheong, Teo, Chua and Chan
Conducted experiments:	Cheong, Teo and Chua
Performed data analysis:	Cheong, Teo, Chua and Chan
Wrote or contributed to the writing of the manuscript:	Cheong, Teo, Chua and Chan

Downloaded from dmd.aspetjournals.org at ASPET Journals on April 20, 2024

DMD Fast Forward. Published on September 10, 2019 as DOI: 10.1124/dmd.119.086918
This article has not been copyedited and formatted. The final version may differ from this version.

REFERENCES

Abduljalil K, Cain T, Humphries H, and Rostami-Hodjegan A (2014) Deciding on success criteria for predictability of pharmacokinetic parameters from in vitro studies: An analysis based on in vivo observations. *Drug Metab Dispos* **42**:1478–1484.

Acharya P, O'Connor MP, Polli JW, Ayrton A, Ellens H, and Bentz J (2008) Kinetic Identification of Membrane Transporters That Assist P-glycoprotein-Mediated Transport of Digoxin and Loperamide through a Confluent Monolayer of MDCKII-hMDR1 Cells. *Drug Metab Dispos* **36**:452–460.

Ahn S-Y, Eraly SA, Tsigelny I, and Nigam SK (2009) Interaction of organic cations with organic anion transporters. *J Biol Chem* **284**:31422–30, American Society for Biochemistry and Molecular Biology.

Bricker NS (1969) On the meaning of the intact nephron hypothesis. *Am J Med* **46**:1–11.

Chugh SS, Havmoeller R, Narayanan K, Singh D, Rienstra M, Benjamin EJ, Gillum RF, Kim YH, McAnulty JH, Zheng ZJ, Forouzanfar MH, Naghavi M, Mensah GA, Ezzati M, and Murray CJL (2014) Worldwide epidemiology of atrial fibrillation: A global burden of disease 2010 study. *Circulation* **129**:837–847.

Darwich AS, Ogungbenro K, Vinks AA, Powell JR, Reny JL, Marsousi N, Daali Y, Fairman D, Cook J, Lesko LJ, McCune JS, Knibbe CAJ, de Wildt SN, Leeder JS, Neely M, Zuppa AF, Vicini P, Aarons L, Johnson TN, Boiani J, and Rostami-Hodjegan A (2017) Why has model-informed precision dosing not yet become common clinical reality? lessons from the past and a roadmap for the future. *Clin Pharmacol Ther* **101**:646–656.

Dias C, Moore KT, Murphy J, Ariyawansa J, Smith W, Mills RM, and Weir MR (2016) Pharmacokinetics, Pharmacodynamics, and Safety of Single-Dose Rivaroxaban in Chronic Hemodialysis. *Am J Nephrol* **43**:229–236.

Emami Riedmaier A, Burt H, Abduljalil K, and Neuhoff S (2016) More Power to OATP1B1: An Evaluation of Sample Size in Pharmacogenetic Studies Using a Rosuvastatin PBPK Model for Intestinal, Hepatic, and Renal Transporter-Mediated Clearances. *J Clin Pharmacol* S132–S142.

Friedrich CM (2016) A model qualification method for mechanistic physiological QSP models to support model-informed drug development. *CPT Pharmacometrics Syst Pharmacol* **5**:43–53.

Frishman WH, and Lazar EJ (1992) Sustained-release verapamil formulations for treating hypertension. *J Clin Pharmacol* **32**:455–62.

Downloaded from dmd.aspetjournals.org at ASPET Journals on April 20, 2024

DMD Fast Forward. Published on September 10, 2019 as DOI: 10.1124/dmd.119.086918
This article has not been copyedited and formatted. The final version may differ from this version.

Glomme A, März J, and Dressman JB (2007) Predicting the Intestinal Solubility of Poorly Soluble Drugs. *Pharmacokinet Profiling Drug Res* 259–280.

Gnoth MJ, Buetehorn U, Muenster U, Schwarz T, and Sandmann S (2011) In vitro and in vivo P-glycoprotein transport characteristics of rivaroxaban. *J Pharmacol Exp Ther* **338**:372–380.

Greenblatt DJ, Patel M, Harmatz JS, Nicholson WT, Rubino CM, and Chow CR (2018) Impaired Rivaroxaban Clearance in Mild Renal Insufficiency With Verapamil Coadministration: Potential Implications for Bleeding Risk and Dose Selection. *J Clin Pharmacol* **58**:533–540.

Grillo JA, Zhao P, Bullock J, Booth BP, Lu M, Robie-Suh K, Berglund EG, Pang KS, Rahman A, Zhang L, Lesko LJ, and Huang S-M (2012) Utility of a physiologically-based pharmacokinetic (PBPK) modeling approach to quantitatively predict a complex drug-drug-disease interaction scenario for rivaroxaban during the drug review process: implications for clinical practice. *Biopharm Drug Dispos* **33**:99–110.

Guest EJ, Aarons L, Houston JB, Rostami-Hodjegan A, and Galetin A (2011) Critique of the two-fold measure of prediction success for ratios: application for the assessment of drug-drug interactions. *Drug Metab Dispos* **39**:170–3.

Haeri A, Javadian B, Saadati R, and Dadashzadeh S (2014) Metabolite parameters as an appropriate alternative approach for assessment of bioequivalence of two verapamil formulations. *Iran J Pharm Res IJPR* **13**:383–9, Shahid Beheshti University of Medical Sciences.

Hsu V, Vieira MDLT, Zhao P, Zhang L, Zheng JH, Nordmark A, Berglund EG, Giacomini KM, and Huang SM (2014) Towards quantitation of the effects of renal impairment and probenecid inhibition on kidney uptake and efflux transporters, using physiologically based pharmacokinetic modelling and simulations. *Clin Pharmacokinet* **53**:283–293.

Hsueh C-H, Yoshida K, Zhao P, Meyer TW, Zhang L, Huang S-M, and Giacomini KM (2016) Identification and Quantitative Assessment of Uremic Solutes as Inhibitors of Renal Organic Anion Transporters, OAT1 and OAT3. *Mol Pharm* **13**:3130–3140, American Chemical Society.

Hsueh CH, Hsu V, Zhao P, Zhang L, Giacomini KM, and Huang SM (2018) PBPK Modeling of the Effect of Reduced Kidney Function on the Pharmacokinetics of Drugs Excreted Renally by Organic Anion Transporters. *Clin Pharmacol Ther* **103**:485–492.

Huang W, and Isoherranen N (2018) Development of a Dynamic Physiologically Based Mechanistic Kidney Model to Predict Renal Clearance. *CPT Pharmacometrics Syst Pharmacol* **7**:593–602.

Ismail M, Lee VH, Chow CR, and Rubino CM (2018) Minimal Physiologically Based Pharmacokinetic

Downloaded from dmd.aspetjournals.org at ASPET Journals on April 20, 2024

DMD Fast Forward. Published on September 10, 2019 as DOI: 10.1124/dmd.119.086918
This article has not been copyedited and formatted. The final version may differ from this version.

and Drug-Drug-Disease Interaction Model of Rivaroxaban and Verapamil in Healthy and Renally Impaired Subjects. *J Clin Pharmacol* **58**:541–548.

Jamei M (2016) Recent Advances in Development and Application of Physiologically-Based Pharmacokinetic (PBPK) Models: a Transition from Academic Curiosity to Regulatory Acceptance, Current Pharmacology Reports.

Jamei M, Dickinson GL, and Rostami-Hodjegan A (2009) A framework for assessing inter-individual variability in pharmacokinetics using virtual human populations and integrating general knowledge of physical chemistry, biology, anatomy, physiology and genetics: A tale of "bottom-up" vs "top-down" recognition of covariates. *Drug Metab Pharmacokinet* **24**:53–75.

January CT, Wann LS, Alpert JS, Calkins H, Cigarroa JE, Conti JB, Ellinor PT, Ezekowitz MD, Field ME, Murray KT, Sacco RL, Stevenson WG, Tchou PJ, Tracy CM, Yancy CW, Members F, Anderson JL, Halperin JL, Albert NM, Bozkurt B, Brindis RG, Creager MA, Curtis LH, Demets D, Guyton RA, Hochman JS, Kovacs RJ, Ohman EM, Pressler SJ, Sellke FW, Shen W-K, Stevenson WG, and Yancy CW (2014) 2014 AHA/ACC/HRS Guideline for the Management of Patients With Atrial Fibrillation. *J Am Coll Cardiol* **63**:e1–e76.

Kubitza D, Becka M, Voith B, Zuehlsdorf M, and Wensing G (2005) Safety, pharmacodynamics, and pharmacokinetics of single doses of BAY 59-7939, an oral, direct factor Xa inhibitor. *Clin Pharmacol Ther* **78**:412–421.

Kubitza D, Becka M, Wensing G, Voith B, and Zuehlsdorf M (2005) Safety, pharmacodynamics, and pharmacokinetics of BAY 59-7939 - An oral, direct Factor Xa inhibitor - After multiple dosing in healthy male subjects. *Eur J Clin Pharmacol* **61**:873–880.

Lumen AA, Li L, Li J, Ahmed Z, Meng Z, Owen A, Ellens H, Hidalgo IJ, and Bentz J (2013) Transport Inhibition of Digoxin Using Several Common P-gp Expressing Cell Lines Is Not Necessarily Reporting Only on Inhibitor Binding to P-gp. *PLoS One* **8**:e69394.

Menochet K, Kenworthy KE, Houston JB, and Galetin A (2012) Simultaneous Assessment of Uptake and Metabolism in Rat Hepatocytes: A Comprehensive Mechanistic Model. *J Pharmacol Exp Ther* **341**:2–15.

Moore KT, Vaidyanathan S, Natarajan J, Ariyawansa J, Haskell L, and Turner KC (2014) An open-label study to estimate the effect of steady-state erythromycin on the pharmacokinetics, pharmacodynamics, and safety of a single dose of rivaroxaban in subjects with renal impairment and normal renal function. *J Clin Pharmacol* **54**:1407–1420.

Mueck W, Kubitza D, and Becka M (2013) Co-administration of rivaroxaban with drugs that share its

Downloaded from dmd.aspetjournals.org at ASPET Journals on April 20, 2024

DMD Fast Forward. Published on September 10, 2019 as DOI: 10.1124/dmd.119.086918
This article has not been copyedited and formatted. The final version may differ from this version.

elimination pathways: pharmacokinetic effects in healthy subjects. *Br J Clin Pharmacol* **76**:455–466.

Mueck W, Stampfuss J, Kubitza D, and Becka M (2014) Clinical pharmacokinetic and pharmacodynamic profile of rivaroxaban. *Clin Pharmacokinet* **53**:1–16.

Naud J, Michaud J, and Beauchemin S (2011) Effects of chronic renal failure on kidney drug transporters and cytochrome P450 in rats. *Drug Metab Dispos* **39**:1363–1369.

Neely M (2017) Scalpels not hammers: The way forward for precision drug prescription. *Clin Pharmacol Ther* **101**:368–372.

Orr STM, Ripp SL, Ballard TE, Henderson JL, Scott DO, Obach RS, Sun H, and Kalgutkar AS (2012) Mechanism-based inactivation (MBI) of cytochrome P450 enzymes: Structure-activity relationships and discovery strategies to mitigate drug-drug interaction risks. *J Med Chem* **55**:4896–4933.

Prasad B, Johnson K, Billington S, Lee C, Chung GW, Brown CDA, Kelly EJ, Himmelfarb J, and Unadkat JD (2016) Abundance of Drug Transporters in the Human Kidney Cortex as Quantified by Quantitative Targeted Proteomics. *Drug Metab Dispos* **44**:1920–1924.

Rodgers T, and Rowland M (2006) Physiologically based pharmacokinetic modelling 2: Predicting the tissue distribution of acids, very weak bases, neutrals and zwitterions. *J Pharm Sci* **95**:1238–1257.

Rostami-Hodjegan A (2018) Reverse Translation in PBPK and QSP: Going Backwards in Order to Go Forward With Confidence. *Clin Pharmacol Ther* **103**:224–232.

Sager JE, Yu J, Ragueneau-Majlessi I, and Isoherranen N (2015) Physiologically Based Pharmacokinetic (PBPK) Modeling and Simulation Approaches: A Systematic Review of Published Models, Applications, and Model Verification. *Drug Metab Dispos* **43**:1823–37.

Scaglione F (2013) New Oral Anticoagulants: Comparative Pharmacology with Vitamin K Antagonists. *Clin Pharmacokinet* **52**:69–82.

Scotcher D, Jones CR, Galetin A, and Rostami-Hodjegan A (2017) Delineating the Role of Various Factors in Renal Disposition of Digoxin through Application of Physiologically Based Kidney Model to Renal Impairment Populations. *J Pharmacol Exp Ther* **360**:484–495.

Shebley M, Fu W, Badri P, Bow D, and Fischer V (2017) Physiologically Based Pharmacokinetic Modeling Suggests Limited Drug-Drug Interaction Between Clopidogrel and Dasabuvir. *Clin Pharmacol Ther* **102**:679–687.

Downloaded from dmd.aspetjournals.org at ASPET Journals on April 20, 2024

DMD Fast Forward. Published on September 10, 2019 as DOI: 10.1124/dmd.119.086918
This article has not been copyedited and formatted. The final version may differ from this version.

Shebley M, Sandhu P, Emami Riedmaier A, Jamei M, Narayanan R, Patel A, Peters SA, Reddy VP, Zheng M, de Zwart L, Beneton M, Bouzom F, Chen J, Chen Y, Cleary Y, Collins C, Dickinson GL, Djebli N, Einolf HJ, Gardner I, Huth F, Kazmi F, Khalil F, Lin J, Odinecs A, Patel C, Rong H, Schuck E, Sharma P, Wu SP, Xu Y, Yamazaki S, Yoshida K, and Rowland M (2018) Physiologically Based Pharmacokinetic Model Qualification and Reporting Procedures for Regulatory Submissions: A Consortium Perspective. *Clin Pharmacol Ther*, doi: 10.1002/cpt.1013.

Stampfuss J, Kubitza D, Becka M, and Mueck W (2013) The effect of food on the absorption and pharmacokinetics of rivaroxaban. *Int J Clin Pharmacol Ther* **51**:549–561.

Takács-Novák K, Szoke V, Völgyi G, Horváth P, Ambrus R, and Szabó-Révész P (2013) Biorelevant solubility of poorly soluble drugs: Rivaroxaban, furosemide, papaverine and niflumic acid. *J Pharm Biomed Anal* **83**:279–285.

Tsuruya Y, Nakanishi T, Komori H, Wang X, Ishiguro N, Kito T, Ikukawa K, Kishimoto W, Ito S, Schaefer O, Ebner T, Yamamura N, Kusuhara H, and Tamai I (2017) Different Involvement of OAT in Renal Disposition of Oral Anticoagulants Rivaroxaban, Dabigatran, and Apixaban. *J Pharm Sci* **106**:2524–2534.

US FDA (2017) Drug Development and Drug Interactions : Table of Substrates , Inhibitors and Inducers, Center for Drug Evaluation and Research.

US FDA (2011a) XARELTO (rivaroxaban). Clinical Pharmacology and Biopharmaceutics Review.

US FDA (2011b) XARELTO (rivaroxaban) product information.

Vermeer LMM, Isringhausen CD, Ogilvie BW, and Buckley DB (2016) Evaluation of Ketoconazole and Its Alternative Clinical CYP3A4/5 Inhibitors as Inhibitors of Drug Transporters: The In Vitro Effects of Ketoconazole, Ritonavir, Clarithromycin, and Itraconazole on 13 Clinically-Relevant Drug Transporters. *Drug Metab Dispos* **44**:453–459.

Wang J, and Flanagan DR (1999) General solution for diffusion- controlled dissolution of spherical particles. 1. Theory. *J Pharm Sci* **88**:731–738.

Wessler JD, Grip LT, Mendell J, and Giugliano RP (2013) The P-glycoprotein transport system and cardiovascular drugs.

Wise DL (2000) *Handbook of Pharmaceutical Controlled Release Technology*, CRC Press.

Xu R, Ge W, and Jiang Q (2018) Application of physiologically based pharmacokinetic modeling to the prediction of drug-drug and drug-disease interactions for rivaroxaban. *Eur J Clin Pharmacol* **74**:755–765, European Journal of Clinical Pharmacology.

Downloaded from dmd.aspetjournals.org at ASPET Journals on April 20, 2024

DMD Fast Forward. Published on September 10, 2019 as DOI: 10.1124/dmd.119.086918
This article has not been copyedited and formatted. The final version may differ from this version.

Zhao X, Sun P, Zhou Y, Liu Y, Zhang Huilin, Mueck W, Kubitza D, Bauer RJ, Zhang Hong, and Cui Y (2009) Safety, pharmacokinetics and pharmacodynamics of single/multiple doses of the oral, direct Factor Xa inhibitor rivaroxaban in healthy Chinese subjects. *Br J Clin Pharmacol* **68**:77–88.

Downloaded from dmd.aspetjournals.org at ASPET Journals on April 20, 2024

DMD Fast Forward. Published on September 10, 2019 as DOI: 10.1124/dmd.119.086918
This article has not been copyedited and formatted. The final version may differ from this version.

FOOTNOTES

This work was supported by the Singapore Ministry of Education Tier 1 Academic Research Funding to E.C.Y.C. [Grant R-148-000-193-112], the National University of Singapore (NUS) President's Graduate Fellowship (PGF) to E.J.Y.C. and the NUS, Department of Pharmacy, Final Year Project Funding to D.W.X.T. and D.X.Y.C. [Grant C-148-000-003-001]. The authors thank Dr. Kathleen Giacomini (University of California, San Francisco, CA) for the kind donation of the hOAT1-transfected and hOAT3-transfected HEK cell lines.

Downloaded from dmd.aspetjournals.org at ASPET Journals on April 20, 2024

DMD Fast Forward. Published on September 10, 2019 as DOI: 10.1124/dmd.119.086918
This article has not been copyedited and formatted. The final version may differ from this version.

LEGENDS FOR FIGURES

Figure 1. PBPK modeling framework detailing the iterative processes of model development and verification that were performed in this study. Successful model verification must precede application of the PBPK model of rivaroxaban for prospective predictions of drug-drug-disease interactions.

Figure 2. Simulated pharmacokinetic profiles of rivaroxaban after single dose administration. Simulated mean (solid line) plasma drug concentration-time profiles of single dose rivaroxaban demonstrated (**A**) the effect of food in increasing bioavailability at the 20 mg dose and accurately recapitulated clinically observed profiles at (**B**) 10 mg and (**C**) 20 mg doses. Open symbols represent clinical data.

Figure 3. *In vitro* investigation of the P-gp-mediated and OAT3-mediated transport kinetics of rivaroxaban. For efflux kinetics, time-and concentration-dependent data in the absorptive direction was analyzed via mechanistic three-compartmental modeling. Goodness of fit between experimentally measured (symbols) and simulated (solid lines) basolateral rivaroxaban concentrations is presented in (**A**) and (**B**). For uptake kinetics, time-and concentration-dependent rivaroxaban uptake into OAT3-transfected HEK cells was analyzed via mechanistic two-compartmental modeling. Goodness of fit between experimentally measured (symbols) and simulated (solid lines) intracellular rivaroxaban concentrations is presented in (**C**) and (**D**).

Figure 4. Development of the mechanistic kidney model (MechKiM) for simulation of rivaroxaban PK in healthy and renal impaired patients. Simulated (**A**) cumulative urinary excretion of rivaroxaban and (**B**) its corresponding plasma concentration-time profile using MechKiM following a single 20 mg dose. Accounting for glomerular filtration (black solid line), glomerular filtration and reabsorption (grey dashed line), glomerular filtration, reabsorption and apical P-gp-mediated active efflux (blue dotted line) as well as glomerular filtration, reabsorption and basolateral OAT3-mediated uptake (red line) were unsuccessful in recapitulating observed clinical profiles (open circles). Recapitulation of observed

Downloaded from dmd.aspetjournals.org at ASPET Journals on April 20, 2024

DMD Fast Forward. Published on September 10, 2019 as DOI: 10.1124/dmd.119.086918
This article has not been copyedited and formatted. The final version may differ from this version.

clinical plasma rivaroxaban concentrations and urinary excretion data required the consideration of basolateral uptake in tandem with apical efflux (orange line). Upon verification of the drug-dependent parameters within the MechKiM model, adjustment of system parameters (glomerular filtration and proximal tubular cells per gram kidney) allowed accurate prediction of the increase in rivaroxaban's systemic exposure in (**C**) mild renal impairment. Open symbols represent clinical data.

Figure 5. Simulated pharmacokinetic profiles of verapamil and its major metabolite norverapamil. Simulated plasma concentration-time profiles of (**A**) 80 mg immediate release verapamil and norverapamil in healthy volunteers verified the basal PBPK model of verapamil provided within Simcyp. (**B**) IVIVC convolution using the reported *in vitro* dissolution profile of a controlled release capsule was unable to recapitulate clinically observed plasma concentration-time profiles following a single 120 mg dose. Iterative refinement of dissolution parameters yielded an *in vivo* dissolution profile (**B**) that adequately described absorption kinetics after (**C**) single and (**D**) multiple dosing based on the administration schedule delineated by Greenblatt *et al.* Open symbols represent clinical data while solid lines depict simulations.

Figure 6. Predicted drug-drug interactions (DDIs) between rivaroxaban and verapamil or ketoconazole in healthy and renal impaired patients. Simulated mean plasma concentration-time profiles of (**A**) 20 mg rivaroxaban in the absence and presence of CYP3A4 inhibitor verapamil demonstrated accurate estimation of DDI magnitude, including (**B**) an increase in the cumulative urinary excretion of rivaroxaban with verapamil co-administration. (**C**) Mild renal impairment potentiated the extent of DDI between rivaroxaban and verapamil. (**D**) Consideration of the inhibitory potential of ketoconazole on CYP3A4/2J2-mediated metabolism and P-gp-mediated efflux of rivaroxaban underestimated the observed DDI magnitude (blue solid line). Optimization of the K_i of ketoconazole against OAT3-mediated rivaroxaban uptake was required to accurately recapitulate the clinically observed DDI (blue dashed line). Open symbols represent clinical data.

Downloaded from dmd.aspetjournals.org at ASPET Journals on April 20, 2024

DMD Fast Forward. Published on September 10, 2019 as DOI: 10.1124/dmd.119.086918
This article has not been copyedited and formatted. The final version may differ from this version.

Table 1. Key input parameters for the PBPK model of rivaroxaban

Parameter	**Value**	**Method/Reference**
Molecular weight (g/mol)	435.88	CAS ID: 366789-02-8
log P	1.5	(Mueck *et al.*, 2014)
Compound type	Neutral	-
B/P	0.71	(Grillo *et al.*, 2012)
fu	0.065	(Grillo *et al.*, 2012)
Main plasma binding protein	Human serum albumin	-
Absorption Model	ADAM Model	
fu_{gut}	0.21	Predicted
$P_{eff,man}$ (10^{-4}cm/s)	3.020492	Predicted
Permeability Assay	Caco-2	(Gnoth *et al.*, 2011)
Apical pH : Basolateral pH	7.4 : 7.4	
Activity	Passive & Active	
$P_{appA:B}$(10^{-6} cm/s)	8	
Reference Compound	Multiple	
Reference Compound $P_{appaA:B}$ (10^{-6} cm/s)	0	
Scalar	1.284077	Predicted
Solubility pH Type	Intrinsic	
Solubility (mg/mL)	0.01	(Takács-Novák *et al.*, 2013)
Transporter	ABCB1 (P-gp/MDR1)	
J_{max} (pmol/min)	37.83	Determined experimentally
K_m (μM)	9.416	Determined experimentally
fu_{inc}	1	Predicted
Insert growth area of the Transwell (cm^2)	0.33	Determined experimentally
System	MDCK	Determined experimentally
RAF/REF	1.5	
Distribution Model	Full PBPK Model	

Downloaded from dmd.aspetjournals.org at ASPET Journals on April 20, 2024

DMD Fast Forward. Published on September 10, 2019 as DOI: 10.1124/dmd.119.086918
This article has not been copyedited and formatted. The final version may differ from this version.

V_{SS} (L/kg)	0.3824139	Predicted - Method 2
Enzyme	CYP3A4	Predicted in Simcyp using the Retrograde Calculator
Pathway	Pathway 1	
CL_{int} (µL/min/pmol)	0.06353705	
Enzyme	CYP2J2	Predicted in Simcyp using the Retrograde Calculator
Pathway	Pathway 1	
CL_{int} (µL/min/pmol)	5.685421	
CL_{int} (HLM) (µL/min/mg protein)	7.998799	Predicted in Simcyp using the Retrograde Calculator
Mechanistic Kidney Model		
$CL_{PD,basal}$ (mL/min/million proximal tubular cells)	1.09E-05	Determined experimentally
$CL_{PD,apical}$ (mL/min/million proximal tubular cells)	1.09E-05	Determined experimentally
$fu_{kidney,cell}$	0.3788975	Predicted in Simcyp
fu_{urine}	1	
Transporter	SLC22A8 (OAT3)	
Function	Uptake	
$CL_{int,T}$ (µL/min/million cells)	43	Scaled using sensitivity analysis
Transporter	ABCB1 (P-gp/MDR1)	
Function	Efflux	
J_{max} (pmol/min/million cells)	80.921	Determined experimentally
K_m (µM)	9.416	Determined experimentally
RAF/REF	4	

B/P, blood to plasma partition ratio; CL_{int}, *in vitro* intrinsic clearance; $CL_{int,T}$, *in vitro* transporter-mediated intrinsic clearance; CL_{PD}, passive diffusion clearance; CL_R, renal clearance; fm (liver), fractional metabolism in the liver; f_u, fraction unbound in plasma; fu_{gut}, fraction unbound in the enterocytes; fu_{inc}, fraction unbound in the *in vitro* incubation; $fu_{kidney,cell}$, fraction unbound in the kidney cell; fu_{inc}, fraction unbound in the urine; J_{max}, maximum rate of transporter mediated efflux or uptake; K_m, Michaelis constant; K_p, tissue to plasma partition

Downloaded from dmd.aspetjournals.org at ASPET Journals on April 20, 2024

DMD Fast Forward. Published on September 10, 2019 as DOI: 10.1124/dmd.119.086918
This article has not been copyedited and formatted. The final version may differ from this version.

coefficient; log P, common logarithm of the octanol:water partition coefficient; MDCK, Madin Darby Canine Kidney cell line; P_{eff}, Human jejunum effective permeability; RAF/REF, Relative activity/expression factor; V_{ss}, volume of distribution at steady state

Downloaded from dmd.aspetjournals.org at ASPET Journals on April 20, 2024

DMD Fast Forward. Published on September 10, 2019 as DOI: 10.1124/dmd.119.086918
This article has not been copyedited and formatted. The final version may differ from this version.

Table 2. Comparison of PK parameters between simulated and observed data for model verification of rivaroxaban in healthy subjects

	Simulated (n=220)		**Observed (n=22)**	
20 mg single dose, fasted (Stampfuss *et al.*, 2013)	**AUC (µg.h/L)**	**C_{max} (µg/L)**	**AUC (µg.h/L)**	**C_{max} (µg/L)**
Geometric mean	1512	111	1477	160
CV (%)	67	28	23	34
Ratio of simulated/observed	1.02	0.69		
Success criteria for ratio of simulated/observed	0.81-1.23	0.74-1.35		

	Simulated (n=220)		**Observed (n=22)**	
20 mg single dose, fed (Stampfuss *et al.*, 2013)	**AUC (µg.h/L)**	**C_{max} (µg/L)**	**AUC (µg.h/L)**	**C_{max} (µg/L)**
Geometric mean	2127	234	2048	281
CV (%)	31	28	23	27
Ratio of simulated/observed	1.04	0.83		
Success criteria for ratio of simulated/observed	0.81-1.23	0.79-1.27		

	Simulated (n=200)			**Observed (n=20)**		
10 mg single dose (Mueck *et al.*, 2013)	**AUC (µg.h/L)**	**C_{max} (µg/L)**	**CL (L/h)**	**AUC (µg.h/L)**	**C_{max} (µg/L)**	**CL (L/h)**
Geometric mean	1103	139	9.06	892	138	11.20
CV (%)	31	24	41	27	22	27
Ratio of simulated/observed	1.24	1.01	0.81			
Success criteria for ratio of simulated/observed	0.78-1.29	0.81-1.23	0.78 - 1.29			

Downloaded from dmd.aspetjournals.org at ASPET Journals on April 20, 2024

DMD Fast Forward. Published on September 10, 2019 as DOI: 10.1124/dmd.119.086918
This article has not been copyedited and formatted. The final version may differ from this version.

	Simulated (n=130)			**Observed (n=13)**		
20 mg single dose (Greenblatt *et al.*, 2018)	**AUC (µg.h/L)**	**C_{max} (µg/L)**	**CL (L/h)**	**AUC (µg.h/L)**	**C_{max} (µg/L)**	**CL (L/h)**
Geometric mean	2685	266	7.45	2583	263	7.92
CV (%)	40	29	49	21	26	23
Ratio of simulated/observed	1.04	1.01	0.94			
Success criteria for ratio of simulated/observed	0.78 - 1.29	0.74- 1.35	0.76 - 1.31			

AUC, area under the concentration-time curve from time zero to infinity; C_{max}, maximum plasma concentration; CV, coefficient of variation

Downloaded from dmd.aspetjournals.org at ASPET Journals on April 20, 2024

DMD Fast Forward. Published on September 10, 2019 as DOI: 10.1124/dmd.119.086918
This article has not been copyedited and formatted. The final version may differ from this version.

Table 3. J_{max} and K_m of P-gp-mediated efflux activity, and passive permeability (P_{pass}) of rivaroxaban in MDCK-MDR1 cell monolayers derived from three compartmental analysis

		Absorptive Transport	
	***In vitro* data** **(initial estimates)**	***Nelder-Mead***	***Hybrid***
J_{max} (pmol/min)	97.98 [a]	37.83 (24.3, 51.4)	41.63 (26.2, 57.1)
K_m (µM)	836.80 [a]	9.42 (7.0, 11.8)	12.36 (8.9, 15.8)
$P_{pass} \times 10^{-6}$(cm/s)	6.37 [b]	12.88 (9.8, 15.9)	12.48 (9.5, 15.4)
R^2	-	0.97	0.97
AIC	-	49.80	59.47
AIC_c	-	50.82	60.40
		Uptake Transport	
$CL_{int,T}$ (µL/min/10^6 cells)	33.91	41.33 (40.18, 42.47)	-
CL_{PD} [c] (µL/min/10^6 cells)	1.09×10^{-5} (Fixed)		
R^2		0.97	-
AIC		-16.92	-
AIC_c		-16.44	-

Confidence intervals (95%) are described in brackets.

[a] $J_{max,app}$ and $K_{m,app}$ derived from conventional Michaelis Menten analysis and $CL_{int,T}$ estimate derived from conventional two step approach (**Supplemental Fig. 2**).

[b] P_{pass} determined from inhibition of P_{app} measured in the absorptive direction in the presence of 100 µM of verapamil.

[c] Fixed using CL_{PD} estimated from P_{pass} of 12.88 × 10-6 cm/s using **eq. 3** as large standard errors have been observed with CL_{PD} estimated using 2 min incubations (Menochet *et al.*, 2012).

Downloaded from dmd.aspetjournals.org at ASPET Journals on April 20, 2024

DMD Fast Forward. Published on September 10, 2019 as DOI: 10.1124/dmd.119.086918
This article has not been copyedited and formatted. The final version may differ from this version.

Table 4. Comparison of PK parameters between simulated and observed data for model verification of the mechanistic kidney model in both healthy and renal impaired patients

	Simulated (n=130)			**Observed (n=13)**		
20 mg single dose, Healthy[a], P-gp Only (Greenblatt *et al.*, 2018)	**AUC (µg.h/L)**	**C_{max} (µg/L)**	**CL_R (L/h)**	**AUC (µg.h/L)**	**C_{max} (µg/L)**	**CL_R (L/h)**
Geometric mean	3901	311	0.37	2583	263	2.42
CV (%)	52	31	27	21	26	23
Ratio of simulated/observed	***1.51***	1.18	***0.15***			
Success criteria for ratio of simulated/observed	0.78 - 1.29	0.74- 1.35	0.76 - 1.31			
	Simulated (n=130)			**Observed (n=13)**		
20 mg single dose, Healthy[a], OAT3 Only (Greenblatt *et al.*, 2018)	**AUC (µg.h/L)**	**C_{max} (µg/L)**	**CL_R (L/h)**	**AUC (µg.h/L)**	**C_{max} (µg/L)**	**CL_R (L/h)**
Geometric mean	2946	269	1.60	2583	263	2.42
CV (%)	45	30	46	21	26	23
Ratio of simulated/observed	1.14	1.02	***0.66***			
Success criteria for ratio of simulated/observed	0.78 - 1.29	0.74- 1.35	0.76 - 1.31			
	Simulated (n=130)			**Observed (n=13)**		
20 mg single dose, Healthy[a], P-gp and OAT3 (Greenblatt *et al.*, 2018)	**AUC (µg.h/L)**	**C_{max} (µg/L)**	**CL_R (L/h)**	**AUC (µg.h/L)**	**C_{max} (µg/L)**	**CL_R (L/h)**
Geometric mean	2563	263	2.70	2583	263	2.42
CV (%)	43	30	49	21	26	23

Downloaded from dmd.aspetjournals.org at ASPET Journals on April 20, 2024

DMD Fast Forward. Published on September 10, 2019 as DOI: 10.1124/dmd.119.086918
This article has not been copyedited and formatted. The final version may differ from this version.

Ratio of simulated/observed	0.99	1	1.12			
Success criteria for ratio of simulated/observed	0.78 - 1.29	0.74- 1.35	0.76 - 1.31			
	Simulated (n=200)			**Observed (n=20)**		
10 mg single dose, Healthy[a], P-gp and OAT3 (Mueck *et al.*, 2013)	**AUC (µg.h/L)**	**C_{max} (µg/L)**	**CL_R (L/h)**	**AUC (µg.h/L)**	**C_{max} (µg/L)**	**CL_R (L/h)**
Geometric mean	1060	120	3.05	892	138	2.5
CV (%)	40	29	55	27	22	26
Ratio of simulated/observed	1.19	0.87	1.22			
Success criteria for ratio of simulated/observed	0.78- 1.29	0.81- 1.23	0.78- 1.28			
	Simulated (n=140)			**Observed (n=14)**		
20 mg single dose, Mild Renal Impairment[b] (Greenblatt *et al.*, 2018)	**AUC (µg.h/L)**	**C_{max} (µg/L)**	**CL_R (L/h)**	**AUC (µg.h/L)**	**C_{max} (µg/L)**	**CL_R (L/h)**
Geometric mean	2899	279	1.46	2864	252	2.25
CV (%)	43	29	50	29	29	42
Ratio of simulated/observed	1.01	1.11	0.65			
Success criteria for ratio of simulated/observed	0.72- 1.38	0.72- 1.38	0.63- 1.58			
Fold Change vs Healthy[c]	**AUC Fold Change (90% CI)**		**CL_R Fold Change (90% CI)**	**AUC Fold Change**		**CL_R Fold Change**
	1.20 (1.09, 1.31)		0.54 (0.49, 0.60)	1.11		0.93
Success Criteria for Fold Change	0.80-1.81		0.30-1.03			

Downloaded from dmd.aspetjournals.org at ASPET Journals on April 20, 2024

DMD Fast Forward. Published on September 10, 2019 as DOI: 10.1124/dmd.119.086918
This article has not been copyedited and formatted. The final version may differ from this version.

AUC, area under the concentration-time curve from time zero to infinity; C_{max}, maximum plasma concentration; CL_R, renal clearance; CV, coefficient of variation

[a]Healthy controls (CrCL > 80mL/min)

[b]Mild Renal Impairment (defined as CrCL: 50-79 mL/min)

[c]PK parameters in healthy controls utilized for comparison were obtained from simulations where the mechanistic kidney model incorporating both P-gp and OAT-3 was used to simulate the plasma concentration-time profile of rivaroxaban after a single 20 mg dose

Downloaded from dmd.aspetjournals.org at ASPET Journals on April 20, 2024

DMD Fast Forward. Published on September 10, 2019 as DOI: 10.1124/dmd.119.086918
This article has not been copyedited and formatted. The final version may differ from this version.

Table 5. Summary of CYP450 and P-gp inhibition parameters with rivaroxaban as probe substrate

***In Vitro* Parameters**		**Verapamil**	**Norverapamil**	**Ketoconazole**
MBI of CYP3A4	K_I **(μM)**	1.65	0.28	-
	K_{inact} **(h^{-1})**	3.92	2.44	-
	K_{inact}/K_I **($\mu M^{-1} h^{-1}$)**	2.38	8.59	-
Reversible Inhibition of CYP3A4	**Mode**	Mixed	Mixed	Mixed
	K_i **(μM)**	0.487	0.270	0.094
	α	1.19	1.15	3.28
Reversible Inhibition of CYP2J2	**Mode**	Competitive	Competitive	Competitive
	K_i **(μM)**	12.2	162	0.082
	α	-	-	-
	R_1[a]	1.00	1.00	
Fraction Unbound in the *In Vitro* Incubation	fu_{inc}	0.67	0.78	1
Inhibition of P-gp	IC_{50} **(μM)**	4.3[b]	-	0.22
Inhibition of OAT3	IC_{50} **(μM)**			

[a]R_1 is the predicted ratio of the victim drug's area under the plasma concentration-time curve in the presence and absence of an inhibitor for basic models of reversible inhibition. $R_1 = 1 + (I_{max,u}/K_i)$ where $I_{max,u}$ is the maximal unbound plasma concentration of the interacting drug.
[b]IC_{50} value of verapamil on the P-gp-mediated efflux of rivaroxaban (1 μM) across L-MDR1 cells after 2 h incubation at 37°C (Gnoth *et al.*, 2011)

Downloaded from dmd.aspetjournals.org at ASPET Journals on April 20, 2024

DMD Fast Forward. Published on September 10, 2019 as DOI: 10.1124/dmd.119.086918
This article has not been copyedited and formatted. The final version may differ from this version.

Table 6. Simulated change in rivaroxaban PK parameters in the presence of drug-drug or drug-drug-disease interactions

	Simulated (n=100)			Observed (n=10)		
Rivaroxaban 20 mg and Verapamil (Greenblatt *et al.*, 2018)	**AUC (µg.h/L)**	**C_{max} (µg/L)**	**CL (L/h)**	**AUC (µg.h/L)**	**C_{max} (µg/L)**	**CL (L/h)**
Geometric mean	3488	314	5.73	3600	278	5.70
CV (%)	43	28	56	20	27	22
Ratio of simulated/observed	0.97	1.13	1.01			
Success criteria for ratio of simulated/observed	0.77-1.31	0.70-1.43	0.75-1.34			
Fold Change vs Healthy[a]	**AUC Fold Change (90% CI)**		**CL Fold Change (90% CI)**	**AUC Fold Change**		**CL Fold Change**
	1.46 (1.33, 1.61)		0.68 (0.62, 0.75)	1.39		0.72
Success Criteria for Fold Change	0.94- 2.05		0.45–1.04			
	Simulated (n=110)			**Observed (n=11)**		
Rivaroxaban 20 mg and Verapamil in Mild Renal Impairment[b] (Greenblatt *et al.*, 2018)	**AUC (µg.h/L)**	**C_{max} (µg/L)**	**CL (L/h)**	**AUC (µg.h/L)**	**C_{max} (µg/L)**	**CL (L/h)**
Geometric mean	4057	327	4.93	4093	267	5.04
CV (%)	41	27	73	29	29	26

Downloaded from dmd.aspetjournals.org at ASPET Journals on April 20, 2024

DMD Fast Forward. Published on September 10, 2019 as DOI: 10.1124/dmd.119.086918
This article has not been copyedited and formatted. The final version may differ from this version.

Ratio of simulated/observed	0.99	1.22	0.98					
Success criteria for ratio of simulated/observed	0.69-1.44	0.60-1.44	0.72-1.39					
Fold Change vs Healthy	**AUC Fold Change (90% CI)**		**CL Fold Change (90% CI)**		**AUC Fold Change**		**CL Fold Change**	
	1.70 (1.54, 1.87)		0.59 (0.53, 0.65)		1.58		0.64	
Success Criteria for Fold Change	0.97-2.57		0.40-1.01					
	Simulated (n=200)				**Observed (n=20)**			
Rivaroxaban 10 mg and Ketoconazole (Mueck *et al.*, 2013)	**AUC (µg.h/L)**	**C_{max} (µg/L)**	**CL_H (L/h)**	**CL_R (L/h)**	**AUC (µg.h/L)**	**C_{max} (µg/L)**	**CL_H[c] (L/h)**	**CL_R (L/h)**
Geometric mean	1676	189	2.66	3.05	2298	237	2.75	1.60
CV (%)	39	23	38	54	26	20	26	33
Ratio of simulated/observed	***0.73***	***0.80***	0.97	***1.91***				
Success criteria for ratio of simulated/observed	0.78-1.28	0.83-1.21	0.78-1.28	0.74-1.36				
Fold Change vs Healthy	**AUC Fold Change (90% CI)**	**CL_H Fold Change (90% CI)**	**CL_R Fold Change (90% CI)**		**AUC Fold Change**	**CL_H Fold Change**	**CL_R Fold Change**	
	1.56 (1.46 , 1.66)	0.45 (0.42, 0.49)	1.01 (0.92, 1.09)		2.58	0.32	0.64	
Success Criteria for Fold Change	1.48-4.50	0.17-0.58	0.38–1.07					
	Simulated (n=200)				**Observed (n=20)**			

Downloaded from dmd.aspetjournals.org at ASPET Journals on April 20, 2024

DMD Fast Forward. Published on September 10, 2019 as DOI: 10.1124/dmd.119.086918
This article has not been copyedited and formatted. The final version may differ from this version.

Rivaroxaban 10 mg and Ketoconazole **OAT3 K_i Optimized** **(Mueck *et al.*, 2013)**	**AUC (µg.h/L)**	**C_{max} (µg/L)**	**CL_H (L/h)**	**CL_R (L/h)**	**AUC (µg.h/L)**	**C_{max} (µg/L)**	**CL_H[c] (L/h)**	**CL_R (L/h)**
Geometric mean	2850	241	2.70	0.81	2298	237	2.75	1.60
CV (%)	35	21	36	30	26	20	26	33
Ratio of simulated/observed	1.24	1.02	0.98	***0.51***				
Success criteria for ratio of simulated/observed	0.78-1.28	0.83-1.21	0.78-1.28	0.74-1.36				

Fold Change vs Healthy	**AUC Fold Change (90% CI)**	**CL_H Fold Change (90% CI)**	**CL_R Fold Change (90% CI)**	**AUC Fold Change**	**CL_H Fold Change**	**CL_R Fold Change**
	2.65 (2.49, 2.82)	0.44 (0.41, 0.48)	0.27 (0.25, 0.29)	2.58	0.32	0.64
Success Criteria for Fold Change	1.48-4.50	0.17-0.58	0.38–1.07			

AUC, area under the concentration-time curve from time zero to infinity; CL, clearance; CL_H, hepatic clearance, CL_R, renal clearance; C_{max}, maximum plasma concentration; CV, coefficient of variation

[a]PK parameters in healthy controls utilized for comparison were obtained from simulations where the mechanistic kidney model incorporating both P-gp and OAT-3 was used to simulate the plasma concentration-time profile of rivaroxaban after a single 10 mg or 20 mg dose (**Table 3**).

[b]Mild Renal Impairment (defined as CrCL: 50-79 mL/min).

[c]CL_H calculated from ($CL/F - CL_R$) assuming F=1 as rivaroxaban is known to have high absolute bioavailability (80-100%) for the 10 mg dose (Mueck *et al.*, 2013).

Downloaded from dmd.aspetjournals.org at ASPET Journals on April 20, 2024

DMD Fast Forward. Published on September 10, 2019 as DOI: 10.1124/dmd.119.086918
This article has not been copyedited and formatted. The final version may differ from this version.

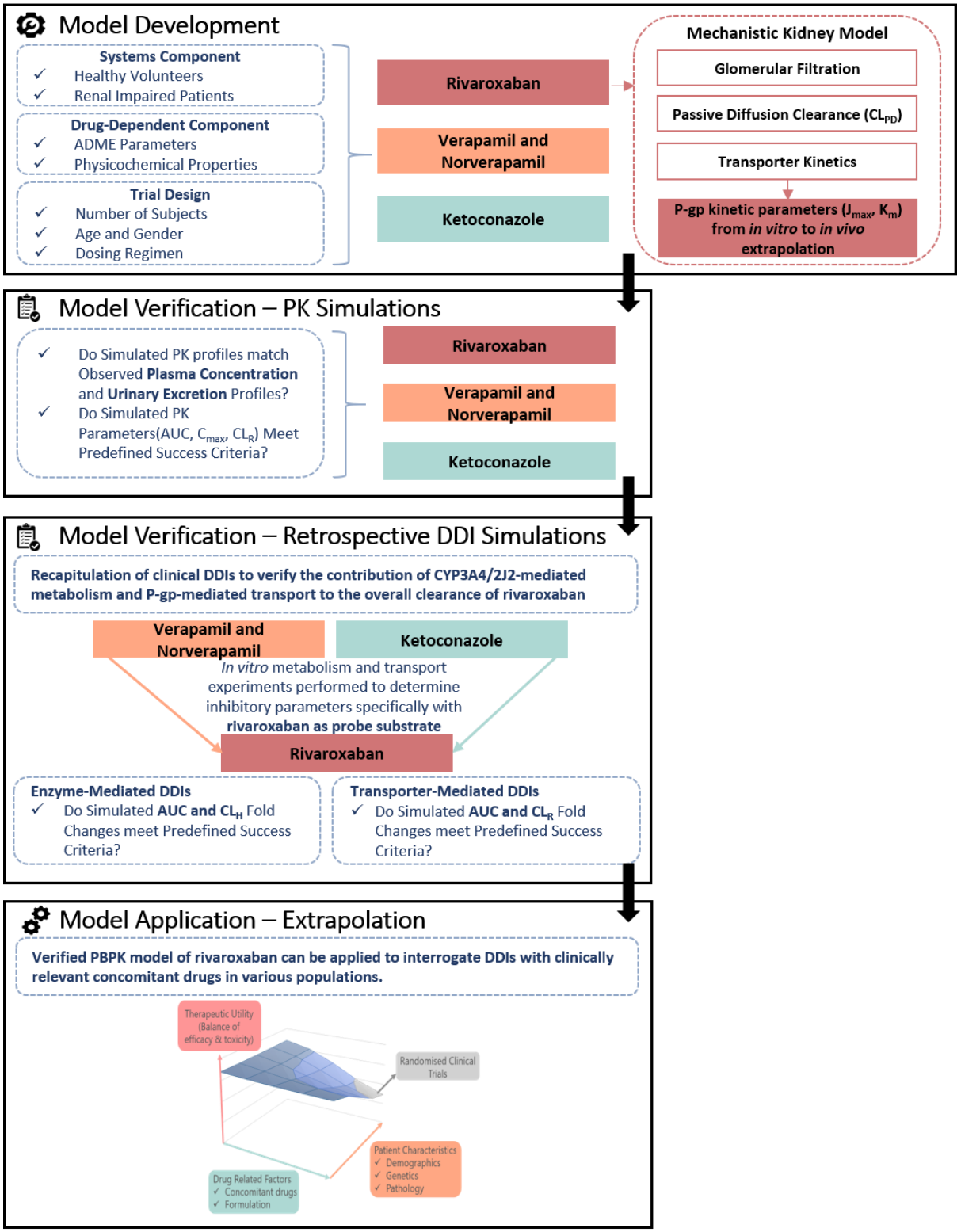

Figure 1

Downloaded from dmd.aspetjournals.org at ASPET Journals on April 20, 2024

DMD Fast Forward. Published on September 10, 2019 as DOI: 10.1124/dmd.119.086918
This article has not been copyedited and formatted. The final version may differ from this version.

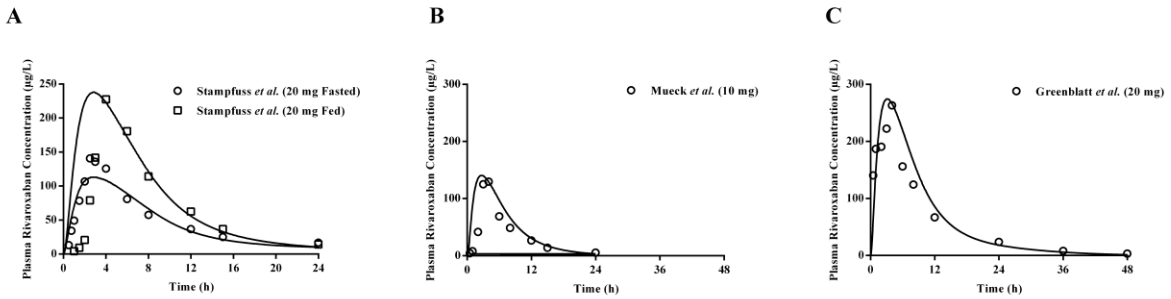

Figure 2

Downloaded from dmd.aspetjournals.org at ASPET Journals on April 20, 2024

DMD Fast Forward. Published on September 10, 2019 as DOI: 10.1124/dmd.119.086918
This article has not been copyedited and formatted. The final version may differ from this version.

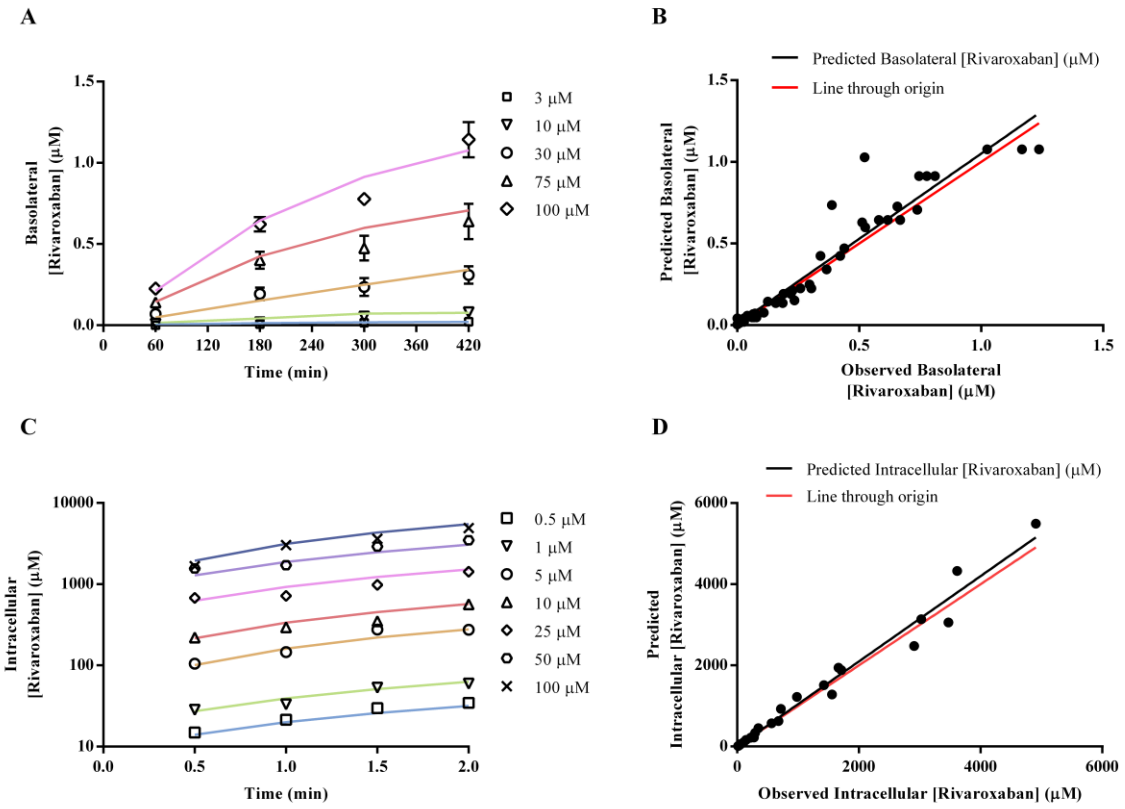

Figure 3

Downloaded from dmd.aspetjournals.org at ASPET Journals on April 20, 2024

DMD Fast Forward. Published on September 10, 2019 as DOI: 10.1124/dmd.119.086918
This article has not been copyedited and formatted. The final version may differ from this version.

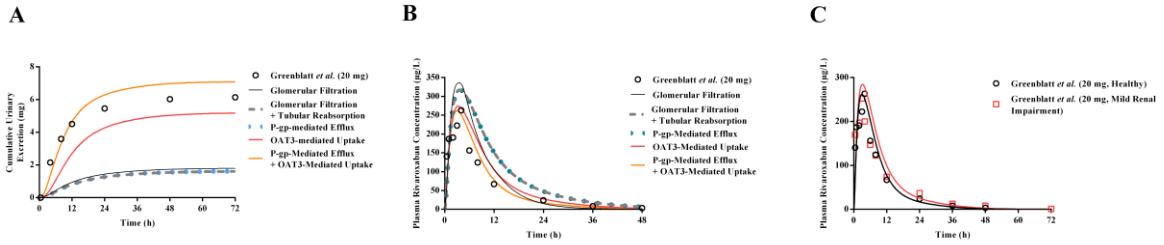

Figure 4

Downloaded from dmd.aspetjournals.org at ASPET Journals on April 20, 2024

DMD Fast Forward. Published on September 10, 2019 as DOI: 10.1124/dmd.119.086918
This article has not been copyedited and formatted. The final version may differ from this version.

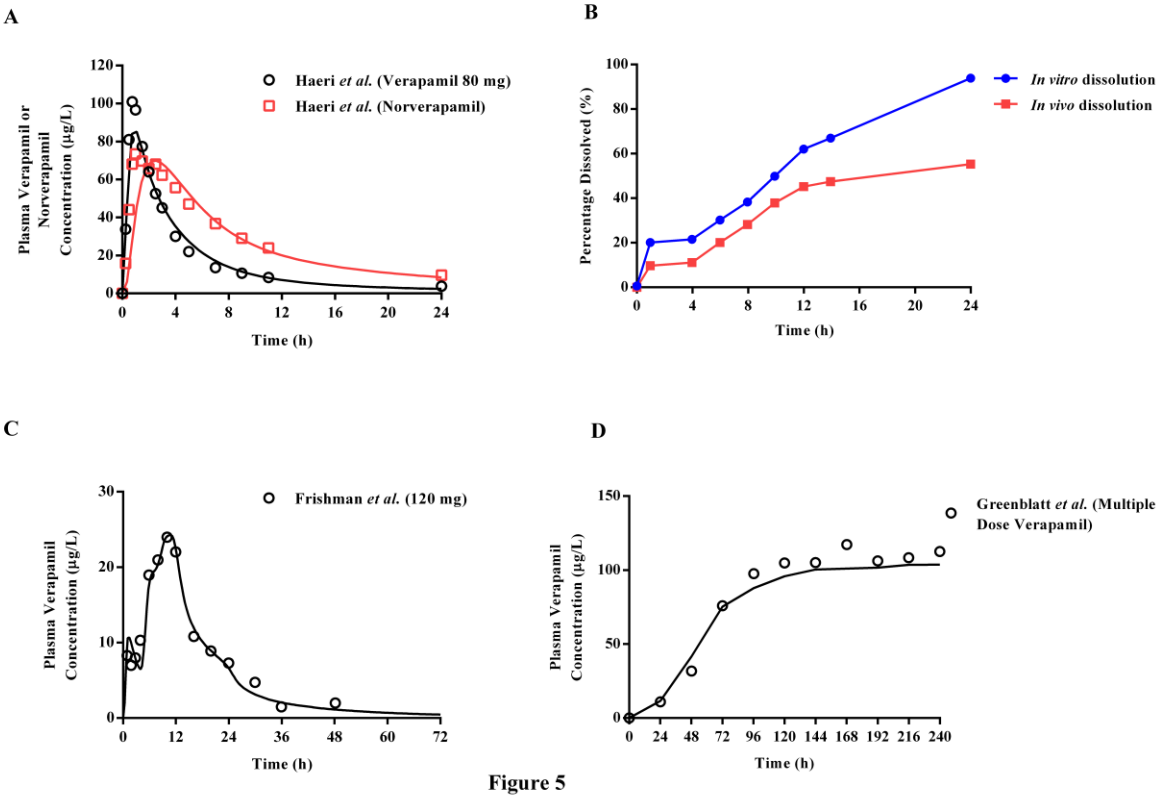

Figure 5

Downloaded from dmd.aspetjournals.org at ASPET Journals on April 20, 2024

DMD Fast Forward. Published on September 10, 2019 as DOI: 10.1124/dmd.119.086918
This article has not been copyedited and formatted. The final version may differ from this version.

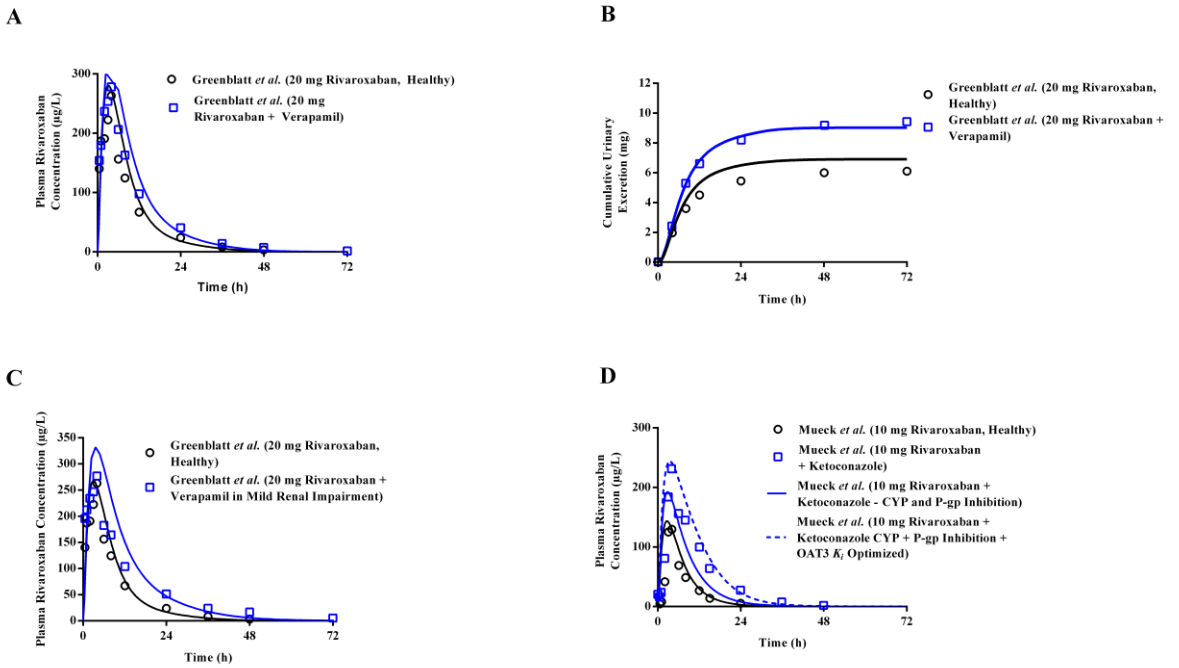

Figure 6

Downloaded from dmd.aspetjournals.org at ASPET Journals on April 20, 2024

Supplemental Data:

Systematic Development and Verification of A Physiologically-Based Pharmacokinetic Model of Rivaroxaban

Eleanor Jing Yi Cheong[1], Denise Wun Xi Teo[1], Denise Xin Yi Chua[1] and Eric Chun Yong Chan[1,2]

[1]Department of Pharmacy, Faculty of Science, National University of Singapore, 18 Science Drive 4, Singapore 117543; [2]Singapore Institute for Clinical Sciences (SICS), Brenner Centre for Molecular Medicine, 30 Medical Drive, Singapore 117609

Drug Metabolism and Disposition

Supplemental Methods

1 Model Development

1.1 PBPK Model of Rivaroxaban

Supplemental Table 1. Clearance parameters of rivaroxaban utilized for retrograde analysis within the Simcyp simulator

Trial	No. of subjects	Dose (mg)	$AUC_{0h-\infty}$ (ng.h/mL)	Apparent Oral Clearance (L/h)
(Kubitza, Becka, *et al.*, 2013)	6	10		8.26
	6	10		6.77
(Kubitza, Becka, Mueck, Halabi, Maatouk, Klause, Lufft, Dominic D. Wand, *et al.*, 2010)	8	10		8

(Kubitza, Roth, *et al.*, 2013)	16	10		6.6
(Kreutz *et al.*, 2017)	24	20		10.9
(Dias *et al.*, 2016)	8	15		8.31
(Moore *et al.*, 2014)	45	20	2277	8.78
(Stampfuss *et al.*, 2013)	24	10	1201	8.33
	24	15	1801	8.33
	24	20	2294	8.72
			Weighted Mean Clearance:	8.61 L/h
			Weighted Mean Renal Clearance:	36% × 8.61 L/h = 3.1 L/h

Mechanistic Kidney Model Development via *In Vitro In Vivo* Extrapolation

Materials for *In Vitro* Uptake and Efflux Assays. Madin-Darby canine kidney sub-clone I cells transfected with multi drug resistance gene (MDCK-MDR1) were donated by A/P Gigi Chiu. Human embryonic kidney 293 (HEK293) cells transfected with OAT1 and OAT3 were obtained from Dr. Kathleen Giacomini (University of California, San Francisco, San Francisco, CA). Dulbecco's modified eagle's medium (DMEM) with L-Glutamine (DMEM Glutamax) and DMEM (high glucose), 4-(2-hydroxyethyl)-1-piperazineethanesulfonic acid (HEPES), heat inactivated foetal bovine serum (FBS), penicillin/streptomycin 10,000 IU antibiotic solution (pen/strep), 10× trypsin-EDTA, hygromycin B, lucifer yellow CH dilithium salt and Hank's balanced salt solution (HBSS) were from Gibco® Life Technologies (Waltham, MA, USA). 1 M stock solution of phosphate buffer saline (PBS) was purchased from Vivantis (Subang Jaya, Malaysia). Lucifer yellow was dissolved in milli-Q water obtained using a milli-Q water purification system (Millipore, Billerica, MA). Rivaroxaban was purchased from Carbosynth (Compton, Oxford, England) and was reconstituted in dimethyl sulfoxide (DMSO). 4-aminohippuric acid was from Cayman Chemical (Ann Arbor, Michigan, USA) Propranolol, quinidine, estrone-3-sulfate and probenecid were from Sigma Aldrich (St. Louis, MO, USA) and were reconstituted in either DMSO or methanol. Subsequent dilutions for all compounds were carried out using DMSO. All other reagents were of analytical grade.

MDCK-MDR1 Cell Culture. MDCK-MDR1 cells were cultured at 37°C and were maintained in DMEM Glutamax culture media supplemented with 10% FBS and 1% pen/strep in humidified air-5% CO_2. Cells were passaged upon reaching approximately 100% confluence using 5× trypsin–EDTA and seeded in T75 flasks. For transport studies, MDCK-MDR1 cells (passage number 20 to 29) were seeded at a density of 200,000 cells on 24 well ThinCert™ cell culture inserts (8.4 mm id, 0.1 µm pore size). After allowing the cells to settle for at least 24 h, the culture media was refreshed. Transport assays were conducted approximately 48 h after seeding (Shirasaka *et al.*, 2008).

Setup of the Bidirectional Transport Assay. Culture media was first removed and each well and insert were washed with PBS before initiation of transport assays to minimize residual metabolic waste. As shown in the setup below, for absorptive transport, solutions (300 µL) containing test drugs and lucifer yellow in DMEM were added to the donor apical compartment (A), with culture media (600 µL) in the receiver basolateral compartment (B). In parallel wells measuring secretory transport, test solutions were added to the donor basolateral compartment (B) with culture media in the receiver apical compartment (A).

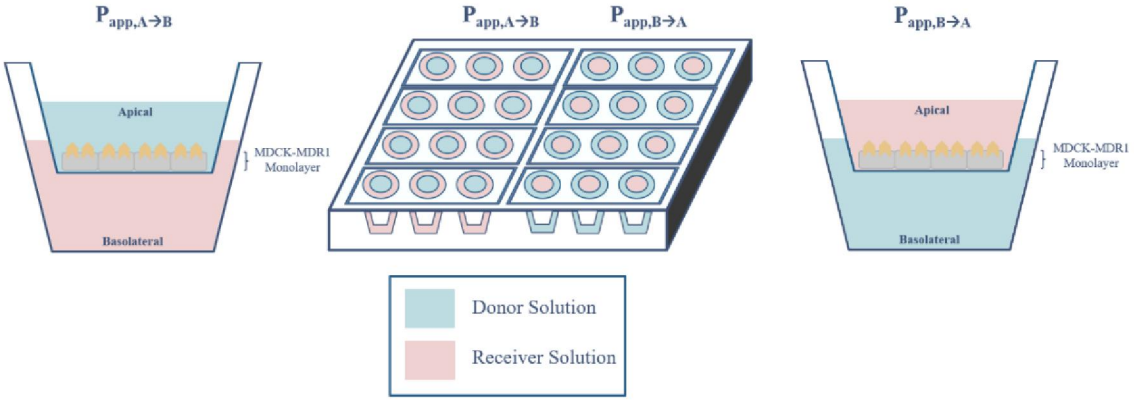

Bidirectional transport assay experimental setup.

Validation of Transport Assay Functionality. To ascertain the functionality of the proposed *in vitro* system in quantifying the P-gp-mediated transport of rivaroxaban, rigorous assay validation was also performed (Volpe, 2016; FDA/CDER, 2017). Monolayer integrity was established via the calculation

of the paracellular flux of low permeability compound lucifer yellow as described in **eq. S1** (Polli *et al.*, 2008).

$$P_{app,AB} \text{ of lucifer yellow (nm/s)} = -\left(\frac{V_D V_R}{(V_D + V_R)At}\right) ln\left[1 - \frac{(V_D + V_R)C_R(t)}{V_D C_D(t) + V_R C_R(t)}\right] \times 10^7 \quad \textbf{(S1)}$$

where V_D is the volume of donor solution (mL), V_R is the volume of receiver solution (mL), A is the surface area of monolayer (cm^2), t is the incubation time (s), $C_D(t)$ is the measured concentration in the donor well at time t (nM), $C_R(t)$ is the measured concentration in the receiver well at time t (nM). Acceptance criteria was defined as a passive permeability (P_{app}) of < 5 x 10^6 cm/s (Ellens *et al.*, 2017). Efflux ratios of positive control (quinidine 10 μM) and negative control propranolol (10 μM) were assessed and compared with literature reported values. As accuracy of the transport ratios could be compromised by poor recovery which can be calculated by **eq. S2**, a mass balance cut-off exceeding 70% was deemed acceptable according to previously published guidelines by the International Transporter Consortium (Brouwer *et al.*, 2013).

$$\text{Percentage recovery (\%)} = \frac{D_t + R_t}{D_0} \times 100\% \quad \textbf{(2)}$$

where D_t and R_t represent the amount of substrate in the donor and receiver chambers at the end of experiment respectively, and D_0 is the amount of substrate in the donor chamber at t = 0 min.

Investigation of the *In Vitro* P-gp-mediated Transport of Rivaroxaban. To ensure that transport studies were conducted under conditions where flux was linearly related to time, time-dependent changes in rivaroxaban transport (10 μM in donor) in both absorptive and secretory directions were monitored by quantifying receiver compartment concentrations at 30, 60, 120, 180, 240, 300 and 360 min. Subsequent concentration-dependent permeation experiments were conducted with 5 different concentrations of rivaroxaban (3, 10, 30, 75, 100 μM) using the optimized incubation time of 90 min. Absorptive (J_{AB}) or secretory (J_{BA}) flux was calculated using **eq. S3**:

$$J_{AB} \text{ or } J_{BA} = \frac{dQ}{dt} \quad \textbf{(S3)}$$

where Q is the amount of compound transported over time t of the experiment. Apparent passive permeability (P_{app}) was derived from flux using **eq. S4**:

$$P_{app} = \frac{J}{S \times C_D} \quad \textbf{(S4)}$$

where C_D is the initial concentration of the test compound added to the donor compartment and S is the surface area of the porous membrane in cm^2. The efflux ratio (ER) was calculated using **eq. S5** (Troutman and Thakker, 2003):

$$Efflux\ Ratio = \frac{P_{app,BA}}{P_{app,AB}} \quad \textbf{(S5)}$$

Rivaroxaban flux (J_{pass}) and apparent permeability solely due to passive diffusion (P_{pass}) were approximated in the presence of 100 μM of verapamil (~20× greater than the reported half maximal inhibitory concentration (IC_{50}) in L-MDR1 cells = 4.3 ± 1.9 μM) (Gnoth *et al.*, 2011), ensuring abolishment of P-gp efflux activity.

Analyzing P-gp Mediated Efflux of Rivaroxaban Using the Conventional Michaelis-Menten Approach. Overall flux during absorptive (J_{AB}) and secretory transport (J_{BA}) can be quantified using **eqs. S6** and **S7**, where J_{pass} and $J_{P-gp,X}$ represent passive and P-gp-mediated flux respectively (Troutman and Thakker, 2003). X denotes transport direction, either A to B or B to A.

$$J_{AB} = J_{pass} - J_{P-gp,AB} \quad \textbf{(S6)}$$

$$J_{BA} = J_{P-gp,BA} + J_{pass} \quad \textbf{(S7)}$$

Relationships specified in e**qs. S4**, **S6** and **S7** can be further modified to obtain permeability equations describing the concentration dependence of clearance (P_{app}×S) derived from both absorptive and secretory directions. **Eqs. S8** and **S9** comprise a saturable component that describes P-gp-mediated efflux where $J_{max,app}$ and $K_{m,app}$ represent the maximal achievable transport rate and the donor chamber concentration associated with half-maximal transport rate respectively. Additionally, passive permeability was quantified via the term denoting first order passive diffusion clearance (P_{pass}×S).

$$P_{app,AB} \times S = P_{pass} \times S - \frac{1000 \times J_{max,app}}{K_{m,app} + C_D} \quad \textbf{(S8)}$$

$$P_{app,BA} \times S = \frac{1000 \times J_{max,app}}{K_{m,app} + C_D} + P_{pass} \times S \quad \textbf{(S9)}$$

P_{app} obtained from concentration-dependent transport experiments along with P_{pass} obtained in the presence of P-gp inhibitor verapamil were fitted to **Eqs. S8** and **S9** using GraphPad PRISM® software version 7.01 (San Diego, CA, USA) to calculate initial estimates of $J_{max,app}$ and $K_{m,app}$.

Analyzing P-gp Mediated Efflux of Rivaroxaban Using A Three Compartmental Model. Measured time- and concentration-dependent data for the absorptive and secretory transport of rivaroxaban were fitted separately to a three-compartment model using the Simcyp *In Vitro* Analysis (SIVA) Toolkit Version 3, where a system of differential equations (**Eqs. S10, S11 and S12**) was applied to dynamically model changes in drug concentration ($\frac{dS}{dt}$) in the apical, intracellular and basolateral compartments respectively (**refer to table and diagram for additional details on system-dependent parameters required**). Given that only unbound concentrations are involved in bidirectional passive diffusion across the apical and basolateral membranes, and apical efflux is also driven by the intracellular unbound concentrations, ultrafiltration was performed to determine the fraction unbound of rivaroxaban in media (fu_{media}) as well as within the cell (fu_{cell}) (**More details on the ultrafiltration protocol are highlighted in the subsequent section**). Naïve pooled fitting was performed to estimate J_{max}, K_m and passive diffusion clearance (CL_{PD}) based on the initial values of $J_{max,app}$, $K_{m,app}$ and $P_{pass,app}$ obtained from the Michaelis-Menten model. Given the potential uncertainty associated with initial estimates, both hybrid (global followed by Nelder-Mead) and local Nelder-Mead optimization were used to minimize the objective function value (OFV), defined by the overall sum of square residuals between the experimental and simulated data which are weighted by the reciprocal of predicted squared. Model performance was assessed via goodness of fit between observed and predicted values, the coefficient of determination (R^2), Akaike information criterion (AIC) and difference in small sample size corrected version of AIC (ΔAICc). Confidence intervals around final estimated parameters were employed as diagnostics of parameter certainty.

$$V_{ap}.\frac{dS_{ap}}{dt} = \frac{J_{max}.SA.[S]_{cell,u}}{K_{m,u} + [S]_{cell,u}} + P_{pass} \times SA \times 60/1000([S]_{cell,u} - [S]_{ap,u}] \quad \textbf{(S10)}$$

$$V_{cell}.\frac{dS_{cell}}{dt} = -\frac{J_{max}.SA.[S]_{cell,u}}{K_{m,u} + [S]_{cell,u}} + P_{pass} \times SA \times 60/1000([S]_{ap,u}] + [S]_{bl,u} - 2[S]_{cell,u}] \quad \textbf{(S11)}$$

$$V_{bl}.\frac{dS_{bl}}{dt} = P_{pass} \times SA \times 60/1000([S]_{cell,u} - [S]_{bl,u}] \quad \textbf{(S12)}$$

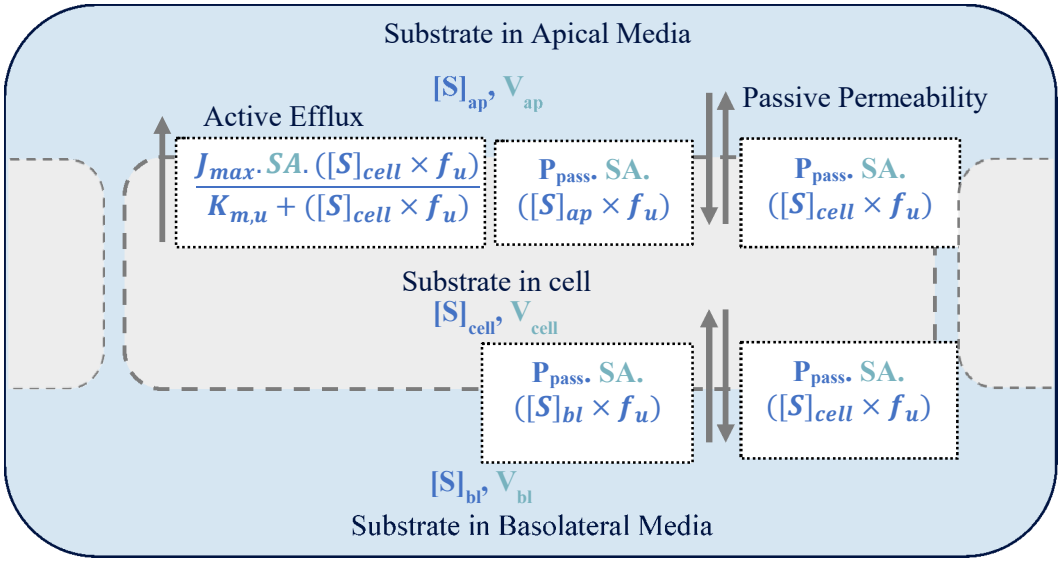

Three-compartment permeability and transport model in the Simcyp *in vitro* analysis (SIVA) toolkit. Drug-dependent parameters include J_{max}: *In vitro* maximal rate of transporter mediated efflux; K_m: Michaelis Menten constant; P_{pass}: Passive permeability, f_u: fraction unbound. System dependent parameters include the surface area occupied (SA) and volumes of the intracellular (V_{cell}), apical (V_{ap}) and basolateral (V_{bl}) compartments respectively.

System-dependent parameters utilized for three-compartmental analysis

Parameter	Value	Method/Reference
Surface area (cm^2)	0.33	Greiner Bio-one Thincert™ Tissue Culture Inserts for 24-well plates
Volume of the apical compartment (V_{ap}) (µL)	300	Defined experimentally
Volume of the basolateral compartment (V_{bl}) (µL)	600	Defined experimentally
Volume of the intracellular compartment (V_{cell}) (µL)	0.47	(von Bonsdorff *et al.*, 1985)

HEK293 Cell Culture. HEK wild type cells were cultured at 37°C and were maintained in DMEM culture media supplemented with 10% FBS and 1% pen/strep in humidified air - 5% CO2. Similar culture conditions were utilized for HEK-OAT3 and OAT1 culture albeit with the addition of hygromycin B (50 µg/mL). For transport studies, wild type and OAT1/3-transfected cells (passage number 3-15) were directly seeded into Biocoat 24-well poly-D-lysine coated plates (Corning, NY) 48 hours before each experiment, at densities of 2.4 (wild type) and 3.6×10^5 (OAT3/1-transfected) cells/well in a volume of 400 µL. Transport assays were conducted approximately 48 h after seeding upon verification of monolayer confluence as described previously (Mathialagan, Piotrowski, *et al.*, 2017; Mathialagan, Rodrigues, *et al.*, 2017).

Setup of the Uptake Assay and Verification of Assay Functionality. Transport buffer was prepared at pH 7.4 using Hank's balanced salt solution supplemented with 20 mM HEPES. Estrone 3-sulfate (2 µM) and para aminohippuric acid (3 µM) were used as control probe substrates for OAT3 and OAT1 respectively, to monitor the functionality of the cells. Immediately before the experiment, the cells were washed twice with 200 µL of transport buffer, leaving the final rinse volume for 10 min to allow equilibration. Uptake was initiated by incubating with 200 µL transport buffer (containing 0.5 -100 µM rivaroxaban) at 37°C. At four different time points from 0.5 to 2 min, cellular uptake was terminated by washing the cells twice with 200 µL of ice-cold PBS and lysed directly on the plate with 100% methanol containing internal standard (IS).

Analyzing OAT-3 Mediated Uptake of Rivaroxaban Using the Conventional Two-Step Approach. Initial estimates for clearances via passive diffusion (CL_{PD}) and active uptake ($CL_{int,T} = J_{max}/K_m$) were derived based on the two-step approach. Uptake rates of rivaroxaban in both wild type and transfected HEK cells were calculated over 2 min (time-linear conditions) and expressed as the slope of the linear regression of the rates of transport versus time plot. Passive diffusion clearance (CL_{PD}) was calculated from the uptake rates measured in wild type cells (**eq. S13**) and inserted into **eq. S14**, which describes total cellular uptake measured at 37°C as a composite of both saturable active uptake and non-saturable passive transport.

$$v = CL_{PD} \times S \tag{S13}$$

$$v = \frac{J_{max} \times [S]}{K_m + [S]} + CL_{PD} \times [S] \tag{S14}$$

v represents the rate of uptake (pmol/min/mg), [S] is the substrate concentration (µM), J_{max} is the maximum rate of active transport (pmol/min/mg), K_m is the Michaelis constant (µM) and CL_{PD} is the passive diffusion clearance (µL/min/mg).

Determination of Uptake Kinetics Parameters using a Mechanistic Two-Compartmental Model. To facilitate the dynamic evaluation of flux in rivaroxaban concentrations due to active transport, bidirectional passive diffusion and intracellular/extracellular binding processes occurring during uptake, naïve pooled concentration-time data of rivaroxaban in the intracellular compartment was fitted to a mechanistic two-compartmental model using the Simcyp *In Vitro* Analysis (SIVA) Toolkit Version 3 (figure above) as described by **eqs. S15** and **S16** (**refer to table and diagram for additional details on system-dependent parameters required**).

$$V_{media} + K_{mem} \times No\ of\ cells\left(\frac{d[S]_{media}}{dt}\right) = -CL_{int,u,uptake}.No\ of\ cells.S_{media}.f_{u,media} + CL_{PD}([S]_{cell} \times f_{u,cell} - [S]_{media}.f_{u,media}) \tag{S15}$$

$$(V_{cell}.No\ of\ cells)\frac{d[S]_{cell}}{dt} = CL_{int,u,uptake}.No\ of\ cells.S_{media}.f_{u,media} + CL_{PD}([S]_{media}.f_{u,media} - f_{u,cell} \times [S]_{cell}) \tag{S16}$$

Initial CL_{PD} and $CL_{int,T}$ values derived from the two-step approach were converted from units of µL/min/mg protein to µL/min/10^6 cells on the basis that 1 million HEK293 cells contain 0.15 mg of total protein (measured). Naïve pooled fitting of measured time-and concentration-dependent uptake data was performed to estimate $CL_{int,u,uptake}$, with CL_{PD} and the surface binding constant (K_{mem}) inserted as constants into the model (see table below). The unbound fraction of rivaroxaban in media and the cellular homogenate was also fixed at 1 and 0.023 respectively.

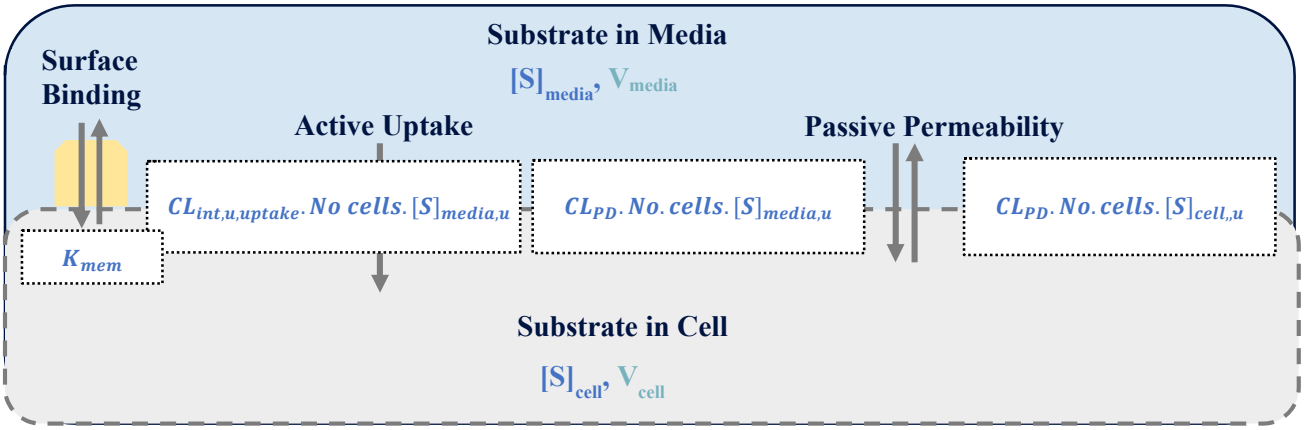

Two-compartment permeability and transport model in the Simcyp *in vitro* analysis (SIVA) toolkit. Drug-dependent parameters include $CL_{int,u,uptake}$: unbound intrinsic clearance for active uptake; CL_{PD}: Passive diffusion clearance, $f_{umedia/cell}$: fraction unbound in media/within the cell and K_{mem}; surface binding constant. System dependent parameters include the volumes of the intracellular (V_{cell}), and media compartments as well as the number of cells.

System-dependent parameters utilized for two compartmental analysis

Parameter	Value	Method/Reference
System-Dependent		
V_{media} (µL)	**300**	Defined experimentally
V_{cell} (µL/10^6 cells)	**1.7**	Measured assuming spherical structure and a cell diameter of 14.8 µm (Mathialagan, Piotrowski, *et al.*, 2017)
No. of cells (10^6 cells)	**0.06**	Calculated based on average measured protein concentration per well and the number of cells per measured protein (0.15 mg/10^6 cells)
Drug-Dependent		
K_{mem} (µL/10^6 cells)	**0.001**	Default value in SIVA
fu_{media}	**1**	Assumed to be 1 despite known non-specific binding to test apparatus for many compounds
fu_{cell}	**0.023**	Assumed to be the same as that measured using ultrafiltration in the MDCK-MDR1 homogenate
CL_{PD} (µL/min/10^6 cells)	**22.64**	Calculated from linear regression of uptake rates across rivaroxaban concentrations measured in wild type HEK cells to be 159.4 µL/min/mg protein (**Supplemental Fig. 2F**) Corrected to units of µL/min/10^6 cells based on 0.15 mg protein/10^6 HEK cells

1.2 PBPK Models of Verapamil, Norverapamil and Ketoconazole

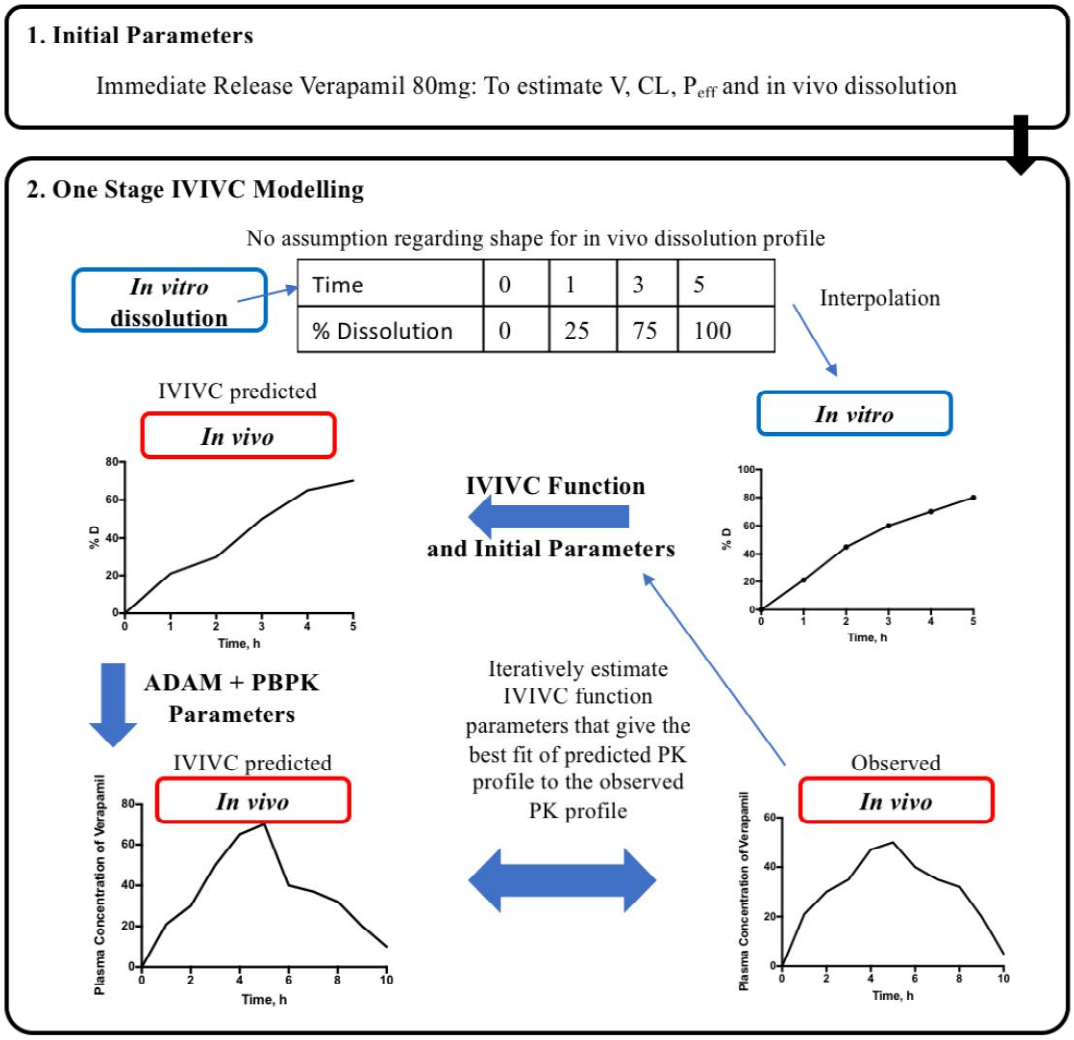

Supplemental Fig. 1 *In vitro in vivo* correlation workflow to recapitulate the PK of a controlled release formulation of verapamil.

Supplemental Table 2.1. Key input parameters for the PBPK model of verapamil

Parameter	**Value**	**Method/Reference**
Molecular weight (g/mol)	454.6	Simcyp compound file
log P	4.46	Simcyp compound file
Compound type	Monoprotic Base	Simcyp compound file
pKa	8.78	Simcyp compound file
B/P	0.709	Simcyp compound file
fu	0.09	Simcyp compound file
Main plasma binding protein	Human serum albumin	Simcyp compound file
Absorption Model	**ADAM Model**	
fu_{gut}	1	Predicted
$P_{eff,man}$ (10^{-4}cm/s)	6.08477	Predicted, Simcyp compound file
Permeability Assay	Caco-2	
Apical pH : Basolateral pH	7.4 : 7.4	
Activity	Passive & Active	
$P_{appaA:B}$(10^{-6} cm/s)	50	
Reference Compound	Propranolol	
Reference Compound $P_{appaA:B}$ (10^{-6} cm/s)	109	
Scalar	0.3944954	
Solubility pH Type	Intrinsic	Predicted
Solubility (mg/mL)	0.022	(Popović-Nikolić *et al.*, 2017)
Transporter	ABCB1 (P-gp/MDR1)	Simcyp compound file
J_{max} (pmol/min/cm^2)	2.814	
K_m (μM)	0.734	
fuinc	1	
Insert growth area of the Transwell (cm²)	1	
System	User	
RAF/REF	0.608	

Transporter	ABCC2 (MRP2)	Simcyp compound file
$CL_{int,T}$ (µL/min/cm^2)	18	
fuinc	1	
Insert growth area of the Transwell (cm^2)	1	
System	User	

Distribution Model	**Full PBPK Model**	
V_{SS} (L/kg)	5.366168	Predicted - Method 2

Enzyme	CYP2C8	Simcyp compound file
Pathway	Norverapamil	
V_{max} (pmol/min/pmol)	221.2	
K_m (µM)	140.5	

Enzyme	CYP3A4	Simcyp compound file
Pathway	Norverapamil	
V_{max} (pmol/min/pmol)	154.3	
K_m (µM)	122	

Enzyme	CYP3A5	Simcyp compound file
Pathway	Norverapamil	
V_{max} (pmol/min/pmol)	169.3	
K_m (µM)	87.5	

Enzyme	CYP2C8	Simcyp compound file
Pathway	D-617	
V_{max} (pmol/min/pmol)	218.9	
K_m (µM)	156	

Enzyme	CYP3A4	Simcyp compound file
Pathway	D-617	
V_{max} (pmol/min/pmol)	174	
K_m (µM)	99.5	

Enzyme	CYP3A5	Simcyp compound file
Pathway	D-617	
V_{max} (pmol/min/pmol)	117.7	
K_m (µM)	73	
CL_{int} (HLM) (µL/min/mg protein)	79.57	Simcyp compound file
CL_R (L/h)	2.52	Simcyp compound file
Enzyme	CYP3A4	Internal Data
K_i (µM)	0.487	
fu_{mic}	0.67	
K_I (µM)	1.653	
k_{inact} (1/h)	3.924	
fu_{mic}	0.67	
Enzyme	CYP2J2	Internal Data
K_i (µM)	12.2	

Supplemental Table 2.2. Key input parameters for the PBPK model of norverapamil

Parameter	**Value**	**Method/Reference**
Molecular weight (g/mol)	440.575	Simcyp compound file
log P	4.66	Simcyp compound file
Compound type	Monoprotic Base	Simcyp compound file
pKa	10.29	Simcyp compound file
B/P	0.675	Simcyp compound file
fu	0.083	Simcyp compound file
Main plasma binding protein	Human serum albumin	Simcyp compound file
fu_{gut}	1	
Distribution Model	Minimal PBPK Model	
V_{SS} (L/kg)	4.166812	Predicted - Method 1
Q (L/h)	18	
V_{SAC} (L/kg)	2	
Enzyme	CYP2C8	Simcyp compound file
Pathway	D-620	
V_{max} (pmol/min/pmol)	38.5	
K_m (µM)	68	
Enzyme	CYP3A4	Simcyp compound file
Pathway	D-620	
V_{max} (pmol/min/pmol)	46	
K_m (µM)	90	
Enzyme	CYP3A5	Simcyp compound file
Pathway	D-620	
V_{max} (pmol/min/pmol)	18.8	
K_m (µM)	19.5	
Enzyme	CYP2C8	Simcyp compound file
Pathway	D-715	

V_{max} (pmol/min/pmol)	113.2	
K_m (μM)	59	
CL_R (L/h)	1.91	Simcyp compound file
Enzyme	CYP3A4	Determined experimentally
K_i (μM)	0.27	
fu_{mic}	0.78	
K_I (μM)	0.28	
k_{inact} (1/h)	2.44	
fu_{mic}	0.78	
Enzyme	CYP2J2	Determined experimentally
K_i (μM)	162	

Supplemental Table 2.3. Key input parameters for the PBPK model of ketoconazole

Parameter	**Value**	**Method/Reference**
Molecular weight (g/mol)	531.4	Simcyp compound file
log P	4.04	Simcyp compound file
Compound type	Diprotic Base	Simcyp compound file
pKa	2.94, 6.51	Simcyp compound file
B/P	0.62	Simcyp compound file
fu	0.029	Simcyp compound file
Main plasma binding protein	Human serum albumin	Simcyp compound file
fu_{gut}	0.06	Simcyp compound file
Distribution Model	Minimal PBPK Model	
V_{SS} (L/kg)	0.345	Simcyp compound file
CL_{po} (L/h)	7.4	Simcyp compound file
CL_R (L/h)	0.147	Simcyp compound file
Enzyme	CYP2J2	
K_i (μM)	0.082	Determined experimentally
Enzyme	CYP3A4	
K_i (μM)	0.094	Determined experimentally
Transporter	ABCB1 (P-gp/MDR1)	
Organ	Gut	
K_i (μM)	0.17	Determined experimentally
Transporter	OAT3	
Organ	Kidney	
K_i (μM)	0.01	Optimized based on experimentally derived IC_{50} of 15.77 μM and reported IC_{50} of 0.86 μM with estrone-3-sulfate

	as the probe substrate (Vermeer *et al.*, 2016)

2 Model Verification – PK and Retrospective DDI Simulations

Supplemental Table 3. Details of clinical study designs for PBPK model verification

Reference Study	Dosing Regimen	Study conditions	Subjects
(Greenblatt *et al.*, 2018)	Rivaroxaban: Single dose of 20 mg on the mornings of day 1 and day 15 Extended Release Verapamil: 120 mg (Day 8), 240 mg (Day 9), 360 mg (Days 10-17)	Fed	Normal renal function: 13 Caucasians (Male/Female: 8/5) Mild renal impairment: 14 Caucasians (Male/Female: 8/6) Age: 38-72
(Kubitza, Becka, Mueck, Halabi, Maatouk, Klause, Lufft, Dominic D Wand, *et al.*, 2010)	Single dose of 10 mg rivaroxaban	Fasted	Normal renal function: 8 Caucasians (Male/Female: 5/3) Mild renal impairment: 8 Caucasians (Male/Female: 5/3) Age: 36-69
(Mueck *et al.*, 2013)	Rivaroxaban: 10 mg once daily (Days 1-10) Ketoconazole: 400 mg once daily (Days 5-10)	Fed	20 healthy Caucasian males Age: 22-45
(Haeri *et al.*, 2014)	Single dose of 80 mg verapamil	Fasted	24 healthy volunteers (Male/Female: 12/12) Age: 21-29
(Frishman and Lazar, 1992)	Single dose of 120 mg controlled release verapamil capsule	Fasted	28 patients with mild to moderate hypertension

Supplemental Table 4. Serum creatinine input for mild renal impaired population

	GFR 30 to 60 mL/min Population in Simcyp		**GFR 50 to 79 mL/min Created Population**	
Age Group (years)	Serum Creatinine (μmol/L)	GFR (mL/min)	GFR (mL/min)	Serum Creatinine (μmol/L)
Male < 61 yo	152	48.8	68.8	107.9
Male > 61 yo	143	51.9	71.9	103.2
Female < 60 yo	152	33.5	53.5	95.2
Female > 60 yo	148	34.4	54.4	93.6
Female > 75 yo	143	28.5	48.5	83.9

Parameterizing the PBPK-DDI Models via *In Vitro* Inhibitory Parameters

***In Vitro* Enzymatic and Transport Inhibition Assays.** The verified PBPK models of rivaroxaban, verapamil, norverapamil and ketoconazole were subsequently used for PBPK-DDI model development. Inhibition potencies (K_i for reversible inhibition and K_I and k_{inact} for mechanism-based inhibition) were derived using rivaroxaban as the probe substrate (FDA/CDER, 2017).

Chemicals. High performance liquid chromatography (HPLC)-grade acetonitrile (ACN) was purchased from Tedia Company Inc (Fairfield, OH). Formic acid was purchased from BDH Chemicals (Radnor, PA). Ketoconazole, verapamil hydrochloride, prednisolone vetranal and dexamethasone were acquired from Sigma-Aldrich (St. Louis, MO). Norverapamil hydrochloride was purchased from Cayman Chemicals (Ann Arbor, MI). Human recombinant cytochrome P450 supersomes (rCYP) and NADPH regenerating system consisting of NADPH A ($NADP^+$ and glucose-6-phosphare) and B (glucose-6-phosphate dehydrogenase) were obtained from BD Gentest (Woburn, MA). All other reagents were of analytical grade.

Mechanism-Based Inactivation of CYP3A4/2J2. Incubations (n=3) were conducted in 96-well plates. In the primary inactivation incubation, either verapamil or norverapamil (0.1 to 5 µM or 2.5 µM for rCYP3A4 and rCYP2J2 respectively) were pre-incubated at 37°C for 5 min with rCYP3A4 (40 pmol/mL) or rCYP2J2 (20 pmol/mL) and NADPH B in potassium phosphate buffer (100 mM, pH 7.4). Reactions were initiated by the addition of 5 µL of NADPH A. The final primary incubation mixture had a total volume of 100 µL and the final organic concentration in the mixture was 1% ACN (v/v). At 0, 3, 8, 15, 22, 30 and 45 min after the addition of NADPH A, 5 µL of the primary incubation was transferred to 95 µL of the secondary incubation containing saturating rivaroxaban concentrations ([S]=50 µM >> K_m), effecting a 20× dilution. Apart from rivaroxaban, the secondary incubation mixture comprised the NADPH regenerating system and 100 mM potassium phosphate buffer (pH 7.4). The secondary incubation mixture was incubated for 2 h (rCYP3A4) or 30 min (rCYP2J2) at 37°C before an 80 µL aliquot was removed and quenched with an equal volume of ice-cold ACN containing 4 µM dexamethasone (internal standard). Quenched samples were subjected to centrifugation at 2755 *g*, 4°C for 30 min. Subsequently, the supernatants were removed for the determination of hydroxylated-rivaroxaban metabolite (main metabolite) by liquid chromatography tandem mass spectrometry (LC/MS/MS).

Calculation of Inactivation Kinetic Parameters (K_I and k_{inact}). The natural logarithm of percentage of enzyme activity remaining versus inactivation pre-incubation time was plotted for each inactivator concentration and k_{obs} values (apparent inactivation rate constants) were described as the negative slopes of the lines. Subsequently, a plot of observed inactivation rate constants (k_{obs}) against inactivator concentration [I] allowed for inactivation kinetic parameters, K_I and k_{inact} to be fitted with non-linear least squares regression using **eq. S13.**

$$k_{obs} = \frac{k_{inact} \times [I]}{K_I + [I]} \quad \textbf{(S13)}$$

Reversible Inhibition of CYP3A4 and CYP2J2. Incubations (n=3) were conducted in 96-well plates. Rivaroxaban (0.5 to 100 µM) was pre-incubated at 37°C for 5 min with rCYP3A4 (40 pmol/mL) and rCYP2J2 (20 pmol/mL), NADPHB and 100 mM potassium phosphate buffer (pH 7.4) in the presence of several concentrations of the test inhibitor (i.e. verapamil, norverapamil). The reactions were commenced by the addition of 5 µL NADPHA and the final mixture had a total volume of 100 µL comprising 1% ACN (v/v). Incubation was carried out for 2 h and 30 min for rCYP3A4 and rCYP2J2 respectively at 37°C and quenched with an equal volume of ice-cold ACN containing 4 µM dexamethasone (internal standard). The quenched samples were subjected to centrifugation at 2755 *g*, 4°C for 30 min. The same protocol was adopted to determine IC_{50} of ketoconazole with rivaroxaban concentration at K_m (10 µM). Subsequently, the supernatants were removed for the determination of hydroxylated-rivaroxaban metabolite (main metabolite) by LC/MS/MS.

Calculation of Reversible Inhibition Parameters (K_i). A series of Michaelis-Menten (substrate-velocity) curves were generated in the presence of various concentrations of the inhibitor. Lineweaver-Burk transformations were used to discern the type of inhibition that was exhibited by the inhibitor-enzyme interaction. The derived inhibition modality dictated the selection of appropriate equations to determine the K_i value via non-linear regression analyses. IC_{50} values computed from log(inhibitor) vs. response variable slope (four parameters) analysis were also corrected to K_i based on the mode of inhibition identified (**eq. S17a** for competitive and **eq. S17b** for mixed mode inhibition)

$$IC_{50} = K_i \times (1 + \frac{[S]}{K_m}) \quad \textbf{(S17a)}$$

$$IC_{50} = \frac{Ki \times (1+\frac{[S]}{K_m})}{1+\frac{K_i}{K_i'} \times \frac{[S]}{K_m}} \quad \textbf{(S17b)}$$

Inhibition of P-gp-mediated Efflux of Rivaroxaban. The inhibitory potential of ketoconazole (0.1-50 µM) on the absorptive transport of rivaroxaban (10 µM) was assessed after the incubation period of 90 min. A model-based approach detailed by Kishimoto *et al* was used for calculation of the IC_{50} value of ketoconazole (**eq. S18**) (Kishimoto *et al.*, 2016).

$$\frac{1}{CL_{AtoB,i}} - \frac{1}{CL_{AtoB(-P-gp)}} = \frac{PS_{P-gp,I=0}}{P_{pass}S_1 \times P_{pass}S_3} \times \frac{1}{1 + \frac{[I]_{cell,u}}{IC_{50}}} \quad \textbf{(S18)}$$

where $CL_{AtoB,i}$ and $CL_{AtoB(-P-gp)}$ represent the observed A to B clearance with inhibitor and complete P-gp inhibition respectively, $P_{pass}S_1$ and $P_{pass}S_3$ represent permeability-surface area products (PS) for influx across apical membrane and efflux across basolateral membrane of MDCK-MDR1 cell monolayers, $PS_{P-gp,I=0}$ represents PS of P-gp in the absence of inhibitor and is defined by $\frac{J_{max}}{K_m}$. J_{max}, K_m *and* P_{pass} estimates were derived from previous three-compartmental analysis. $[I]_{cell,u}$ represents the unbound intracellular ketoconazole concentrations obtained from three-compartmental modelling of ketoconazole's bidirectional transport at t = 90 min. All regression analyses were performed using GraphPad Prism version 7 (GraphPad Software, San Diego, CA).

Inhibition of OAT3-mediated Uptake of Rivaroxaban. Investigation of the potential inhibition of OAT3-mediated rivaroxaban uptake by ketoconazole and verapamil adhered to the protocol previously outlined by Vermeer *et al* (Vermeer *et al.*, 2016). Prior to addition of ketoconazole, OAT3-transfected HEK cells were washed once with HBSS containing 20 mM HEPES (pH 7.4). Subsequently, HBSS containing varying concentrations of ketoconazole and verapamil (0.1 – 100 µM) was added for 15 min. Following pre-incubation, inhibitor solutions were aspirated and replaced with HBSS containing the inhibitors (or solvent control, dimethylsulfoxide) and rivaroxaban (1 µM) probe substrate . After 5 min, cellular uptake was terminated by washing the cells twice with 200 µL of ice-cold PBS and lysed directly on the plate with 100% methanol containing internal standard. IC_{50} values were determined from the average percent inhibition values fitted to log(inhibitor) vs. response variable slope (four parameters) analysis.

Ultrafiltration in the Determination of Fraction Unbound. To estimate the extent of non-specific binding of rivaroxaban (victim substrate) and inhibitors within the *in vitro* system, ultrafiltration was performed using the Centrifree® device. The calculated fraction unbound was subsequently used to correct the apparent kinetic and inhibition constants previously derived.

Non-Specific Binding (NSB) of Substrates and Inhibitors to Centrifree Device. Binding to the Centrifree tube sample reservoir and collection cup (as annotated in the diagram below) was determined by adding rivaroxaban 100 µM and the inhibitors (verapamil, norverapamil and ketoconazole) in protein free buffer (pH 7.4) directly to the reservoir (1000 µL) and cup (500 µL) followed by incubation for 20 min (Ballard and Rowland, 2011).

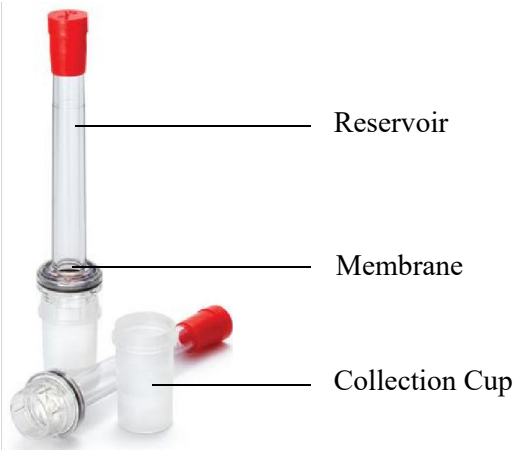

Centrifree device consisting of sample reservoir, membrane and collection cup.

Fraction unbound to the sample reservoir (fu_R) and collection cup (fu_C) was obtained using **eqs. S19a** and **S19b**.

$$fu_R = \frac{Cu_R}{C_{tot}} \quad \textbf{(19a)} \qquad fu_C = \frac{Cu_C}{C_{tot}} \quad \textbf{(19b)}$$

Where Cu_R, Cu_C and C_{tot} represent the unbound concentration of drug in the sample reservoir, collection cup and total concentration of test substrate respectively. Fraction unbound to the membrane, fu_{mem}, determined from a control filtration containing no protein in the supernatant, can be calculated using **eq. S20**.

$$fu_{mem} = \frac{Cu_C}{Cu_R \times fu_C} \quad \textbf{(S20)}$$

Unbound Fraction of Rivaroxaban in Media and within the Cell. Binding of rivaroxaban to culture media (DMEM + 10% FBS) and the MDCK-MDR1 cell homogenate was determined by the addition of rivaroxaban 100 µM to media and cell homogenate respectively. After incubation at 37℃ for 90 min, aliquots of the solutions were added to the reservoir, incubated for 20 min to ensure equilibration and subsequently centrifuged (2000 *g*) using a swing bucket for 30 min at 37℃. The ultrafiltrate was incubated for another 20 min to ensure equilibration with the collection cup. Both fraction unbound to DMEM (fu_{media}) as well as the diluted intracellular fraction unbound ($fu_{cell,d}$) were obtained using **eq. S21**.

$$fu_{media}/fu_{cell,d} = \frac{1}{1 + [\left(\frac{C_{tot,X} \times fu_{mem} \times fu_C}{Cu_{UF}}\right) - \frac{1}{fu_R}]} \quad \textbf{(S21)}$$

Where $C_{tot,X}$ represent the total concentration measured in DMEM or cell homogenate and Cu_{UF} is the concentration measured in the ultrafiltrate (Ballard and Rowland, 2011).

Calculation of fu_{cell}. $fu_{cell,d}$ that is determined under incubation conditions needs to be corrected by the dilution factor, D, to obtain the intrinsic undiluted $f_{u\,cell}$ (**Eq. S22**) (Riccardi *et al.*, 2018).

$$fu_{cell} = \frac{{}^1/_D}{\left(\left({}^1/_{fu_{cell,d}}\right) - 1\right) + {}^1/_D} \quad \textbf{(S22)}$$

Where D at $10 \times 10^6 cells/mL = \frac{Total\ suspension\ volume}{Cell\ volume}$ and $Cell\ volume = \frac{4}{3}\pi(\frac{Cell\ diameter}{2})^3$

Unbound Fraction of Verapamil, Norverapamil and Ketoconazole in the *In Vitro* Enzymatic Incubation. Binding of the inhibitors (1 μM) in the enzymatic incubation containing 40 pmol/mL of rCYP3A4 or 20 pmol/mL of rCYP2J2 was determined via the same protocol defined above.

Sample Processing for LC/MS/MS Quantitation

Efflux Assay. A calibration curve was built using 0.001, 0.005, 0.01, 0.1, 0.3, 0.5, 0.75, 1, 2, 5 μM of rivaroxaban. For sample concentrations above 5 μM, samples were diluted using media before sample processing to minimize any matrix effects during quantitation. To ascertain accuracy, quality control (QC) samples were prepared in triplicates using a similar method where low and high QCs were 0.05 and 3.5 μM respectively. To account for chemical degradation that might have occurred during the cell assay, the calibrants were also exposed at room temperature for the same duration as the transport assay. For rivaroxaban samples, calibration standards and controls, the samples were spiked with 2.02 μL of 50 μM prednisolone (IS) and subjected to a 2-step liquid-liquid extraction (LLE). In the first extraction, 1 mL of methyl tert butyl ether (MTBE) was aliquoted into each tube and vortexed at high speed for 5 min. Samples were then centrifuged using a microfuge at 18 000 *g* for 5 min at 4°C to ensure complete separation of the media from the extraction solvent. 800 μL of MTBE was carefully aliquoted from each tube to a corresponding 2 mL Eppendorf tube. For the second extraction, another 500 μL of MTBE was added, vortexed and spun down in a similar manner before 600 μL of MTBE was aliquoted and added to the same corresponding tube. The extraction solvent was then dried down in a turbovap using nitrogen gas at 3-5 psi before reconstitution in 100 μL of a 0.1% formic acid in ACN and 0.1% formic acid in water mixture (85:15 v/v) for LC/MS/MS analysis.

Uptake Assay. For *in vitro* studies of rivaroxaban uptake, the matrix was a mammalian cell lysate derived from HEK293 cells. Confluent monolayers were lysed with 100 μL of ice-cold methanol/cm^2 for 1 h before centrifugation at 18000 *g* for 15 min to pellet precipitated protein. Culture lysates were spiked with rivaroxaban working solutions to obtain final rivaroxaban concentrations of 0,0025, 0,005, 0.0125, 0.025, 0.05, 0.1, 0.25, 0.75, 1, 2 and 2.5 μM, containing the IS prednisolone at a concentration of 1 μM. QC samples were prepared independently at concentrations of 0.01 (low), 0.5 (medium) and 1.5 (high) μM of rivaroxaban.

NSB Assay. Collected samples were quenched by the addition of ACN containing 1 μM of prednisolone as IS. All samples were centrifuged at 4℃, 18000 *g* for 30 min and the supernatant was subjected to LCMS/MS analysis.

LC/MS/MS Quantitation

All samples were analysed using an Agilent 1290 Infinity ultra-high pressure liquid chromatography (UHPLC) (Agilent Technologies Inc., Santa Clara, CA, USA) interfaced with the AB SCIEX QTRAP 5500 tandem mass spectrometry (MS/MS) system (AB SCIEX, Framingham, MA, USA). The ACQUITY UPLC BEH C_{18}, 1.7 µM, 2.1 × 50 mm column (Waters, Mildord, MA, USA) was used for chromatographic separation. Samples were delivered using injection volumes of 1-4 µL. The aqueous mobile phase (A) was 0.1% formic acid in milli-Q water whereas the organic mobile phase (B) consisted of 0.1% formic acid in ACN. Mobile phases were delivered at a flow rate of 0.6 ml/min. The column was maintained at 45°C.

Transport Assay. The gradient program for rivaroxaban, propranolol, quinidine and prednisolone was as follows: linear gradient from 15 % to 85 % B (0-1.2 min), isocratic at 100 % B (1.21-2 min), linear gradient from 100 % to 15 % B (2-2.01 min) and isocratic at 15 % B (2.01-2.5 min).

Enzymatic Inhibition Assay. The gradient program for hydroxylated rivaroxaban metabolite and dexamethasone was as follows: linear gradient from 20% B to 80% B (0-1.2 min), isocratic at 100% B (1.21–2 min), linear gradient from 100% to 20% B (2-2.01 min) and isocratic at 20% B (2.01 – 2.5 min).

Transport Inhibition Assay. The gradient program for rivaroxaban, ketoconazole and prednisolone was as follows: linear gradient from 30 % to 70 % B (0 – 1.2 min), isocratic at 100 % (1.21 – 2 min) and isocratic at 20 % B (2.01 – 2.5 min).

NSB to PBS, DMEM culture media and cell homogenates. The gradient program for rivaroxaban, ketoconazole and prednisolone was as follows: linear gradient from 15% to 85% B (0 – 1.2 min), isocratic at 100% B (1.21 – 2 min) and isocratic at 15% B (2.01 – 2.5 min).

The MS source conditions were: source temperature 500 °C, curtain gas 30 psi, ion source gas 1 (sheath gas) 25 psi, ion source gas 2 (drying gas) 25 psi, ion spray voltage +5000V, collision gas (nitrogen) medium. All analyses were performed in ESI positive mode. Acquisition and analysis of data were performed with Analyst software ver. 1.6.2 (Applied Biosystems). For all LC/MS/MS analyses, the peak area of the analyte was expressed as a ratio to the peak area of the internal standard. The MRM transitions and compound dependent MS parameters of the analytes are summarized in the following table.

Optimized compound-specific MS parameters for LC/MS/MS analysis

Compound	MRM Transition (*m/z*)	Collision Energy (CE) (*V*)	Declustering Potential (DP) (*V*)	Entrance Potential (EP) (*V*)	Collision Exit Potential (CXP) (*V*)	Dwell Time (ms)
Rivaroxaban	436.200→145.000	33	95	10	9	100
Rivaroxaban Metabolite	452.200→406.100	25	100	10	9	100
Ketoconazole	531.200→489.200	40	103	9	25	100
Quinidine	325.300→172.100	27	100	7	6	100
Propranolol	260.300→116.200	23	45	11	6	100
Estrone-3-Sulfate (E3S)	349.200→269.200	-40	-116	-11	-8	100
Pregnenolone Sulfate (IS for E3S)	395.300→97.000	-79	-136	-8	-6	100
Para-aminohippuric acid (PAH)	195.300→120.200	18	34	7	8	100
Acetaminophen (IS for PAH)	152.100→110.000	23	64	12	8	100
Prednisolone	361.200→147.000	29	100	6	9	100
Dexamethasone	393.200→355.100	14	112	4	14	100

Supplemental Results

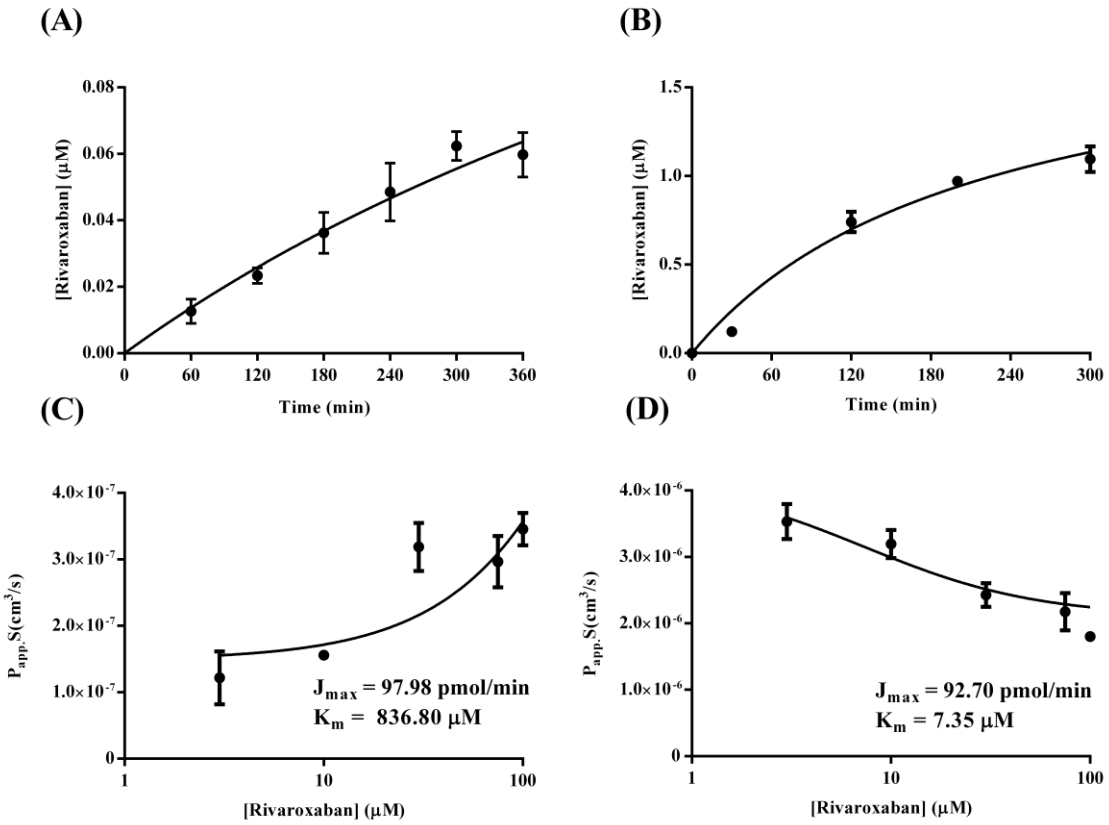

Supplemental Fig 2. Investigation of the P-gp-mediated transport kinetics of rivaroxaban. Time-dependent (**A**) A to B and (**B**) B to A transport of rivaroxaban. Both graphs were fitted with nonlinear regression Michaelis-Menten models. Concentration-dependent (**C**) A to B and (**D**) B to A transport of rivaroxaban was investigated at 180 min and 120 min respectively. Fitting of concentration-dependent absorptive and secretory clearances using **eqs. S8** and **S9** yielded $J_{max,app}$ and $K_{m,app}$ values. Each point represents the mean of triplicate determinations.

Supplemental Table 5. Non-specific binding of rivaroxaban and ketoconazole to ultrafiltration apparatus, culture media and cell homogenate.

	Rivaroxaban	***Ketoconazole***
fuR	0.94	0.80
fuC	0.90	1
fu_{mem}	0.88	0.49
fu_{media}	1	0.57
fu_{cell}	0.023	0.01
Cell diameter (µm)	13.6	13.6
Cell volume (µL/million cells)	1.317	1.317
D	75.9 *at* 10×10^6 *cells/mL*	25.3 *at* 30×10^6 *cells/mL*

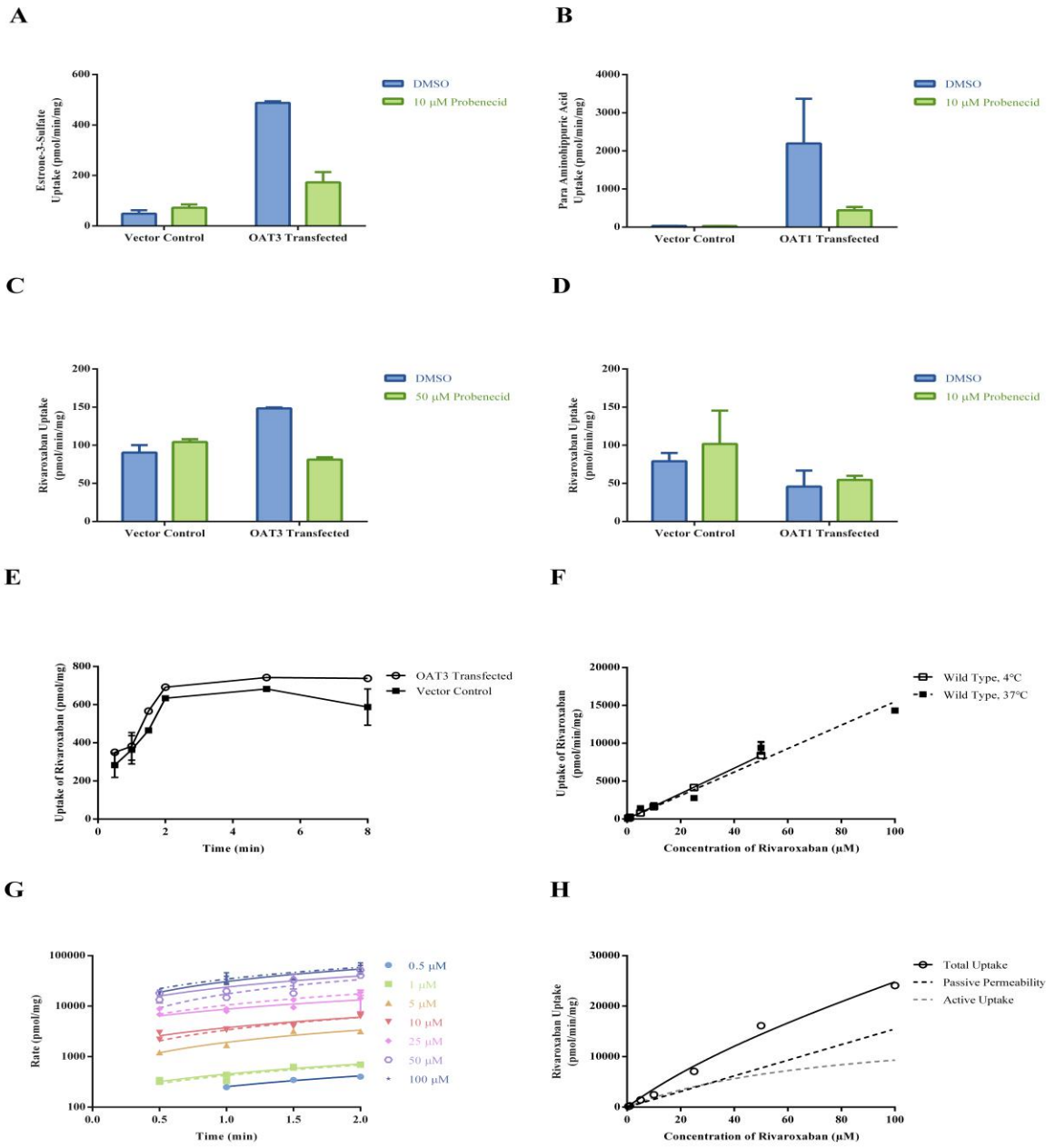

Supplemental Fig. 3. Investigation of the hOAT-mediated uptake transport kinetics of rivaroxaban. Uptake for 5 min by wild type HEK293 cells and those stably expressing hOAT3/1 was determined at 37°C for (**A**) estrone-3-sulfate (2 µM) and (**B**) para-aminohippuric acid (3 µM) to verify uptake functionality. Uptake of rivaroxaban (1 µM) in the absence and presence of prototypical OAT inhibitor, probenecid was subsequently investigated in (**C**) hOAT3-expressing HEK293 cells compared to wild type cells and (**D**) hOAT1-expressing HEK293 cells compared to wild type cells. Time course of uptake kinetics in wild type and OAT3-transfected cells is presented in (**E**). Time-dependent passive permeability up to 2 min was determined across 0.5 to 100 µM of rivaroxaban in wild type cells at both 4°C and 37°C (data not shown). Uptake rates obtained in wild type cells were plotted against rivaroxaban concentration in (**F**) to obtain the passive diffusion clearance (CL_{PD}) via linear regression (**eq. S13**). (**G**) Time-dependent total uptake up to 2 min was also quantified across 0.5 to 100 µM of rivaroxaban in OAT3-transfected HEK cells at 37°C. (**H**) Total uptake (black solid line) in OAT3-transfected HEK cells was analyzed via non-linear regression (**eq. 14**), and active uptake (grey dashed line) was obtained after subtracting the passive diffusion component (black dashed line) determined in wild type HEK cells. Uptake experiments carried out in (**E-H**) are represented as the mean ± SD of two experiments. All other data are results from a single experiment carried out in triplicate.

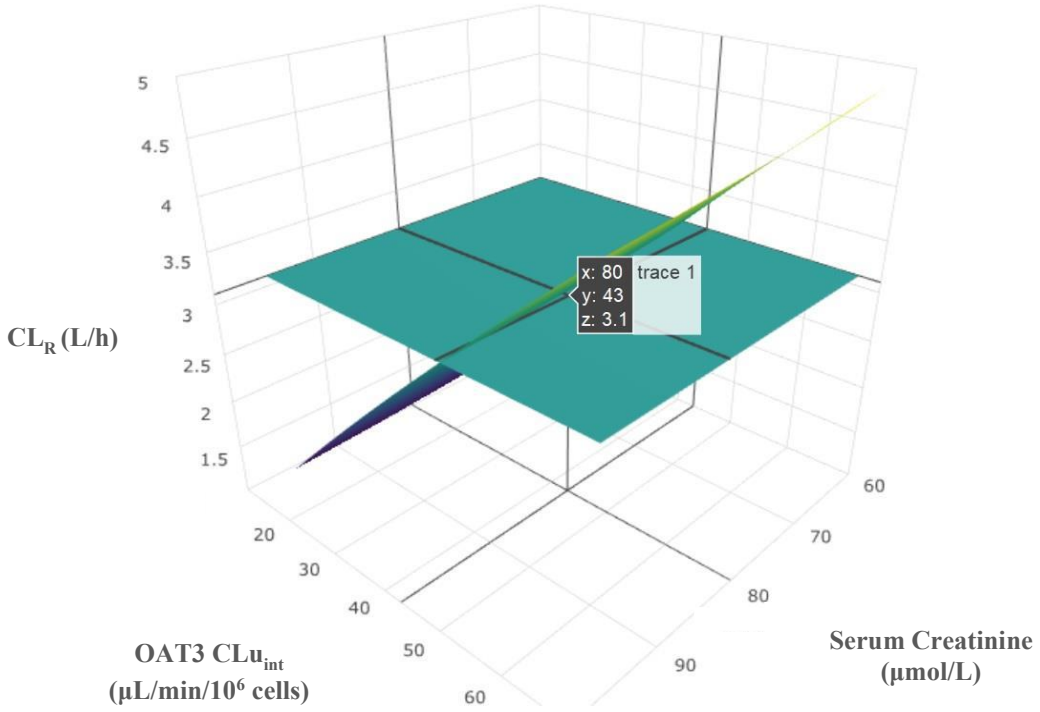

Supplemental Fig. 4. Top-down optimization of the OAT3-mediated basolateral uptake of rivaroxaban. Estimates of OAT3 CLu_{int} were obtained via a sensitivity analysis approach and was defined to be 43 µL/min/10^6 cells where simulated CL_R converged with the weighted mean CL_R of 3.1L/h when serum creatinine was fixed at 80 µmol/L (healthy volunteers).

Supplemental Table 6. Comparison of PK parameters between simulated and observed data for model verification of verapamil and norverapamil

	Simulated (n=200)	**Observed (n=20)**
Verapamil 80 mg	**AUC (µg.h/L)**	**AUC (µg.h/L)**
Geometric mean	404	389
CV (%)	45	66
Ratio of simulated/observed	1.04	
Success criteria for ratio of simulated/observed	0.58-1.73	
	Simulated (n=200)	**Observed (n=20)**
Norverapamil 80 mg	**AUC (µg.h/L)**	**AUC (µg.h/L)**
Geometric mean	722	674
CV (%)	42	38
Ratio of simulated/observed	1.07	
Success criteria for ratio of simulated/observed	0.72-1.39	

AUC, area under the concentration-time curve from time zero to infinity; CV, coefficient of variation

Supplemental Table 7. Comparison between Simcyp and experimental inhibitory parameters

		Simcyp (Index substrate)			**Experimental (Rivaroxaban Substrate)**		
In vitro parameter		V	NV	K	V	NV	K
MBI on CYP3A4	K_I (μM)	2.21	10.3	-	1.653	0.284	-
	k_{inact} (h^{-1})	2	18	-	3.924	2.440	-
	Potency	0.90	1.74	-	2.37	8.59	-
Reversible Inhibition on CYP3A4	K_i (μM)	-	-	0.015	0.487	0.270	0.094
Fraction Unbound	fu_{inc}	1	1	1	0.67	0.78	1

V, verapamil; NV, norverapamil; K, ketoconazole

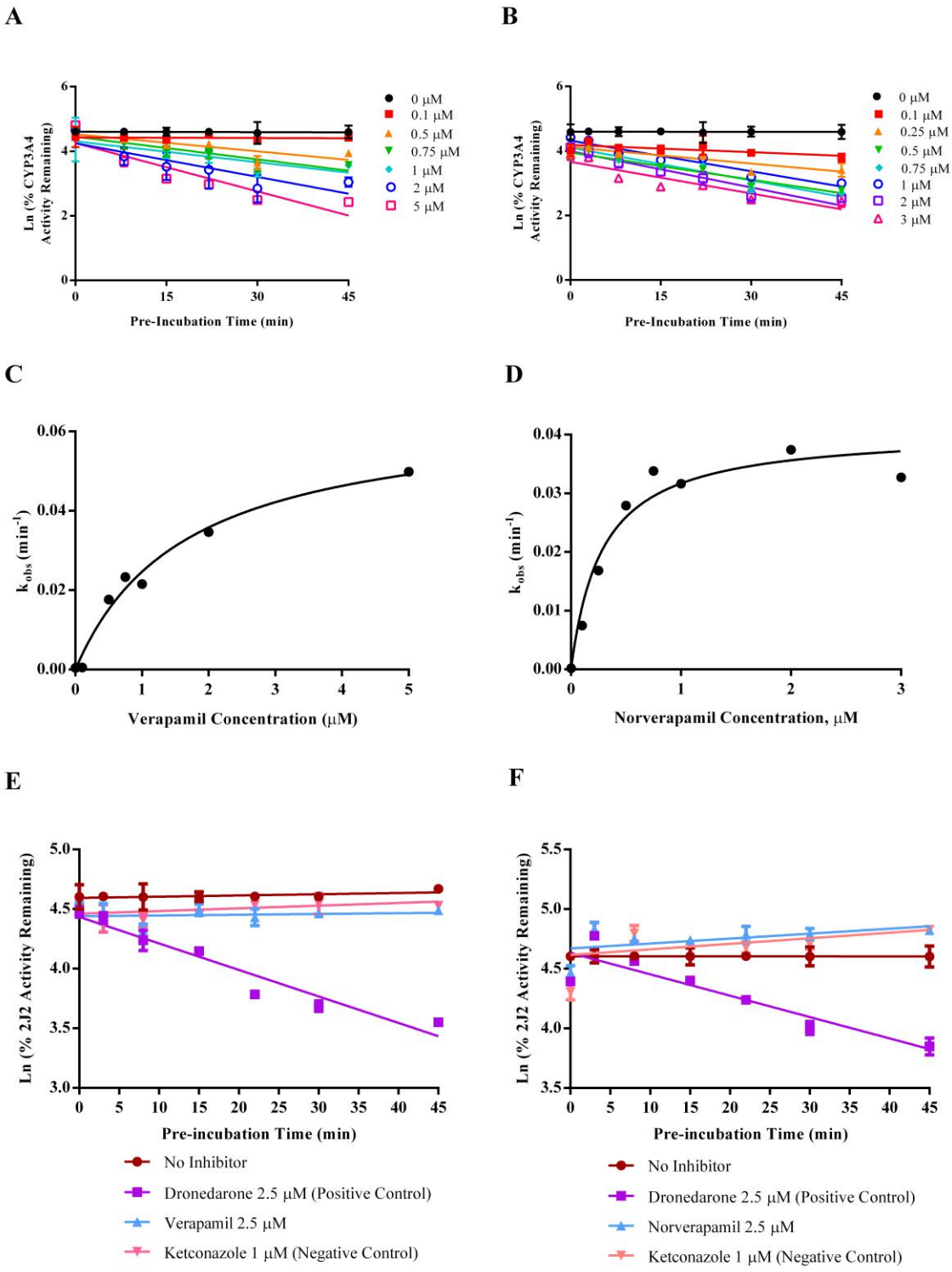

Supplemental Fig. 5. MBI of CYP3A4 and CYP2J2-mediated metabolism of rivaroxaban by verapamil and norverapamil. Semi-logarithmic plots demonstrate time- and concentration-dependent inhibition of CYP3A4 by **(A)** verapamil and **(B)** norverapamil using rivaroxaban as probe substrate and enabled the determination of pseudo-first order rates of inactivation (k_{obs}) at various verapamil and norverapamil concentrations. In **(C)** and **(D)**, the relationship between k_{obs} values determined from **(A)** and **(B)** and inhibitor concentration was further investigated via non-linear regression analysis to derive inactivation kinetic constants, K_I and k_{inact}. In contrast, time-dependent decrease in CYP2J2 activity across pre-incubation times was not apparent with verapamil (**E**) and norverapamil (**F**) as the putative inhibitors. Each point in the semi-logarithmic plots represents the mean of triplicate determinations.

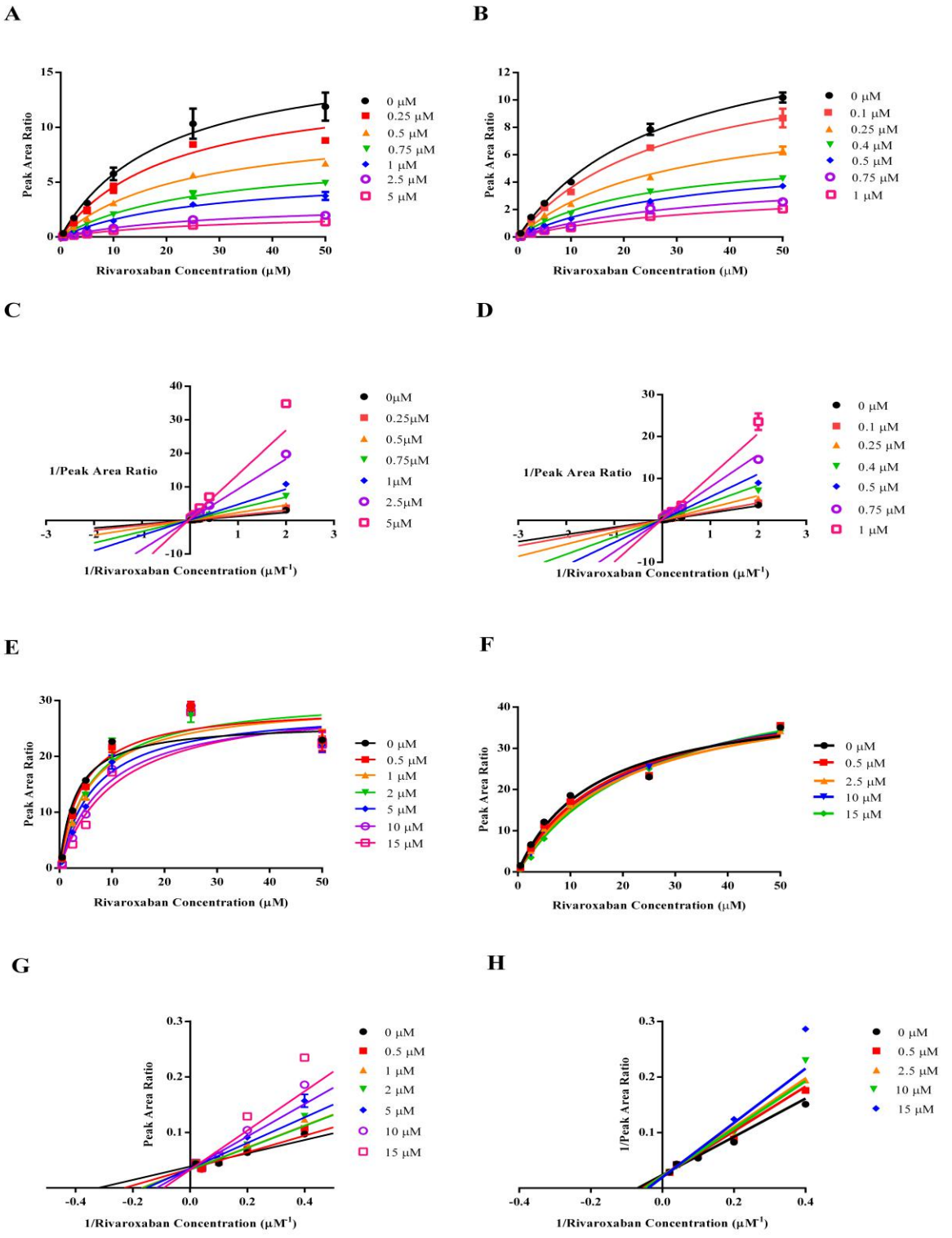

Supplememtal Fig. 6. Reversible inhibition of CYP3A4 and CYP2J2-mediated metabolism of rivaroxaban by verapamil and norverapamil. Michaelis-Menten plots illustrate reversible inhibition of CYP3A4 and CYP2J2 in the presence of (**A and E**) verapamil as well as (**B and F**) norverapamil. Data from (**A, B, E and F**) were transformed to corresponding Lineweaver-Burk plots in to reveal mixed mode inhibition of CYP3A4 in (**C, D**) and competitive inhibition of CYP2J2 in (**G, H**) when rivaroxaban was used as the probe substrate. Each point represents the mean of triplicate determinations.

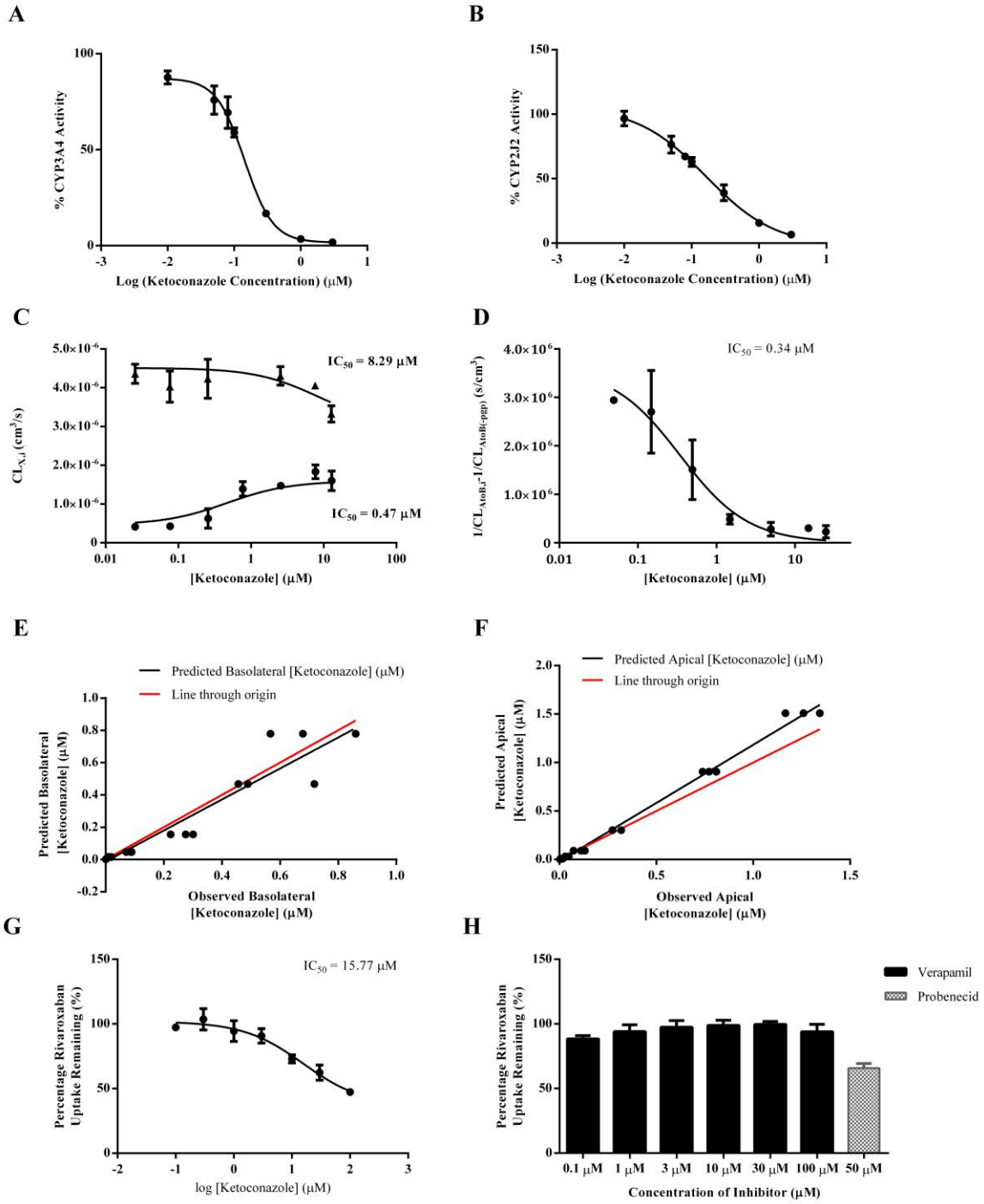

Supplemental Fig. 7. Inhibition of the enzyme and transporter-mediated elimination of rivaroxaban by ketoconazole and verapamil. (**A and B**) represent *in vitro* IC_{50} curves used to quantify the reversible inhibition of CYP3A4- and CYP2J2-mediated metabolism of rivaroxaban respectively. (**C and D**) illustrate the inhibitory effects of intracellular unbound concentrations of ketoconazole on the $CL_{AtoB,i}$; $CL_{BtoA,i}$ and $1/CL_{AtoB,i}$ - $1/CL_{AtoB}$(-P-gp) values of rivaroxaban. Intracellular unbound concentrations derived from three compartmental modeling were verified via assessing the goodness of fit between measured versus predicted ketoconazole concentrations in the (**E**) basolateral and (**F**) apical compartments of the transwell apparatus. The *in vitro* IC_{50} values describing the inhibition of the P-gp-mediated efflux of rivaroxaban by ketoconazole was converted to the inhibition constant K_i by applying the Cheng Prusoff equation (eq. S14a) assuming competitive inhibition. (**G and H**) illustrate the inhibitory effects of ketoconazole and verapamil respectively on the OAT3-mediated uptake of rivaroxaban into HEK cells. Inhibition experiments performed in (**G**) is represented as the mean ± SD of two experiments. All other data are results from a single experiment carried out in triplicate.

A

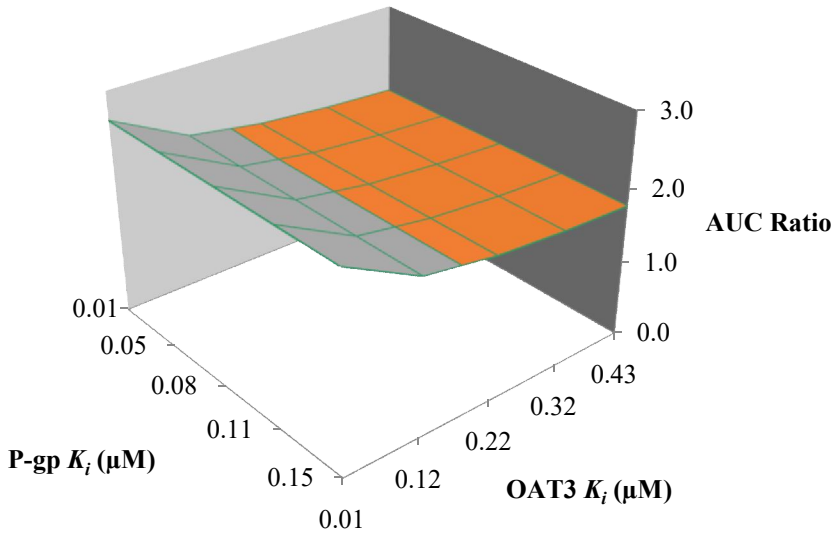
3.0
2.0
AUC Ratio
1.0
0.0
0.01
0.05
0.08
0.11
0.15
P-gp K_i (µM)
0.01
0.12
0.22
0.32
0.43
OAT3 K_i (µM)

B

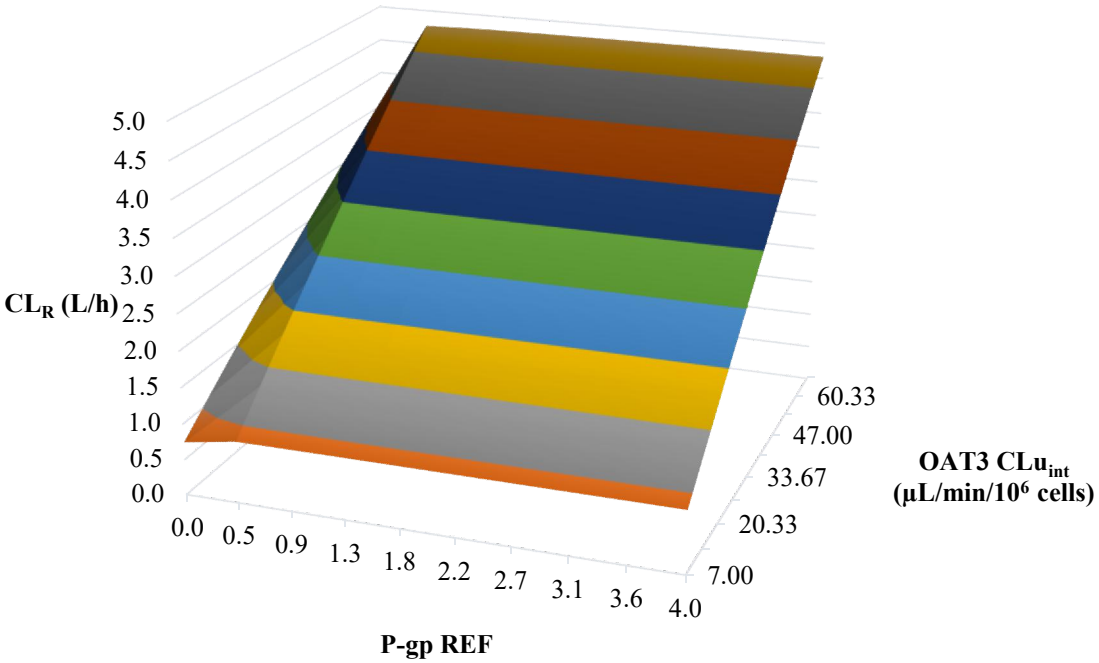
5.0
4.5
4.0
3.5
3.0
2.5
2.0
1.5
1.0
0.5
0.0
CL_R (L/h)
0.0
0.5
0.9
1.3
1.8
2.2
2.7
3.1
3.6
4.0
P-gp REF
60.33
47.00
33.67
20.33
7.00
OAT3 CLu_{int} (µL/min/10^6 cells)

C

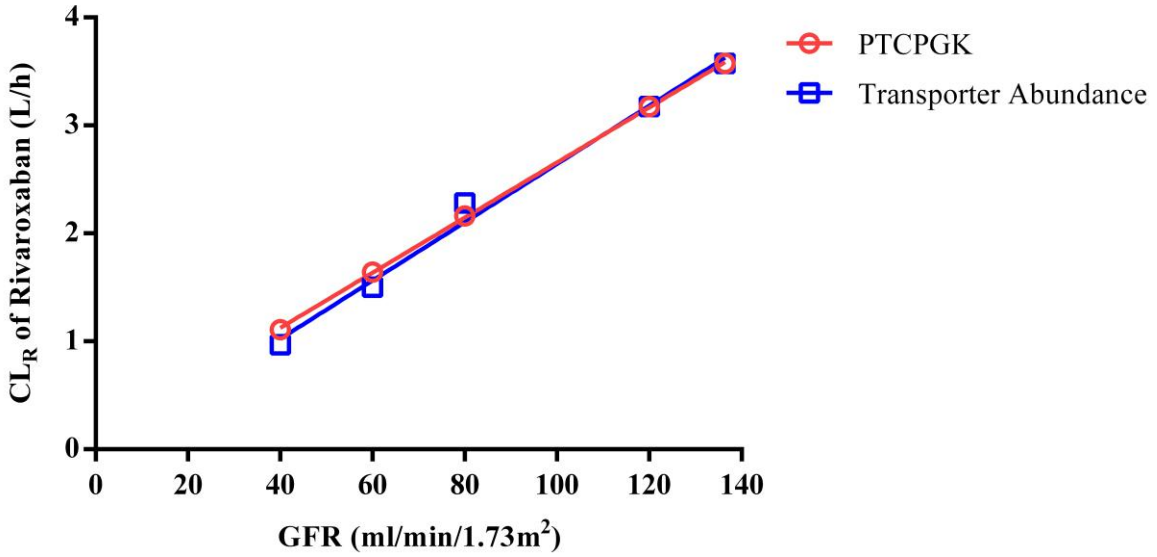

Supplemental Fig. 8. (**A**) Simulated rivaroxaban AUC ratio at different input values of OAT3 K_i and P-gp K_i. (**B**) Simulated rivaroxaban CL_R at different input values of OAT3 $CL_{int,T}$ and P-gp REF. Values of OAT3 $CL_{int,T}$, P-gp REF, OAT3 K_i and P-gp K_i were varied using the automated sensitivity analysis tool in the Simcyp simulator in a population representative following the clinical trial design reported by (Mueck *et al.*, 2013). (**C**) Predicting the effect of various physiological changes (either reductions in PTCPGK or transporter abundance) characterizing mild and moderate renal impairment on the CL_R of rivaroxaban

Supplemental Table 8. Comparison of **(A)** clinically observed renal clearance with simulated renal clearances of rivaroxaban using the **(B)** 35-compartment mechanistic kidney model versus **(C)** MechKiM module within the Simcyp simulator

$f_{u,p}$	Reported Apparent Permeability (10^{-6} cm/s)	$CL_{api,scr}$ (L/h)[a]	$CL_{bsl,scr}$ (L/h)[a]	Observed CL_R (L/h) (A)	Simulated CL_R (L/h)[b] (B)	Simulated CL_R (Mech KiM) (L/h)[b] (C)	Fold difference
0.065	21.8 (Caco-2)	0	0	3.1	0.27		
	12.7 (L-MDR1)				0.32		
	25.8 (LLC-PK1)				0.26		
	12.88 (MDCK-MDR1)				0.32	0.35	B/C = 0.91
0.065	12.88 (MDCK-MDR1)	42.3	0	3.1	0.37	0.35	B/A = 0.12
0.065	12.88 (MDCK-MDR1)	42.3	52.9	3.1	4.4	3.26	B/A = 1.41 C/A = 1.05

[a] Prediction of *in vivo* rivaroxaban basolateral and apical secretion clearances based on *in vitro* transporter data (**Supplemental Table 1**) using scaling factors of 60 million proximal tubule cells per gram kidney and 341.5 g of kidney per person.

[b] Renal clearance was calculated as the steady state urinary excretion rate (amount of drug excreted into the urine in a unit time) divided by the plasma rivaroxaban concentration at steady state.

Supplemental Table 9: Physiological changes in renal impairment

GFR (mL/min/1.73m^2)	Tubular Flow (L/h) (Percentage of Cardiac Output)[a]	OAT3 Abundance[b]	P-gp Abundance[b]	PTCPGK[b]
136.4	59.0	1	1	60
120	59.0	0.88	0.88	52.8
80	59.0	0.59	0.59	35.2
60	54.6	0.44	0.44	26.4
40	54.6	0.29	0.29	17.6

Reduction in both filtration and secretion was performed to represent changes in renal impairment. Simulated population representative of the healthy "NEurCaucasian" population available in Simcyp population had an age, weight, and body surface area of 58 years, 82 kg, and 1.97 m^2 respectively.

[a]Cardiac output for the population representative was defined as CO = BSA×60×(3-0.01*(age-20)). Tubular flow was defined as 19% of cardiac output for a healthy population (GFR > 80 mL/min/1.73 m^2), 17.67% of cardiac output for GFR 30-60 mL/min/1.73m^2 and 16.98% for GFR < 30 mL/min/m^2

[b]Relative change in GFR for each scenario was calculated using the value of 136.4 ml/ min/m^2 as baseline and applied to the OAT3 abundance, P-gp abundance or PTCPGK parameter. Reductions in renal transporter expression was represented in MechKiM by assigning relative abundances for the OAT3 and P-gp transporters in kidney in the "poor transporter" (PT) phenotype as a proportion of the Simcyp "extensive transporter" phenotype value of 1 and setting the frequency of PT in the modified population to 1 (Scotcher *et al.*, 2017). Changes were applied equally to each of the 3 sub-regions of the proximal tubule.

REFERENCES

Ballard P, and Rowland M (2011) Correction for nonspecific binding to various components of ultrafiltration apparatus and impact on estimating in vivo rat clearance for a congeneric series of 5-ethyl,,5-n-alkyl barbituric acids. *Drug Metab Dispos* **39**:2165–2168.

Brouwer KLR, Keppler D, Hoffmaster KA, Bow DAJ, Cheng Y, Lai Y, Palm JE, Stieger B, and Evers R (2013) In Vitro Methods to Support Transporter Evaluation in Drug Discovery and Development. *Clin Pharmacol Ther* **94**:95–112.

Dias C, Moore KT, Murphy J, Ariyawansa J, Smith W, Mills RM, and Weir MR (2016) Pharmacokinetics, Pharmacodynamics, and Safety of Single-Dose Rivaroxaban in Chronic Hemodialysis. *Am J Nephrol* **43**:229–236.

Ellens H, Johnson M, Lawrence SK, Watson C, Chen L, and Richards-Peterson LE (2017) Prediction of the transporter-mediated drug-drug interaction potential of dabrafenib and its major circulating metabolites. *Drug Metab Dispos* **45**:646–656.

FDA/CDER (2017) In Vitro Metabolism- and Transporter- Mediated Drug-Drug Interaction Studies Guidance for Industry. *FDA Guid*.

Frishman WH, and Lazar EJ (1992) Sustained-release verapamil formulations for treating hypertension. *J Clin Pharmacol* **32**:455–62.

Gnoth MJ, Buetehorn U, Muenster U, Schwarz T, and Sandmann S (2011) In vitro and in vivo P-glycoprotein transport characteristics of rivaroxaban. *J Pharmacol Exp Ther* **338**:372–380.

Greenblatt DJ, Patel M, Harmatz JS, Nicholson WT, Rubino CM, and Chow CR (2018) Impaired Rivaroxaban Clearance in Mild Renal Insufficiency With Verapamil Coadministration: Potential Implications for Bleeding Risk and Dose Selection. *J Clin Pharmacol* **58**:533–540.

Haeri A, Javadian B, Saadati R, and Dadashzadeh S (2014) Metabolite parameters as an appropriate alternative approach for assessment of bioequivalence of two verapamil formulations. *Iran J Pharm Res IJPR* **13**:383–9, Shahid Beheshti University of Medical Sciences.

Kishimoto W, Ishiguro N, Ludwig-Schwellinger E, Ebner T, Maeda K, and Sugiyama Y (2016) Usefulness of A Model-Based Approach for Estimating In Vitro P-Glycoprotein Inhibition Potency in a Transcellular Transport Assay. *J Pharm Sci* **105**:891–896.

Kreutz R, Persson PB, Kubitza D, Thelen K, Heitmeier S, Schwers S, Becka M, and Hemmrich M (2017) Dissociation between the pharmacokinetics and pharmacodynamics of once-daily rivaroxaban and twice-daily apixaban: a randomized crossover study. *J Thromb Haemost* **15**:2017–2028.

Kubitza D, Becka M, Mueck W, Halabi A, Maatouk H, Klause N, Lufft V, Wand Dominic D, Philipp T, and Bruck H (2010) Effects of renal impairment on the pharmacokinetics, pharmacodynamics and safety of rivaroxaban, an oral, direct Factor Xa inhibitor. *Br J Clin Pharmacol* **70**:703–712.

Kubitza D, Becka M, Mueck W, Halabi A, Maatouk H, Klause N, Lufft V, Wand Dominic D., Philipp T, and Bruck H (2010) Effects of renal impairment on the pharmacokinetics, pharmacodynamics and safety of rivaroxaban, an oral, direct Factor Xa inhibitor. *Br J Clin Pharmacol* **70**:703–712.

Kubitza D, Becka M, Roth A, and Mueck W (2013) The influence of age and gender on the pharmacokinetics and pharmacodynamics of rivaroxaban-an oral, direct factor xa inhibitor. *J Clin Pharmacol* **53**:249–255.

Kubitza D, Roth A, Becka M, Alatrach A, Halabi A, Hinrichsen H, and Mueck W (2013) Effect of hepatic impairment on the pharmacokinetics and pharmacodynamics of a single dose of rivaroxaban, an oral, direct Factor Xa inhibitor. *Br J Clin Pharmacol* **76**:89–98.

Mathialagan S, Piotrowski MA, Tess DA, Feng B, Litchfield J, and Varma M V. (2017) Quantitative prediction of human renal clearance and drug-drug interactions of organic anion transporter substrates using in vitro transport data: A relative activity factor approach. *Drug Metab Dispos* **45**:409–417.

Mathialagan S, Rodrigues AD, and Feng B (2017) Evaluation of Renal Transporter Inhibition Using Creatinine as a Substrate In Vitro to Assess the Clinical Risk of Elevated Serum Creatinine. *J Pharm Sci* **106**:2535–2541.

Moore KT, Vaidyanathan S, Natarajan J, Ariyawansa J, Haskell L, and Turner KC (2014) An open-label study to estimate the effect of steady-state erythromycin on the pharmacokinetics, pharmacodynamics, and safety of a single dose of rivaroxaban in subjects with renal impairment and normal renal function. *J Clin Pharmacol* **54**:1407–1420.

Mueck W, Kubitza D, and Becka M (2013) Co-administration of rivaroxaban with drugs that share its elimination pathways: pharmacokinetic effects in healthy subjects. *Br J Clin Pharmacol* **76**:455–466.

Polli JW, Humphreys JE, Harmon KA, Castellino S, Mara MJO, Olson KL, John-williams LS, Koch KM, and Serabjit-singh CJ (2008) The Role of Efflux and Uptake Transporters in N - { 3-Chloro-4- [(3-fluorobenzyl) oxy] phenyl } -6- [5- ({[2- (methylsulfonyl) ethyl] amino } methyl) -2-furyl] -4-quinazolinamine (GW572016 , Lapatinib) Disposition and Drug Interactions. **36**:695–701.

Popović-Nikolić MR, Popović G V., and Agbaba DD (2017) The Effect of Nonionic Surfactant Brij 35 on Solubility and Acid-Base Equilibria of Verapamil. *J Chem Eng Data* **62**:1776–1781.

Riccardi K, Ryu S, Lin J, Yates P, Tess D, Li R, Singh D, Holder BR, Kapinos B, Chang G, and Di L (2018) Comparison of Species and Cell-Type Differences in Fraction Unbound of Liver Tissues, Hepatocytes, and Cell Lines. *Drug Metab Dispos* **46**:415–421.

Shirasaka Y, Sakane T, and Yamashita S (2008) Effect of P-glycoprotein expression levels on the concentration-dependent permeability of drugs to the cell membrane. *J Pharm Sci* **97**:553–565, Elsevier Masson SAS.

Stampfuss J, Kubitza D, Becka M, and Mueck W (2013) The effect of food on the absorption and pharmacokinetics of rivaroxaban. *Int J Clin Pharmacol Ther* **51**:549–561.

Troutman MD, and Thakker DR (2003) Efflux ratio cannot assess P-glycoprotein-mediated attenuation of absorptive transport: Asymmetric effect of P-glycoprotein on absorptive and secretory transport across Caco-2 cell monolayers. *Pharm Res* **20**:1200–1209.

Vermeer LMM, Isringhausen CD, Ogilvie BW, and Buckley DB (2016) Evaluation of Ketoconazole and Its Alternative Clinical CYP3A4/5 Inhibitors as Inhibitors of Drug Transporters: The In Vitro Effects of Ketoconazole, Ritonavir, Clarithromycin, and Itraconazole on 13 Clinically-Relevant Drug Transporters. *Drug Metab Dispos* **44**:453–459.

Volpe DA (2016) Transporter assays as useful *in vitro* tools in drug discovery and development. *Expert Opin Drug Discov* **11**:91–103, Informa Healthcare.

von Bonsdorff C-H, Fuller SD, and Simons K (1985) Apical and basolateral endocytosis in Madin-Darby canine kidney (MDCK) cells grown on nitrocellulose filters. *EMBO J* **4**:2781–2792.

Modelling Supplemental Data.

Modelling Supplemental Data File 1: Simulated PK of rivaroxaban in mild renal impairment.

Modelling Supplemental Data File 2: Predicted extent of DDI between rivaroxaban and verapamil in a healthy population.

Modelling Supplemental Data File 3: Predicted magnitude of DDI between ketoconazole and rivaroxaban in a healthy population where the K_i of ketoconazole against OAT3-mediated rivaroxaban uptake has been optimized.

Modelling Supplemental Data File 4: Simulated PK of rivaroxaban in the absence of mechanistic kidney modelling

Modelling Supplemental Data File 5: Simulated PK of rivaroxaban in the presence of mechanistic kidney modelling